A NUMERICAL STUDY ON PERFORMANCE ENHANCEMENT OF PEM FUEL CELLS USING VARIABLE LENGTH SERPENTINE FLOW FIELDS

A Numerical study on performance enhancement of PEM Fuel cells using Variable Length Serpentine Flow Fields

A Dissertation
Submitted in partial fulfillment of the requirements for
the award of the Degree of

DOCTOR OF PHILOSOPHY

in

MECHANICAL ENGINEERING

by

Gundalabhagavan Amarnath

(Roll No.: 718032)

Under the Supervision of

Prof. A. Veeresh Babu
Professor

Mechanical Engineering Department

DEPARTEMENT OF MECHANICAL ENGINEERING
NATIONAL INSTITUTE OF TECHNOLOGY,
WARANGAL (TS), INDIA−506004,
July, 2023

A Numerical study on performance enhancement of PEM Fuel cells using Variable Length Serpentine Flow Fields

A Dissertation
Submitted in partial fulfillment of the requirements for
the award of the Degree of

DOCTOR OF PHILOSOPHY

in

MECHANICAL ENGINEERING

by

Gundalabhagavan Amarnath

(Roll No.: 718032)

Under the Supervision of

Prof. A. Veeresh Babu
Professor

Mechanical Engineering Department

DEPARTEMENT OF MECHANICAL ENGINEERING
NATIONAL INSTITUTE OF TECHNOLOGY,
WARANGAL (TS), INDIA−506004,
July, 2023

राष्ट्रीय प्रौद्योगिकी संस्थान वारंगल National Institute of Technology Warangal

Department of Mechanical Engineering

CERTIFICATE

This is to certify that the dissertation work entitled — A NUMERICAL STUDY ON PERFORMANCE ENHANCEMENT OF PEM FUEL CELLS USING VARIABLE LENGTH SERPENTINE FLOW FIELDS, which is being submitted by **Mr. GUNDALABHAGAVAN AMARNATH (**Roll No. 718032), is a bonafide work submitted to the Department of Mechanical Engineering, National Institute of Technology, Warangal in partial fulfillment of the requirement for the award of the degree of **Doctor of Philosophy in Mechanical Engineering.**

To the best of our knowledge, the work incorporated in this thesis has not been submitted elsewhere for the award of any degree.

Prof. A. Veeresh Babu
Supervisor
Department of Mechanical Engineering
National Institute of Technology
Warangal- 506004

Prof. V. Suresh Babu
Head of the Department
Department of Mechanical Engineering
National Institute of Technology
Warangal-506004

राष्ट्रीय प्रौद्योगिकी संस्थान वारंगल National Institute of Technology Warangal

Department of Mechanical Engineering

DECLARATION

This is to certify that the work presented in the thesis entitled, **"A NUMERICAL STUDY ON PERFORMANCE ENHANCEMENT OF PEM FUEL CELLS USING VARIABLE LENGTH SERPENTINE FLOW FIELDS"** is a bonafide work done by me under the supervision of Prof. A. Veeresh Babu, Professor, Department of Mechanical Engineering, NIT Warangal, India and was not submitted elsewhere for the award of any degree.

I declare that this written submission represents my ideas in my own words and where others' ideas or words have been included, I have adequately cited and referenced the original sources. I also declare that I have adhered to all principles of academic honesty and integrity and have not misrepresented or fabricated or falsified any idea / data / fact / source in my submission. I understand that any violation of the above will be a cause for disciplinary action by the Institute and can also evoke penal action from the sources which have thus not been properly cited or from whom proper permission has not been taken when needed.

Gundalabhagavan Amarnath

(Roll No.: 718032)

Date:

Dedicated to

My Mother (Smt.B. Santha Kumari) &
My Wife (Smt. D. Aruna Sree)

ABSTRACT

Fuel cells have been identified as a promising technology to meet future electric power requirements. Out of various fuel cells, Proton Exchange Membrane Fuel Cells (PEMFC) has been staged up as they can operate at low temperatures and also have high power density. The main idea of the current work is to enhance the contact time of the reactants against the products, which doesn't require much time to evacuate. In view of the above, an L-Serpentine Flow Field (LSFF) and Variable length serpentine flow field was considered as it also avoids flooding in the channel. These enhancements included a more uniform distribution of membrane water content, an impressive 8% increase in O_2 consumption, a remarkable 22% improvement in product evacuation demonstrated by the H_2O species profile, attributed to a 40% reduction in product travel distance. Additionally, a noteworthy 10% increase in power density was achieved.

An another attempt has been made to compare the flow behavior of parallel and counter split serpentine flow field with dual serpentine flow field. Where, pressure drop has decreased almost by five fold in Split serpentine when compared to SS and LSFFs. Moreover, a counter flow configuration possible in split serpentine helped to adopted variable length flow concept to this design. Polarization characteristics for all three cases were plotted and it was observed that split serpentine with counter flow field has better current density among other designs. In comparison to the dual serpentine flow field, split serpentine parallel flow and counter flow enhanced their power densities by 6.5% and 10.6%, respectively, and their oxygen consumption by 1.5% and 5%.

Further, the split serpentine flow field study was extended to bigger active areas of 73 x 53 mm^2, with horizontal and vertical configurations. Pressure drop has increased by 100 folds upon increasing the active area from 21x21 to 73x53 or 35x73. Due to the obvious reason of increased length of travel and increased flow resistance. With the adoption of bigger sizes the accumulation of water was observed towards the outlet. Moreover, the accumulation was higher in vertical configuration due to the length of the single flow field. Further the accumulation was reduced with counter flow configuration. Hence, horizontal configuration with counter flow split serpentine showed better performance among the other. However, this problem was further minimized with adoption of variable length to split serpentine.

Variable length to split serpentine flow field of 1 mm and 2 mm were studied. Among these, 2 mm showed better membrane water content and water evacuation characteristics. A 2% and 2.3% increase in current density observed for 1 mm VSS and 2 mm VSS respectively, compared to Split serpentine with counter flow configuration. Though the improved current density seems to be insignificant value of only 2%, it is always to be noticed that this 2% is an additional current density obtained to increase 10% current density in split serpentine alone when compared to dual serpentine.

CONTENTS

LIST OF FIGURES

LIST OF TABLES

NOMENCLATURE

$u_{a,in}, ; u_{c,in}$	Inlet velocities of reactant (m/s)	k_f	Thermal conductivity of fluid (W/m^{2}K)
$\zeta_a ; \zeta_c$	Stoichiometry ratio	k_s	Thermal conductivity of Solid (W/m^{2}K)
I_{ref}	Reference current density (A/cm^2)	y_i	Mass fraction of the species
F	Faradays constant (96485 C/mol)	D_i	Mass diffusion coefficient
R	Ideal gas constant (8.314 J/mol.K)	D_i^o	Mass diffusion coefficient at standard conditions
P	Pressure (Pa)	S_s	Species source term
T	Temperature (K)	$R_{a,c}$	Volume exchange current density at anode and cathode
A_{active}	Active area of the fuel cell (m^2)	$\sigma_{sol}, \sigma_{mem}$	Ionic conductivity in solid and membrane
A_{ff}	Area of cross section of Flow Field (m^2)	$\emptyset_{sol}, \emptyset_{mem}$	Potential of the cell in solid and membrane
$X_{H_2}; X_{O_2}$	Mole fraction of Hydrogen and Oxygen	R_{sol}, R_{mem}	Conductive current (A/m^2)
		V_o	Open Circuit Voltage (V)
ρ	Density of fluid	λ	Membrane water content
V	Velocity vector	a	Water activity
ε	Porosity	$I_{a,c}^{ref}$	Reference exchange current density at anode, cathode (A/m^2)
S_m	Mass source term	$\gamma_{a,c}$	Concentration exponent
MW	Molecular weight of the species (kg/mol)	$\eta_{a,c}$	Activation losses at anode, cathode
τ	Viscous shear stress tensor (N/m^2)	$[H_2], [O_2]$	Concentration of species
S_p	Source term due to porous media	α_a^a	Anodic transfer coefficient at anode
μ	Viscosity of fluid	α_c^a	Cathodic transfer coefficient at anode

k_p	Permeability of porous media	α_a^c	Anodic transfer coefficient at cathode
k_{eff}	Effective thermal conductivity (W/m^2K)	α_c^c	Cathodic transfer coefficient at cathode
T_E	Electrolyte thickness		
T_G	Gas Diffusion Layer thickness		
T_C	Catalyst Layer thickness		
W	Channel width		
H	Channel height		
C_T	Current collector thickness		
R	Rid width		

ABBREVIATIONS

PEMFC	Proton Exchange Membrane Fuel cells	DSFF	Dual Serpentine Flow Field
GDLC	Gas Diffusion Layer Cathode	SSFF	Split Serpentine Flow Field
CLC	Catalyst Layer Cathode	SSPFF	Split Serpentine Parallel Flow Field
PEM	Proton Exchange Membrane	SSCFF	Split Serpentine Counter Flow Field
RH	Relative Humidity	RAT321S	Right Angle Turned 3-2-1 Serpentine
BCGSTAB	Bi-Conjugate Gradient STABilizion	SIMPLE	Semi-Implicit Method for Pressure Linked Equations

Chapter 1
INTRODUCTION

Energy, the vital essence that courses through the veins of existence of human being as it propels the force that fuels the very fabric of our world. It is the pulsating heartbeat that ignites the dynamism of progress, empowering the growth and prosperity of civilizations, industries, and innovation. From the sun's radiant warmth that sustains life to the electrifying currents that power our modern marvels, energy pervades every corner of our existence, an intangible symphony orchestrating the dance of creation and advancement.The very essence of life itself is intertwined with the utilization of energy, consciously or unconsciously, to ensure survival of human being. Solar energy is the primary source that sustains not only the solar system but also all living organisms on Earth. Beyond solar power, other renewable energy sources like wind, tidal and geothermal play crucial roles in supporting human existence. Although the exploration and utilization of these renewable sources are still in the research phasesince long, their immense potential holds promise for a sustainable future. Throughout history, humankind has constantly sought new and alternative energy forms, recognizing the vital role energy plays in facilitating daily life. Thus, the quest for energy remains a fundamental requirement of human existence, providing the basic foundation for progress and enabling the world to achieve substantial success.

1.1.Energy demand and supply

Across the globe, there is a swift surge in the demand for energy to fuel transportation and power various modern household appliances, signaling a remarkable escalation in demand. Over the past 50 years, global electricity consumption has consistently grown, reaching an estimated 25,300 terawatt-hours in 2021. Whereas, India’s electricity consumption 5,800 terawatt-hours. During the period from 1980 to 2021, electricity consumption more than tripled, while the global population saw a growth of approximately 75 percent. This surge in electricity usage can be attributed to the expanding industrialization and improved access to electricity across the globe, which have further fueled the demand for power[1][2].

In order to meet the demand and reduce the dependency on fossil fuels, every country around the world is striving to invest towards clean energy, investments on the fossil fuel has strictly reduced from 1300 to 1000 Billion USD during period 2015 to 2023. Simultaneously, clean energy investment rose from 1100 to 1700 Billion USD in the same duration [3] [4].

Bio-fuel for automobiles reduces the dependency on fossil fuels to very small extent, researcher are still trying to find the economical and suitable fuel for automobiles [5]. However, they would reduce consumption of fossil fuels but pollution remains more or less same.

1.2.Renewable energy sources and their utilization

Despite imposed restrictions on carbon foot print methods for power production. Nations like India are looking for pollution-free energy production methods. In order to meet this requirement, government is planning India'sreduced dependency on thermal power plants to 50-55% by 2030 and switch over to Renewable Energy. Since, India accounts for 49% of total CO_2 emissions, compared to the global average of 41% [6]. As per International Energy Agency (IEA) report, in 2022, the India's primary energy mix consisted of approximately 84% fossil fuels and nuclear power, and 16% renewable energy sources (figure 1.1 and 1.2). Consumption of energy by various sources is plotted in figure.1.1and their percentages are indicated in a pie chart (figure 1.2) from 2022 statistics.

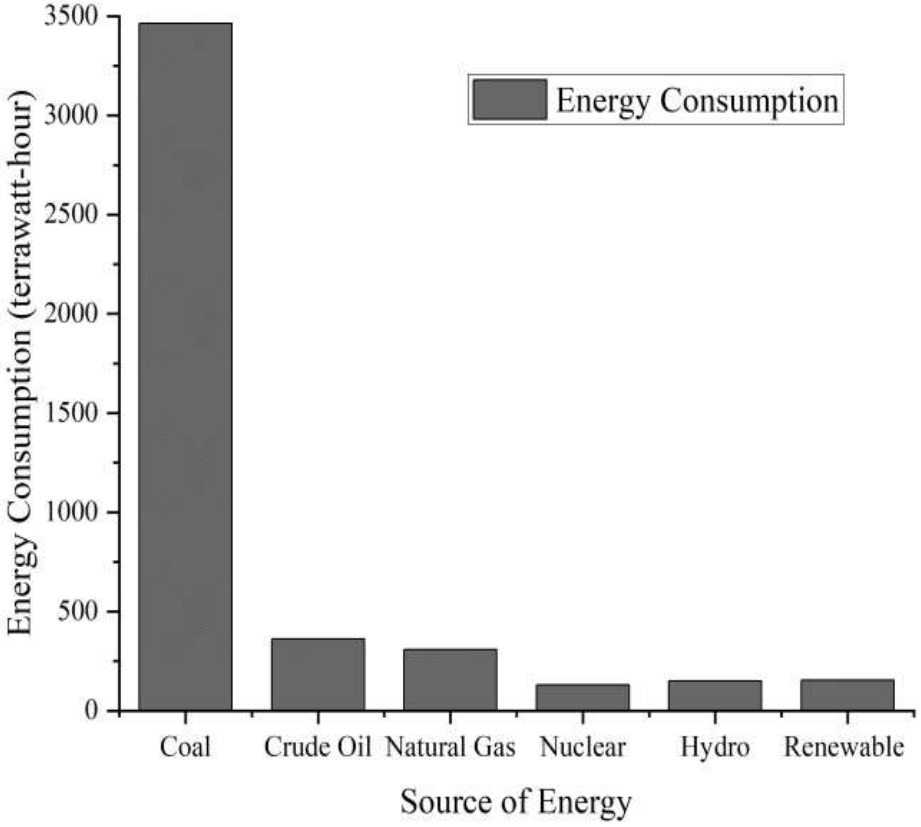

Figure 1.1 Energy consumption in twh[1]

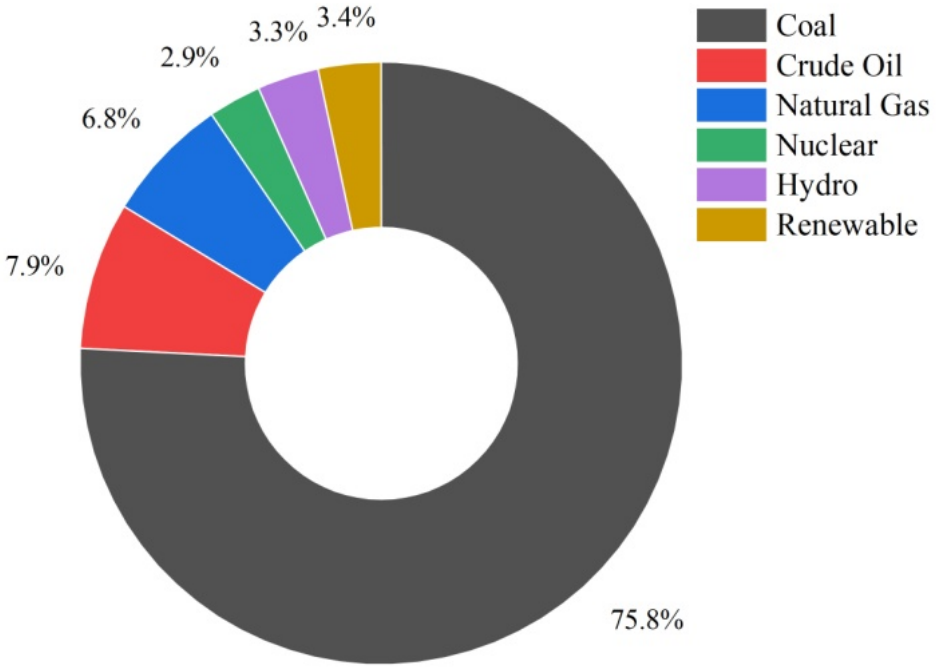

Figure 1.2 Percentage of energy consumption produced from various sources[1]

Figures 1.1 and 1.2 depict the distribution of energy production from different sources. Notably, coal accounts for 75% of the energy generated, highlighting India's heavy reliance on this non-renewable resource. Conversely, renewable sources, namely solar and wind, contribute a meager 3.4% of the total energy production. The IEA projects that renewable energy sources will grow significantly in the coming years, with their share of the global energy mix expected to reach 30% by 2040 [7]. Several factors contribute to this limited utilization. Firstly, solar and wind energy require substantial initial investments, which may hinder their widespread adoption. Additionally, their intermittent nature, contingent upon seasons, poses a challenge to consistent energy generation. Moreover, the installation of solar and wind power systems necessitates significant land area. To enhance the utilization of renewable energies, it becomes imperative to explore alternative energy sources. One of the potential solutions is the integration of various energy sources, which can foster sustainability in energy production. Hydrogen production from renewable energy could be directly used for fuel cell in automobiles and off-grid power plants. The utilization of hydrogen production and its subsequent usage represents a method that effectively addresses the intermittent nature of power generated from renewable energy sources. By converting excess renewable energy into hydrogen during periods of low demand and high renewable power generation, it becomes possible to store and distribute this hydrogen for use in different locations during periods of high demand and low renewable power generation. This

approach not only mitigates the issue of intermittency but also ensures efficient utilization of renewable energy resources based on varying energy demands[8]. Another way to store renewable energy is batteries. Battery power and Fuel Cells which ensure pollution-free energy [9]. Batteries have specific energy of 100-250 Wh/kg. Whereas, the Proton Exchange Membrane Fuel Cells (PEMFC) has specific energy of 600-1000 Wh/kg [10]. Hence, fuel cells can be considered as alternative power generation source for replacing the conventional methods.

1.3.Fuel cells working and categorization

This thesis proposes fuel cell working mechanisms into two categories: cation transfer fuel cells and anion transfer fuel cells.

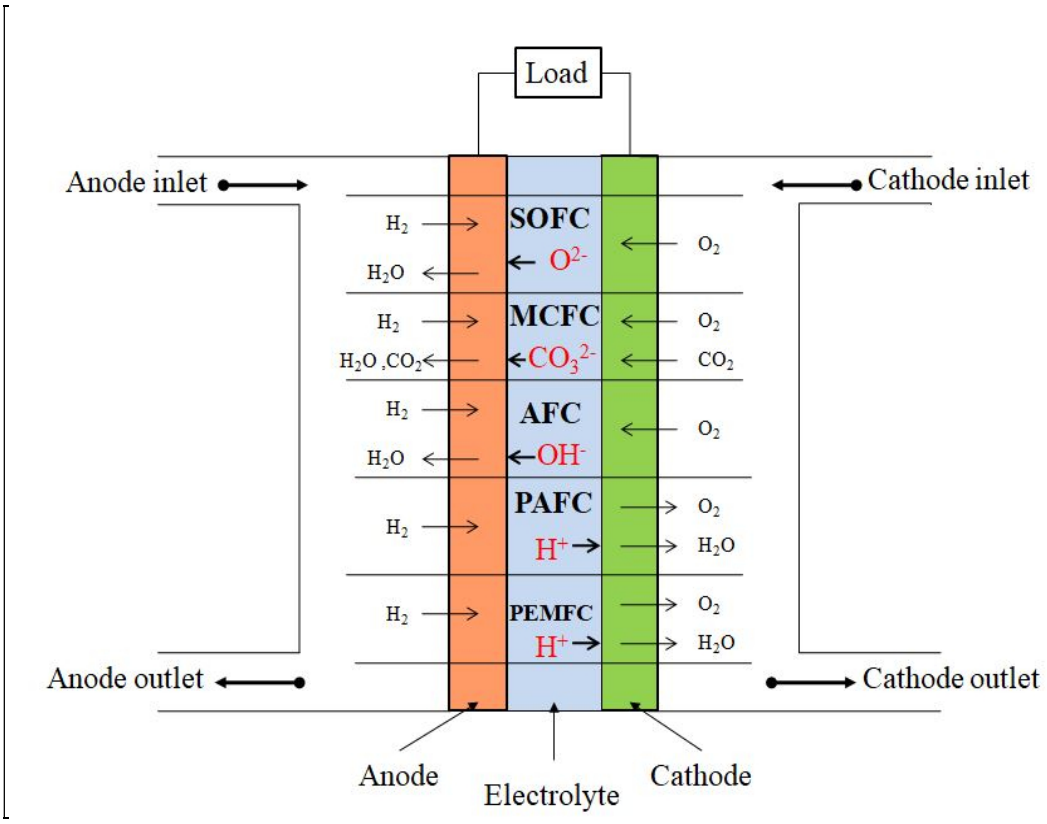

Figure. 1.3 Ion transfer layout of various fuel cells

This categorization helps in understanding the ion transfer mechanism based on the operating temperature and type of electrolyte used. Different cations and anions produced and their transfer mechanism is given in figure 1.3.

In cation transfer fuel cells, cations, which are positively charged ions, are produced at the anode through the loss of electrons. These cations then transfer from the anode to the

cathode through an electrolyte. Examples of cation transfer fuel cells include Proton Exchange Membrane Fuel Cells (PEMFC) and Phosphoric Acid Fuel Cells (PAFC), where H+ ions travel from the anode to the cathode via a proton exchange membrane or phosphoric acid electrolyte.

On the other hand, in anion transfer fuel cells, anions, which are negatively charged ions, are produced at the cathode by consuming electrons from the external circuit. Unlike cation transfer fuel cells, anions in these fuel cells travel back to the anode. Further details regarding specific anion transfer fuel cell types can be provided based on the available information. Eg. Solid Oxide Fuel cells (SOFC), Molten Carbonate Fuel Cells (MCFC) and Alkaline Fuel Cells (AFC).

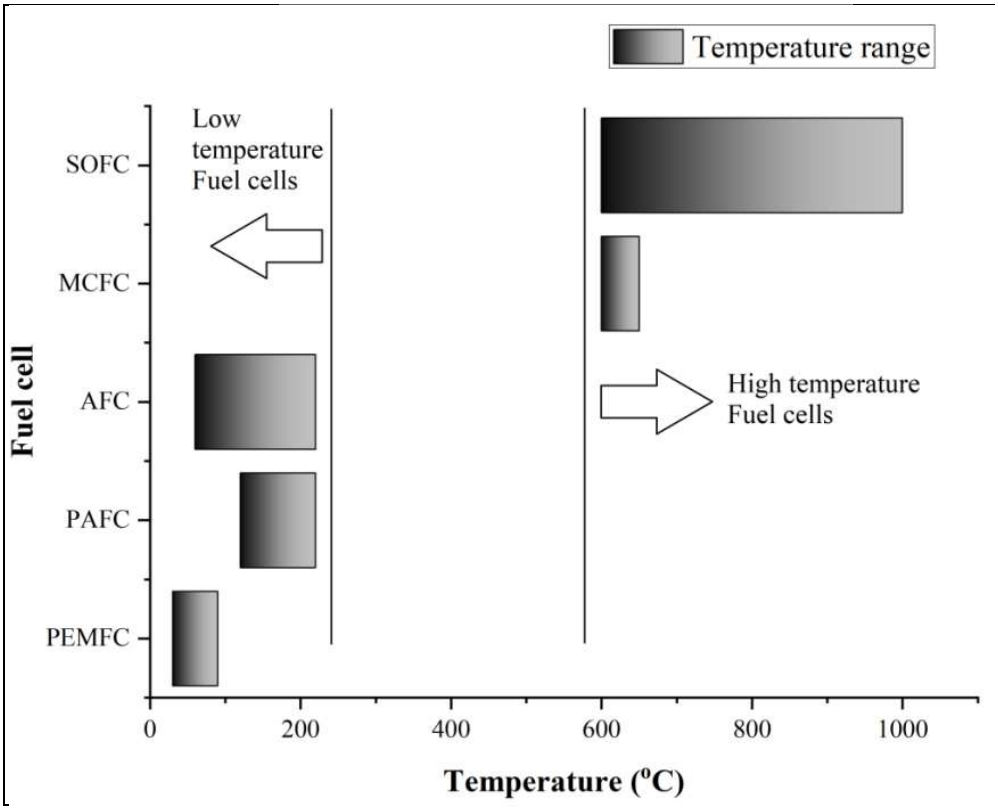

Figure 1.4 Temperature ranges of various fuel cells

Figure 1.4, explains the operating temperature ranges of various fuel cell. With the help of this figure fuel cells can be categorized into low temperature and high temperature operating fuel cells also [11]. Among various performance factors to be considered for selecting a fuel cell, here in this thesis five factors like operating temperature, fuel conversion efficiency, combined heat power plant capability, Quick start and cost of the whole system were considered.

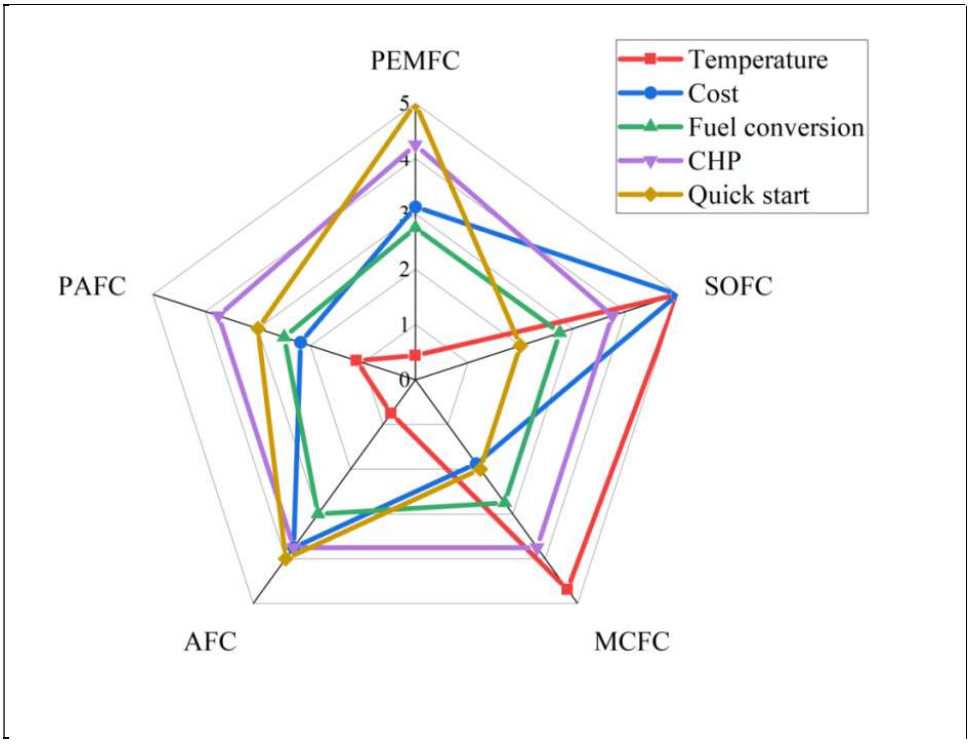

Figure 1.5 Various properties comparison for different fuel cells

From Figure 1.5, a comparison of various factors reveals that all the fuel cells exhibit nearly equal fuel conversion efficiency and combined heat and power plant capacity. However, the operating temperature plays a crucial role in determining the system's cost and quick-start capability. High-temperature fuel cells like SOFC and MCFC require additional subsystems for proper functioning, demanding careful attention. Conversely, low-temperature fuel cells offer quick starting characteristics and utilize hydrogen as fuel along with oxygen as an oxidant. AFC operates across a wide temperature range but is highly sensitive to CO poisoning. PAFC, although possessing a suitable working temperature, presents significant challenges in electrolyte management. Therefore, among the lower temperature fuel cells, PEMFC emerges as an optimal and efficient choice, mitigating the aforementioned drawbacks to a certain extent. Therefore, in this thesis, study was conducted to improve the performance of PEMFC.

Low-temperature fuel cells, specifically PEMFCs, prove convenient for automotive applications due to their quick starting ability, reduced subsystems, and lower setup costs. Among the low-temperature options, PEMFCs excel in terms of fuel conversion efficiency, operating temperature, and ease of operation[12].

1.4.Proton Exchange Membrane Fuel Cell (PEMFC)

In 1980s it was observed that liquid electrolytes offer resistance, which limits the performance of the cell. This problem has been overcome by replacing liquid electrolyte with thin proton exchanging sheet, Nafion[13]. PEMFC are trending fuel cells due to their quick start and high energy density nature. Most of the times PEMFCs operated by H_2 dominant fuel. Some of these fuel cells were also operated by methanol, alcohols solutions. PEM fuel cells are expected to be good substitute for IC engines in automobile sector, with onboard reformer for H_2 production [14]. These fuel cells operate in the temperature range of 20^0-90^0C, CO poisoning is a major problem of consideration, where CO is adsorbed on Pt surface and makes the fuel cell deactivate [15][16]. So researcher are trying to remove CO from the H_2 gas during fuel processing [17]. Strong acid fuel cells like PAFC are capable enough to oxidise CO to CO_2 to some extent. Moreover, PAFC performance was expected to be higher, but the results obtained with solid membrane (PEMFC- Nafion) were reasonably good compared to liquid electrolyte fuel cell (PAFC) [18] [19].

PEMFC mainly consumes Hydrogen as fuel and Oxygen/air as oxidizer. The primary products of this reaction are water and heat. PEMFC consists of Proton Exchange Membrane (PEM), catalyst layer (CL), Gas Diffusion Layer (GDL) and Bipolar plates or Current collectors (CC). Flow field or flow channels are engravings on current collectors on both anode and cathode. Flow field facilitate reactants to catalyst sites through GDL. Simultaneously, formed water at the cathode catalyst transferred to the flow field via capillary action [20]. Flow field collects the water and drive them out due to the pressure difference in them. Among the various studies on PEMFCs, Flow field design is considered as a primary factor which affects the performance significantly. Flow field designs were played a vital in other fuel cells like SOFC [21] [22].

Flow fields have undergone development over time, with various designs such as pin-fin, parallel U and Z, spiral, radial, serpentine, and interdigitated (figure 1.6). Pin-fin or grid layouts have lower flow resistance, resulting in less pressure drop. However, they suffer from blind spots or low pressure zones that arise due to insufficient driving pressure, which can cause certain areas of the active zone to experience a dearth of species or a buildup of product water. Blind spots were only partially eliminated with the implementation of parallel flow fields, as compared to pin-fin or grid flow fields[23].The parallel flow field was a simple and popular design, but it was found to be ineffective in distributing species [24].

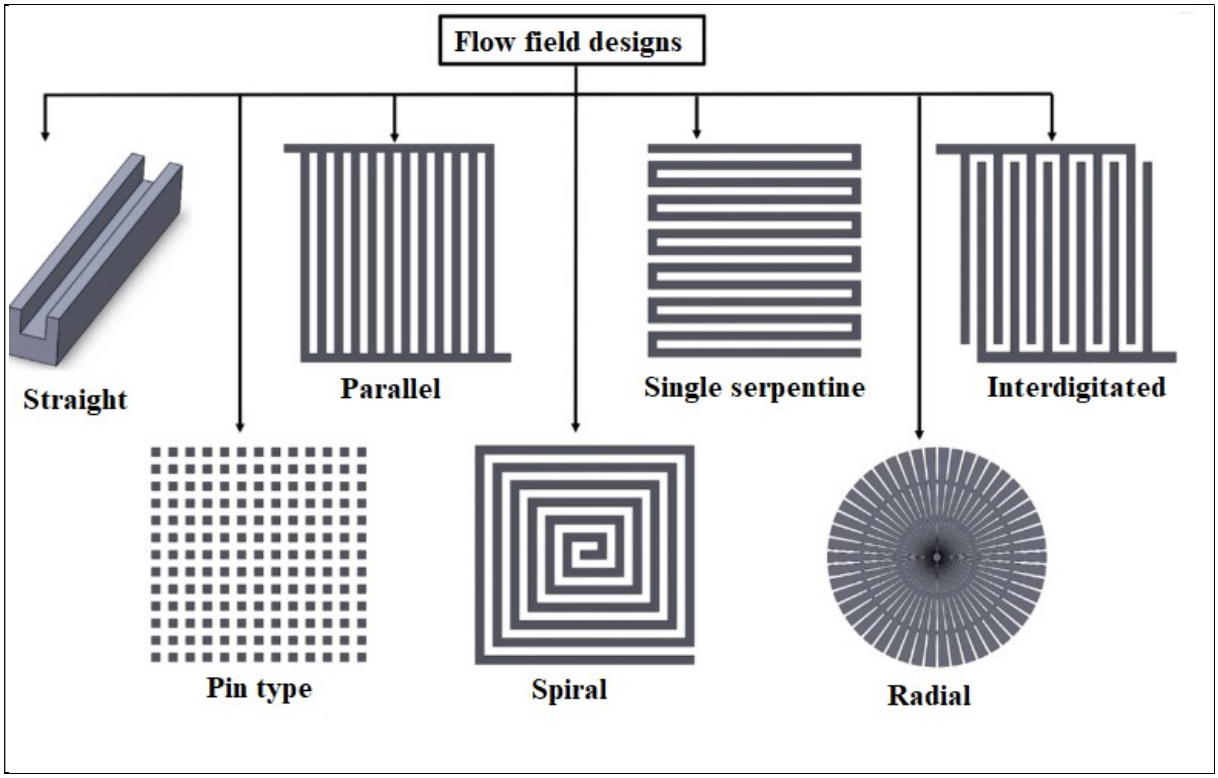

Figure 1.6 Developments in flow field designs [25]

Subsequent improvements were made, resulting in designs such as serpentine, interdigitated, and bio-inspired flow fields, which had greater transport capabilities[26]. In a study by Ozedimir et al., U and Z parallel flow fields were simulated and it was found that they also exhibited lower pressure drops, similar to pin-fin or grid layouts, poor distribution of species with blind spots was observed in certain corners of both designs. These findings suggest that blind spots remain a persistent challenge in the development of efficient and effective flow fields [27]. However, this issue can be resolved by using a single serpentine flow field which ensures continuity and prevents the accumulation of species. This design resulted in increased reactivity and current density, but it also leads to a higher pressure loss, requiring more compressor work at the inlet. Single serpentine flow field was further modified into double, triple, multiple parallel and parallel in series (RAT321S) serpentines in order to reduce the pressure drop and enhances distribution (figure 1.7). However, distribution of species still need to be improved [28].

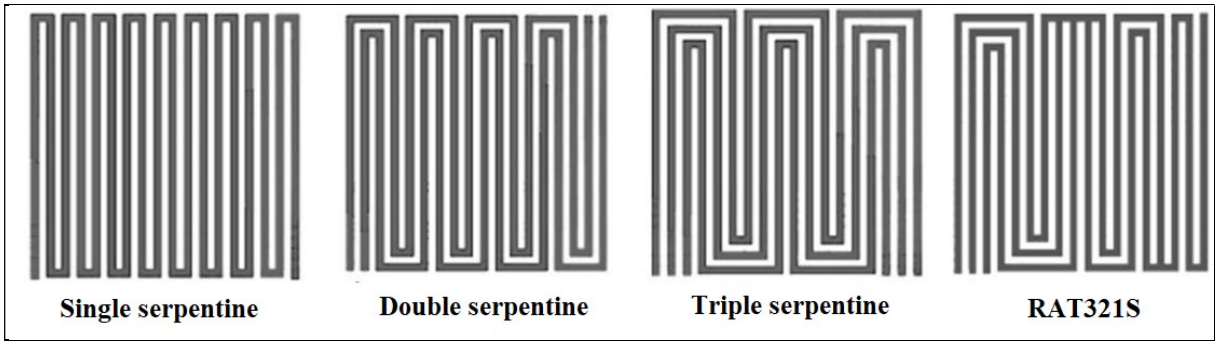

Figure 1. 7 Developments in Serpentine flow field [29]

Furthermore, Interdigitated shows higher pressure drop than single serpentine but improves reactivity by creating a dead-end flow pattern. However, the pressure drop is even higher than that of a single serpentine flow field [23]. Another modification is a positive tapered fuel cell flow channel, which has a tapered slope and can handle high current density and water removal [30] [31] [32]. Nevertheless, this design requires a large gas pressure at the inlet [31][32][33]. On the other hand Bumpy flow fields were developed to improve the reactivity, these flow fields drives the reactants towards the catalyst for better reaction [34]. Similar to tapered flow fields, these flow fields also induces large pressure drop. Hence, amongst all designs, serpentine design was found to be good [35][36][11] due to its ability to flush out products and reduce blind spots due to condensed water [37].

Various flow fields designs were development methods by researchers in order address the performance issues in serpentine flow fields were discussed in the next chapter.

Chapter 2
LITERATURE SURVEY

The performance of a PEMFC is heavily influenced by a variety of parameters, the most important of which is the flow field design, efficient distribution of reactants and removal of products is crucial for the optimal functioning of a fuel cell. Rostami et.al, mentioned bipolar plates weight is 50% of the total weight of the fuel cell. Next to catalyst bipolar plates cost is the second expensive cost of the fuel cell [38]. As the gases move through the channels, they are dispersed to the Gas Diffusion Layer (GDL) and reach the catalyst layer. Any water produced is carried by diffusion towards the channel, which then drains the water from the cell. Therefore, the design of the flow channels plays a critical role in ensuring the fuel cell performs optimally by facilitating the effective supply of reactants and removal of products [39]. Also, efficient Flow fields also aid in the reduction of pressure drop losses and heat buildup. Fuel cells exhibit temperature and water gradients due to the reaction distribution, affecting the reaction rate and potentially leading to local flooding. Moreover, water transport across the membrane between the anode and cathode is impacted by electro-osmosis and diffusion, and changes in the membrane's conductivity result from variations in the local water activity on the anode. These effects significantly impact fuel cell performance [40]. Considerable quantum of work has been carried out to increase the life of PEMFC by decreasing minor losses arising due to non uniform distribution of spices.

Detailed studies of various researchers on serpentine flow fields and their performance evaluation using mathematical models are going to be discussed in the following literature.

Watkins, Dircks and Epp (1991)[41] patented single serpentine design for the first time. They explained its structure by giving the details of inlet and outlets provided for their design. Unlike the other designs, this design was having direct connection of inlet and outlet and it is continuous in nature of flow.

Watkins, Dircks and Epp (1992) [42] further modified single serpentine to multi serpentine and been awarded with a patent. This design takes forward the single serpentine in terms of species distribution by shorter flow fields.

Kazim, Liu and Forges (1999) [43]used a mathematical model and compared singe serpentine with interdigitated. In this analysis single serpentine was considered as

conventional flow field. This analysis used various mathematical models like Darcy's equation, standard diffusivity equations for porous media to calculate mass transfer effectively.

Dutta, shimpalee and Van Zee (2001) [44]usedAnsys Fluentmodel to study the mass distribution of single serpentine flow channels, with 20 channels in anode and cathode flow channels and results states that channel affects the consumption pattern on the membrane electrode assembly. Density and viscosity varies with respect to space and hence, a model similar to compressible flow is considered. Change in density at various locations was considered as consumption or production of the species. Hydrogen consumption was about 28% more near the outlet than the inlet. It is found that pressure drop on anode side smaller than cathode side. Moreover, flow over porous media is insignificant, and hence, the overall pressure drop is lower than that expected in a single serpentine.

Wang et.al (2003) [45]**:**The mathematical model developed by this group is considered as most authentic in validating the experimental results. Model active area was 72x72 mm^2 with 18 single serpentine channels. This work established the co-relation between experimental and simulation studies. This study presents results on various parameters operating- cell temperature, humidifying temperature, pressure, etc. It is observed that increasing in cell and humidifying temperature (50 to 90^0C) has increased the power output, due to increased diffusivity of species with temperature and also reduces activation losses. Anode and cathode humidification temperature keeping the cell temperature constant helps in increasing power density. Operating pressure increase has resulted in improved current density.

Nguyen, Berning and Djilali(2004) [46]in their 3D Ansys Fluent CFD simulations, investigated the primary transport phenomena in a single-phase, steady-state operation with a fully humidified membrane. The model treated product water as a vapor phase only. It focused on a single turn flow channel, encompassing only two channels. A novel feature included a voltage-to-current algorithm, enabling the calculation of local activation overpotentials to predict the distribution of current density. The model successfully determined oxygen distribution beneath the channel and ribs. Moreover, it established the characteristics of current distribution, active overpotentials, and ohmic overpotential.

Li and Sabir (2005) [35]in their review of bipolar plates, it was observed that various bipolar or current collectors, such as pure graphite and coated plates, account for 88% and 81% of the total weight of the stack, respectively. This highlights the significance of current collectors

with efficient flow fields in enhancing the performance of the fuel cell. Among the different flow fields examined, including pin fin, parallel, serpentine, interdigitated, and bio-inspired flow fields. Particular attention was given to serpentine flow fields also. Notably, spirally linked serpentine configurations exhibit both the characteristics of a single serpentine flow field and smaller flow length portions.

Shimpalee, Greeway and Van Zee (2006) [40]considered four different serpentine flow-field configurations were studied using CFD simulations, each having an active area of 200 cm2. Single serpentine channels were modified to dual, triple, and more, aiming to reduce pressure drop by increasing the number of passages and minimizing parasitic losses. The researchers also investigated parallel serpentine designs, which further reduced the species' travel length and subsequently the pressure drop in flow fields. However, increasing the number of channels did not show significant benefits, as the distribution characteristics exhibited only minimal variations.

Ming and Su (2007) [47] in their comprehensive 3D CFD simulation to examine the impact of various flow channel designs on PEMFC performance. The study encompassed parallel and serpentine flow channels. The model's predictions aligned well with experimental results, demonstrating its reliability. The parallel flow channel, featuring a step-wise depth design, notably improved PEMFC performance. Nonetheless, the serpentine flow channel still outperformed the PEMFC in terms of overall performance.

Jeon et.al (2008) [48]investigated the effect of serpentine flow-field designs on performance of PEM fuel cell was studied.CFD simulations were performed for four 10cm^2 serpentine flow-fields with single, double channel, cyclic-single, and symmetric-single channel patterns (cycle and symmetric are single serpentine flow channels which were divided into small segments) to investigate the effect of flow-field design and it was observed that cyclic and symmetric flow fields showed consistently recurring patterns of various factors like membrane water content and current density distribution.

Zhang et.al (2008) [49] considered the effect of RH on PEM fuel cell performance was studied at elevated temperatures under ambient back pressure using Nafion based MEAs. The results revealed that fuel cell performance could be depressed significantly by decreasing RH from 100 to 25%. AC impedance and cyclic voltammetry techniques were employed to diagnose the RH effect on fuel cell reaction kinetics. Reducing RH can result in slower electrode kinetics, including electrode reaction and mass diffusion rates and the proton

conductivity of the membrane, resulting in a significant degradation in performance of fuel cell.

Chena, Li and Peng (2008) [50] study revealed that the membrane vapor transfer rate in PEM fuel cells significantly increased with water channel temperature, air channel temperature, and air flow rate during steady-state tests. This validation model holds vital importance for designing external humidifiers and controlling fuel cell humidification effectively. Understanding membrane humidification behavior and its controllability can lead to enhanced efficiency and reliability of PEM fuel cells. Notably, the study obtained a new water vapor transfer coefficient for Nafion membrane, which showed an exponential increase with membrane temperature.

Wang et.al (2009) [51] carried out CFD study to analyze the effects of active area on the performance and local transport processes of species in a PEM fuel cell with parallel design, interdigitated, and serpentine flow channel design. At the operating voltage of 0.7 V, the polarization curves and power density curves, size effect is not noticeable for all three cells. However, at operating voltage of 0.3 V, the size effect for parallel flow cells is significant. As the active area was increased from 11x11 mm^2 to 41x41 mm^2 (13.9 times increased) for parallel cell, the average current density decreases by 10.6% at 0.4 V and by 11.6% at 0.3 V. Owing to limited oxygen supply, size effect is minimal at high operating voltages.

Lin et.al (2009) [52]used an optimization method for the fuel cell flow fields, basically to optimize the geometry of a serpentine flow field with varying channel heights and widths and it was observed that tapered middle flow channel enhances liquid water removal capacity from the porous electrode and reduces the oxygen transfer resistance by increasing the sub-rib convection. Tapered outlet flow channel has a greater impact on the cell performance than the flow channel width.

Wang et.al (2010) [53]this research investigates the influence of channel size (channel height and width were changed symmetrically) on PEMFC performance using serpentine flow fields. The study indicates that smaller channel sizes improve liquid water removal and enhance oxygen transport to the porous layer, leading to enhanced cell performance. Moreover, smaller channels result in a more uniform current density distribution. However, it is important to note that reducing the channel size increases the pressure drop. Nevertheless, when accounting for the pressure drop losses, the use of smaller channels exhibits higher net power density. In summary, the study highlights the trade-off between improved cell

performance and increased pressure drop, with smaller channels ultimately offering higher net power density when all factors are considered.

Choi, Kim and Moon (2010) [54] investigation showed that raising the channel height above the base design reduced the overall pressure drop, which caused liquid water to collect at the anode and cathode's outlet. Higher channel heights were shown to enhance the back diffusion-induced buildup of anode liquid water near the outflow. The evacuation of liquid water was accelerated and the pressure drop was reduced, however, when the channel width was increased beyond the base design. Due to the identical area of the cross-section for electrochemical processes, the distributions of current density remained largely unaltered.

Iranzo et al (2010)[55]created a CFD model to study a 50 cm^2 fuel cell flow fields. This model used parallel and serpentine flow field bipolar plates and its accuracy was confirmed by comparing it to real-world experimental data. The numerical results obtained from the computer simulations, which were done with two different bipolar plate designs and operating conditions, matched well with the experimental findings. The model was used to analyze various factors such as reactant distribution, heat management, water management, and current density distribution for a specific scenario at different current levels. This simulation model can be further used to better understand the complex processes that occur within fuel cells.

Hashemia, Rowshanzamira and Rezakazemia (2011) [56]compared the performance of PEM fuel cells using CFD simulations on straight and serpentine flow fields. The study showed that the serpentine flow field shows better distribution of current density and temperature. Also, modeling results were compared with the experimental data available in the literature for different values of current densities and results augur well with the experimental data. In high current densities the modeling results differ from experimental results because of assumption of one-phase model which negates the water flooding towards cathode and drying in anode side. Current density is higher in some regions where the electrical current path is little longer. Also, the simulation results revealed that the reactant gases distribution was uniform in the fuel cell.

Aiyejinaand Sastry (2012)[12] in their review on geometry of the flow channels inside a PEMFC, and theireffects on reactant transport, water management, and reactant utilisation efficiency, and consequently the overall performance of a PEMFC system. Flow field optimisation is one strategy for addressing these challenges. This paper examines some recent

work on modelling PEMFCs, investigating their phenomena, and enhancing their performance, particularly through flow field optimisation. This work demonstrates how such modelling can offer helpful data for PEMFC optimisation and offers recommendations for improving the performance of a PEMFC bipolar design based on the literature review. The examined study demonstrates that a serpentine flow field with small channel and rib size outperforms more conventional configurations.

Bachman et.al (2012) [57]In this study, the focus was on parallel flow fields with varying channel lengths (5 mm, 15 mm, 20 mm, and 25 mm). The results showed that longer channel (25 mm) parallel flow fields effectively minimized water buildup and eliminated liquid water slugs. However, the longer flow path also led to a significant pressure drop across the cell, resulting in substantial concentration gradients between the inlet and outlet, as well as considerable pumping losses. The research explores the optimal channel length for both serpentine and parallel flow fields, where the aim is to ensure efficient water content removal without excessive pressure drop. The findings provide valuable insights into achieving a balance between effective water management and minimizing pressure-related challenges in fuel cell designs.

Sierra et.al (2014)[58] compared tubular designs to the usual flow fields, it was discovered that tubular designs provide more consistent distributions of pressure, hydrogen, oxygen concentration, and current density. Among the tubular designs, the straight channel design had the least decrease in pressure along the flow path. This caused more water to gather at the cathode. On the contrary, the serpentine design showed the most even distributions of hydrogen concentration, temperature, and current density across the active area of the cell.

Vazifeshenas, Sedighi and Shakeri (2015)[59] in their new compound flow field design (combination of parallel flow fields at inlet and parallel serpentines) was tested alongside the conventional serpentine and parallel designs using computer simulations in three dimensions. The simulations confirmed that the novel compound flow field design effectively prevented flooding, which is a common problem. Additionally, the performance of the PEMFC was not negatively affected by implementing this new flow field design.

Limjeerajarus and Charoen-Amornkitt (2015)[28] in the similar lines to above research, investigated the performance of various serpentine flow-field configurations in proton exchange membrane fuel cells (PEMFCs) with a 5 cm^2 active area using ANSYS Fluent. They studied 1-, 3-, and 5- parallel serpentine flow fields, as well as 3- and 5- parallel in

series (PIS) flow fields. The results showed that the parallel flow field performed poor, while the PIS flow fields demonstrated better uniformity and water management, although they required slightly higher pressure to force the reactants through the channels. Interestingly 1S flow field provided the best performance and uniformity among all the configurations tested.

Lim et.al (2016)[24]according to this review, flow fields have a significant impact on the functionality and durability of fuel cells. Fuel cells experience a fundamental occurrence called flooding, which lowers their performance and shortens their lifespan. Flooding happens when there is a high current density and a high water generation rate as a result of an electrochemical reaction. In order to reduce the contact surface of the reactant for diffusing into the catalyst layer for the electrochemical reaction, the produced water collects and prevents reactants from flowing into the channel. Therefore, suitable flow field design choices could enhance fuel cell water management. In terms of flow field design, serpentine and integrated flow fields show the highest rates of liquid water removal.

Wang, Yue and Wang (2017)[60] proposed a new design for the cathode flow field in a PEM fuel cell. This design includes a sub-channel that affects the amount of water and the distribution of oxygen within the fuel cell. The sub-channel design helps reduce the amount of pressure lost in the main flow channel. The specific location and rate of flow at which the sub-channel connects to the main channel have a significant impact on the overall performance of the cell. By finding the right combination, it becomes possible to improve both the limiting current density and the maximum power density of the cell.

Singdeo et.al (2017) [61]suggested a compensated serpentine geometry to enhance the distribution. Through simulations, it was observed that the new design exhibits higher uniformity index values compared to the traditional serpentine design. The performance of the fuel cell using the compensated serpentine geometry improved by 27% at an operating voltage of 0.57 V. To validate these findings experimentally, a CDMD (Cell Distribution and Monitoring Device) was developed and tested in the fuel cell. The experimental results closely matched the simulation data, with a small discrepancy of around ±4%.

Alizadeh et.al (2017)[62] in this research, the main goal was to investigate how cascade-type flow fields affect different factors like current density, temperature distribution, and water saturation. The researchers focused on understanding how the width of the channels, the width of the ribs, and the depth of the channels influenced the performance of the PEMFC with reduction serpentine flow field. By analyzing the data, they identified the best

dimensions for these parameters. The results showed that a flow field design with channel width, rib width, and channel depth of 1.2 mm, 0.8 mm, and 0.8 mm, respectively, had the highest performance among all the configurations that were tested.

Mubinet.al (2017)[63] This paper investigates how the performance of PEMFC is influenced by two parameters using a mathematical model: temperature and pressure. The study finds that increasing both temperature and pressure in the system leads to improved performance. However, it is important to note that excessively high input pressure and temperature can cause damage to the membrane of the PEMFC. Therefore, finding the optimal balance is crucial for maximizing performance without jeopardizing the integrity of the membrane.

VenkateswarluVelisala,G. Naga Srinivasulu (2018) [64] This work investigated, computationally and experimentally, the impact of single (1-S), double (2-S), and triple (3-S) serpentine flow field configurations on the performance of PEM fuel cell (PEMFC). First, a thorough 3-D PEMFC model was created. Then, simulations were run using the commercial CFD tool ANSYS FLUENT to look at how 1-S, 2-S, and 3-S flow field design affected PEMFC performance. Important data including pressure distribution, hydrogen and oxygen mass fractions, liquid water activity, current flux density distribution, and membrane water content have also been shown along with the cell performance. The numerical predictions are then validated through an experimental research using a PEMFC with different 1-S, 2-S, and 3-S flow field configurations. 1-S flow channel exhibit better performance as compared to 2S and 3S flow channels.

Abdulla and Patnaikuni(2019) [65] A three-dimensional (3-D) multiphase computational fluid dynamic (CFD) model has been used to undertake a detailed performance evaluation of the enhanced cross-flow split serpentine flow field (ECSSFF) design for PEMFC. A single serpentine flow field and modified the same into three segments of shorter flow channels, which enhanced mass transport properties even when compared to triple serpentine design.For the cathode portion of the cell, ECSSFF design is employed, and for the anode portion, parallel flow field. By maintaining the same anode side flow field design and all other parameters, the performance of PEMFC with ECSSFF has been compared to the performance of triple serpentine flow design on the cathode side. Their polarization curves are used to assess performance. Variable operating conditions, such as cell temperature and inlet humidity on the air and fuel sides, are used to conduct a parametric research. Under all

these conditions, the ECSSFF has demonstrated superior performance over the triple serpentine design.

Vijayakrishnan et.al (2020) [66] primarily made attempt to study common issue of water accumulation at the cathode in fuel cells. To overcome this challenge, the researchers propose and assess a novel sinuous flow field design using both computer simulations and practical experiments. The study compares the dwelling time and its impact on performance between serpentine and sinuous flow designs. Among various configurations, the single serpentine at the anode end and sinuous flow field on the cathode side demonstrated superior performance.Additionally, the research investigates the size effect on power density. Scaling the active area from 25 to 100 mm^2 resulted in a 24.44% lower power density due to increased overpotentials.

Ozdemir and Taymaz(2021) [27]numerical analysis to investigated the influence of steady-state cell performance in three different flow field configurations: U-type, Z-type, and serpentine. The study employed the CFD approach and the ANSYS FLUENT PEMFC module for simulations. The results demonstrate that the serpentine flow field configuration outperforms the other designs significantly. Specifically, the serpentine flow field yields a much higher power density, almost twice as much as the U-type and Z-type flow fields. These findings highlight the superiority of the serpentine flow field arrangement for enhancing the power output of PEMFCs.

Gundlapalli and Jayanti (2021)[67]modified serpentine flow field toflip-flop serpentine flow field. The performance of this modified design was compared with three other configurations: three-parallel split, enhanced cross-flow, and the traditional serpentine flow field. The flip-flop serpentine flow field demonstrates improvements in reducing pressure drop and enhancing cross-flow in the bend regions. This feature is especially important for effectively removing liquid water in hydrogen-fed fuel cells. Additionally, the modified design reduces the travel distance, leading to better water evacuation, primarily due to the reduced pressure drop. These advancements highlight the potential of the flip-flop serpentine flow field as a promising solution to address the pressure drop challenges in fuel cell applications.

Ponnaiyan et.al (2022)[68] research presents a numerical analysis that examined the impact of the steady-state cell performance on the U-type, Z-type, and serpentine flow field configurations using the CFD approach and the ANSYS FLUENT PEMFC module. The

primary objective of this study is to improve the design of the PEMFC in order to get greater performance. The findings show that when compared to the other designs, the PEMFC with serpentine flow field arrangement produces a much greater power density due to enhanced reactant distribution and temperature uniformity.

Hamrang et.al (2022)[69] examined, how the performance of polymer electrolyte membrane fuel cells can be enhanced by making changes to the outlet/inlet configuration of the parallel-serpentine flow field. The results show a remarkable improvement of 26.7% in regions with a high concentration of oxygen when comparing these two configurations. This enhancement is attributed to an increased supply of oxygen to the catalyst layer and better removal of water on the cathode side. As a result, a significant performance increase of 38.5% was achieved at a current density of 1.5 A/cm^2, in comparison to the parallel-serpentine configuration.

2.1. Literature summary:

Serpentine flow fields are recognized as highly effective in enhancing heat and mass transfer in various applications, including PEMFCs. However, their main limitation is the significant pressure drop they induce, resulting in reduced system efficiency. To address this issue, the concept of dual serpentine channels was introduced, involving two parallel serpentine flow paths instead of a single channel. This design modification aims to reduce pressure drop by distributing the flow between two channels. While dual serpentine channels can mitigate the pressure drop problem, they may lead to new challenges, such as uneven temperature and membrane water content distributions. Optimizing the design and exploring alternative approaches are essential to overcome these challenges and improve PEMFC performance.

2.2. Objectives of the thesis:

The main aim of the research work is to focus on design and analyze variable length serpentine flow fields for better fuel reactions and reduced pressure drop in PEM Fuel Cells. To accomplish this, two kinds of variable length flow fields were studied. A L-serpentine flow field which adopts variable length concept to single serpentine and the second was variable length to split serpentine. L-serpentine can be directly compared with single serpentine. However, split serpentine variable length requires comparison with dual serpentine. Further split serpentine was studied with increases active area and best performed among them was provided with variable lengths. The objectives for the study were given below.

- Objective 1: A Comparative Investigation of L-Serpentine and Single Serpentine Flow Fields Efficiency in Proton Exchange Membrane Fuel Cells Using Computational Fluid Dynamics.
- Objective 2: Comparative Computational Fluid Dynamic analysis between Split and Dual Serpentine Flow Field for Proton Exchange Membrane Fuel Cells.
- Objective 3: Assessment of Split Serpentine Flow Fields for Increased Active Area: Exploring Horizontal and Vertical Configurations.
- Objective 4: Design and Performance Investigation of Variable Length Split Serpentine Flow Fields.

Chapter 3
METHODOLOGY

Computational Fluid Dynamic (CFD) analysis and experimental studies were conducted on different flow fields (Lung, Leaf, Zigzag, Sinusoidal, etc., [70][26][71][72]) to evaluate their characteristics. CFD results showed close relation with experimental results. Furthermore, numerical model of fuel cell sets the base frame-work to scrutinize the electrochemical performance by varying the flow field design and its operating parameters effecting in the reduction of time and cost for experimentation [10][21].

In this chapter governing equations, methods, material properties, boundary conditions and assumptions used for the CFD analysis were discussed in the followings sections.

3.1.Governing equations

The entire study utilized Ansys Fluent, a commercial software, which considered various governing equations, including the Conservation of Mass equation, Navier-Stokes Momentum equation, Energy equation, Species equation, Electrochemical equation, and Current Conservation equation. For solving the electrochemistry, Ansys FLUENT employed two potential equations: one for electron transfer (equation (1)) applicable in catalyst and current collector regions, and the other for proton transfer (equation (2)) applicable within the membrane region.

$$\nabla.(\boldsymbol{\sigma_{sol}}\nabla\emptyset_{\boldsymbol{sol}}) = \boldsymbol{R_{sol}} \qquad \text{.....(1)}$$

$$\nabla.(\boldsymbol{\sigma_{mem}}\nabla\emptyset_{\boldsymbol{mem}}) = \boldsymbol{R_{mem}} \qquad \text{.....(2)}$$

The source terms R_{sol} and R_{mem} are calculated by using Buttler-Volmer equations (3) & (4). Whereas R_a and R_c are exchange current densities calculated at anode and cathode side for both solid and membrane phases.

$$R_a = I_a^{ref}\left(\frac{[H_2]}{[H_2]_{ref}}\right)^{\gamma a}\left[exp\left(\frac{\alpha_a^a F\,\eta_a}{RT}\right) - exp\left(-\frac{\alpha_c^a F\,\eta_a}{RT}\right)\right] \qquad \text{.....(3)}$$

$$R_c = I_c^{ref}\left(\frac{[O_2]}{[O_2]_{ref}}\right)^{\gamma c}\left[-exp\left(\frac{\alpha_a^c F\,\eta_c}{RT}\right) + exp\left(-\frac{\alpha_c^c F\,\eta_c}{RT}\right)\right] \qquad \text{.....(4)}$$

Membrane conductivity (σ_{mem}) is found by equation (5), this equation again depends on the operating temperature and membrane water content (λ) (equation (6)).

$$\sigma_{mem} = (0.00514\lambda - 0.00326)exp\left(1268\left(\frac{1}{303} - \frac{1}{T}\right)\right) \quad \text{.....(5)}$$

$$\lambda = 0.043 + 17.81a - 39.84\,a^2 + 36\,a^3, \qquad (a < 1)$$
$$\lambda = 14 + 1.4(a - 1), \qquad (a > 1) \quad \text{.....(6)}$$

Water activity (a) calculated by (7),

$$a = \frac{X_w p}{p^{sat}} + 2s \quad \text{.....(7)}$$

Potential difference at anode (η_a) and cathode (η_c) found by (8) and (9) respectively.

$$\eta_a = \emptyset_{sol} - \emptyset_{mem} \quad \text{.....(8)}$$

$$\eta_c = \emptyset_{sol} - \emptyset_{mem} - V_o \quad \text{.....(9)}$$

Open Circuit Potential(V_o) was considered as function of temperature (equation (10)).

$$V_o = 0.0025T + 0.2329 \quad \text{.....(10)}$$

3.1.1. Conservation of mass

$$\boldsymbol{\nabla.(\rho \varepsilon V) = S_m} \quad \text{.....(11)}$$

Conversation of mass was determined by equation (11). The sources terms (S_m) changes according to location and were estimated with equation (12):

$$S_m = 0, for\ Flow\ fields, GDLs \qquad \left.\begin{aligned} S_{ma} &= -\frac{MW_{H_2}}{2F} i_a \\ S_{mc} &= \frac{MW_{H_2O}}{2F} i_c - \frac{MW_{O_2}}{4F} i_c \end{aligned}\right\} For\ CLs \quad \text{.....(12)}$$

3.1.2 Conservation of Momentum

$$\boldsymbol{\nabla.(\rho \varepsilon V V) = -\nabla P + \nabla \tau + S_p} \quad \text{.....(13)}$$

Conservation of momentum in the whole domain modeled using equation (13). Shear stress (equation (14)) different in various regions due to the effect of porosity, porosity brings additional terms in porous regions. Source terms in different regions are calculated using equation (15).

$$\nabla\tau = \begin{cases} \mu\nabla^2 V;\ for\ Flow\ fields \\ \mu\nabla^2 V + 2.25\dfrac{(1-\varepsilon)^2}{\varepsilon^2}\mu\nabla^2 V - \dfrac{\varepsilon\mu}{k_p}V\ ;\ for\ porus\ media \end{cases} \quad \text{……..(14)}$$

$$\mathrm{S_p} = 0\ for\ flow\ fields; \mathrm{S_p}\ = -\left(\frac{\mu}{\mathrm{k_p}}\right)\mathrm{V}\ for\ porous\ media \quad \text{…….(15)}$$

3.1.3. Conservation of Energy

$$\boldsymbol{\nabla.\left(V(\rho\varepsilon c_p T)\right) = \nabla.(k_{eff}\nabla T) + S_e} \quad \text{…….(16)}$$

Conservation of energy is obtained by equation (16). The effective conductivity (k_{eff}) is calculated by considering the fluid conductivity in flow fields and the solid conductivity, as shown in equation (17).

$$k_{eff} \begin{cases} k_f\ for\ FFs \\ -2k_s + \left(\dfrac{\varepsilon}{2k_s + k_f} + \dfrac{1-\varepsilon}{3k_s}\right)^{-1} for\ porus\ media \end{cases} \quad \text{……(17)}$$

Energy source terms (equation (18)) obtained by combining heats generated through ohmic losses, phase change from liquid to vapour, heat of reaction and current conduction heat.

$$S_e = i^2 R_{ohm} + h_{reaction} + \eta R_{a,c} + h_{phase} \quad \text{…….(18)}$$

3.1.4. Species transport

Species transport can be considered as given in equation (19). Diffusivity of the species calculated with equation (20), since this depends on operating and temperature and pressure.

$$\boldsymbol{\nabla.(\rho\varepsilon V y_i) = -\nabla.\left(\rho(D_i \nabla.y_i)\right) + S_s} \quad \text{…….(19)}$$

$$D_i = \varepsilon^{1.5} D_i^o \left(\frac{P_0}{P}\right)\left(\frac{T}{T_0}\right)^{3/2} \quad \text{…….(20)}$$

Sources terms for species transport are estimated by equation (21).

$$S_{H_2} = -\frac{MW_{H_2}}{2F}R_a; \qquad S_{O_2} = -\frac{MW_{O_2}}{2F}R_c; \qquad S_{H_2O} = -\frac{MW_{H_2O}}{2F}R_c \quad \text{…….(21)}$$

3.2. Material properties

The materials properties considered for the CFD study were given in table 3.1. Current collector material considered as graphite and carbon cloth or carbon fiber for gas diffusion layers. Catalyst used in the study was dispersed platinum on carbon cloth.

Table 3.1 Material properties used in the numerical study

Properties	Catalyst and GDL	Current Collector	Membrane	Tab	Units	Ref.
Density	2719	2719	1980	2719	kg/m^3	
Specific heat	871	871	2000	871	$J/(kg \times K)$	
Thermal conductivity	10	100	2	202.4	$W/(m \times K)$	[73]
Electrical conductivity	5000	1×10^6	10^{-16}	3.541×10^7	$1/(\Omega \times m)$	
Permeability	10^{-12}	-	-	-	m^3	

3.3.Boundary conditions:

The study utilized an ANSYS-Fluent add-on module specifically designed for fuel cell analysis. The flow in the system was assumed to be steady, isothermal, isotropic, and incompressible, with single-phase models taken into account. To simplify the analysis, the current model assumed the fluid to be incompressible and laminar due to the very low Reynolds number of the flow. The current terminal walls were maintained at a constant temperature to achieve isothermal operation. For simplicity, all materials were assumed to be isentropic.

The fuel cell structure included Gas Diffusion Layers, Catalyst Layers, and a Membrane, with the membrane acting as an impermeable barrier to electrons and fully saturated. The velocity at the anode and cathode inlet was calculated based on the equations presented in the study by Nguyen et al. (equation (22) and (23)) (Nguyen, Berning, and Djilali, 2004).

Four boundary conditions were imposed for the simulations, namely, the inlet mass flow rates and the voltage at the anode and cathode. The inlet mass flow rate was determined by evaluating the velocity of the inlet fluid and its density. The applied voltage ranged from 0.4 to 0.9 V, specifically at the cathode current collector terminal. Calculation of mass flow rates using python code is given in Appendix-I.

$$\boldsymbol{u_{a,in} = \zeta_a \frac{I_{ref}}{2F} \frac{RT}{P} \frac{A_{active}}{A_{ff}} \frac{1}{X_{H_2}}} \quad \text{……(22)}$$

$$\boldsymbol{u_{c,in} = \zeta_c \frac{I_{ref}}{4F} \frac{RT}{P} \frac{A_{active}}{A_{ff}} \frac{1}{X_{O_2}}} \quad \text{……(23)}$$

The fluids used were considered as ideal gas which obeys ideal gas laws. This assumption helps to estimate the mole fractions at operating conditions.

Table 3.2. Parameters & boundary conditions for the model

Parameter		**Anode**		**Cathode**	**Ref.**
Stoichiometry	ζ_a	2	ζ_c	2	
Reference current density	I_{ref}	10,000 A/m^2	I_{ref}	10,000 A/m^2	
Humidifying Temperature	T	60, 70, 80^{0}C	T	60, 70, 80 ^{0}C	
Pressure	P	3 atms	P	3 atms	
Relative humidity	RH	100%	RH	100%	
Voltage		0		0.4 – 0.9 V	[45]
Concentration exponents	γ_a	0.5	γ_c	1	[74]
Exchange coefficients	α_a^a, α_c^a	0.5	α_a^c, α_c^c	2	
Area of cross section of flow field	A_{ff}	1x1 mm^2	A_{ff}	1x1 mm^2	
Hydrogen mole fraction	X_{H_2}	0.897	-	-	
Oxygen mole fraction	-	-	X_{O_2}	0.1885	
Gas Diffusion Layer Porosity		0.7		0.7	[36]
Catalyst Layer Porosity		0.38		0.38	

All the equations are solved individually by the solver, and they are combined using SIMPLE solver. Subsequently, the relevant equations were discretized using the second-order upwind scheme for better accuracy. Solution controls were applied for momentum (0.3) and pressure (0.7). BiConjugate Gradient STABilization method (BCGSTAB) was employed for anode and cathode potential stabilization methods along with F-cycle method to enhance the convergence speed. Advanced solution controls for potentials were set to 0.0001. All residuals were set to 10^{-8}. Additionally, a convergence criterion 10^{-6} was used for output current density. Parameters used in the numerical study were given in table 3.2. Parameters were followed for all configurations. Simulation strategy was considered from Abdulla et.al [65].

3.4.Grid dependency test

The fuel cell model's meshing is depicted in figure 3.1 and was performed using Ansys-workbench meshing. For grid independence study 0.1 million to 2.5 million elements were considered and shown in table 3.3. The deviation found was very minimal at 0.6 million elements 0.73%and at 2.5 million elements 0.87%.Hence, 0.6 million elements were taken for the simulation.

This meshing was utilized for correcting studies, figure 3.1 (a) L-Serpentine flow field mesh was used for chapter 4 analysis. Similarly, figure 3.1(b) mesh was used for chapters 5,6 and 7. The front view of mesh show fine divisions of flow channels and also membrane electrode assembly (GDL, CL and Membrane). This fine divisions ensures proper gradients propagation of gradients especially in flow pertaining regions. Structured mesh was obtained by using split by surfaces of the bodies. Structured mesh helps to obtain consistent and precise values. In case of using unstructured mesh, a change in output was observed with simulation to simulation. Hence, structured mesh gave accurate results for this study. The values and contours reproduced in this thesis are obtained by repeating the simulations at least for three times and average values were considered for study. Furthermore, due to consistency of the simulation output all simulations gave almost accurate results.

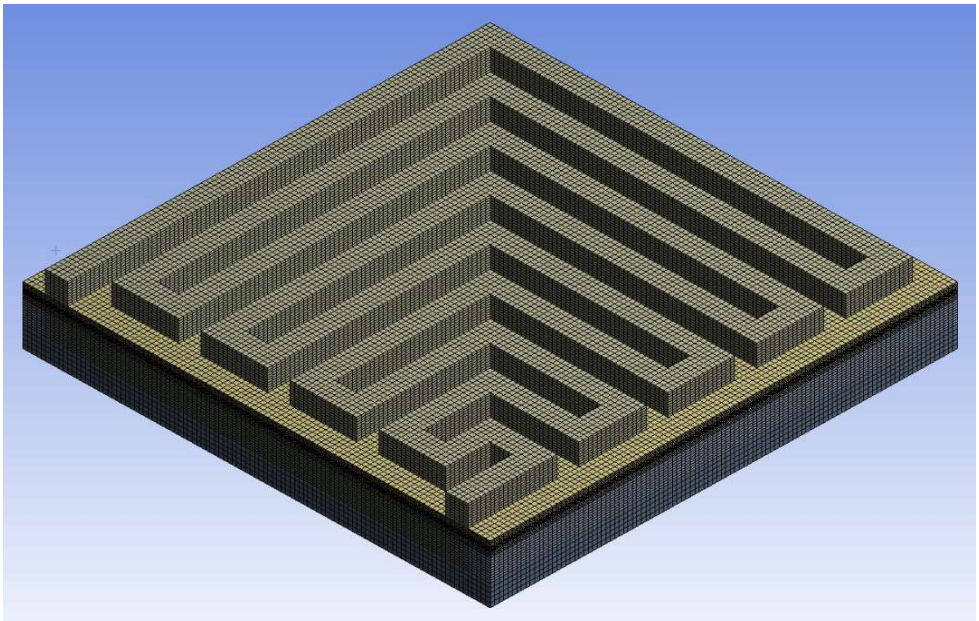

a) Isometric view meshing of L-serpentine flow field

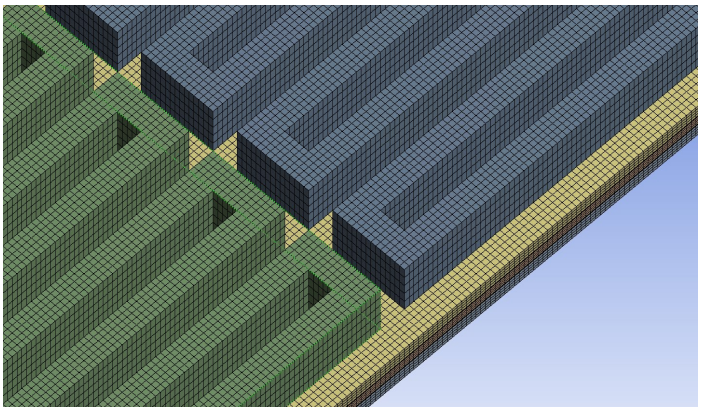

b) Isometric view of meshing for Split serpentine flow field

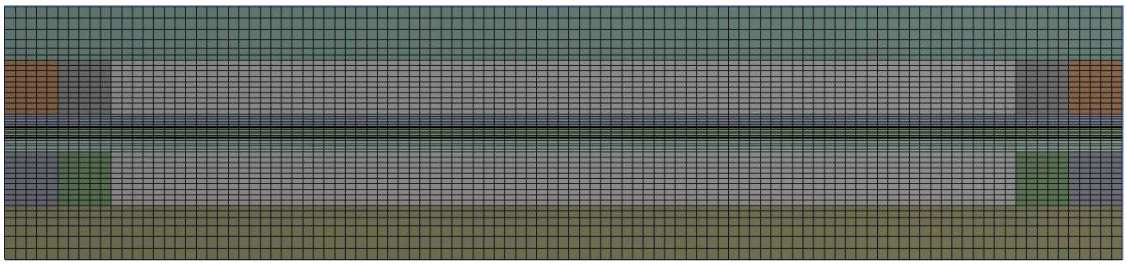

c) Front view of fuel cell meshing

Figure 3.1 Meshing a) and b) isometric view LS and SS, and c) front view fuel cell meshing

Table 3.3 Grid independence study

Elements	Current density (A/cm^2)	Deviation	Percentage Deviation
97,020	1.0062		
388,080	1.0309	0.0247	2.46
606,375	1.0385	0.0076	0.73
2,425,500	1.0475	0.009	0.87

3.5.Validation

The simulation was validated with the experimental study of Lin Wang et.al.Among the various parameters studied in this study. A temperature of 70^0C and 3 bar operating pressure considered with 100% humidification [45]. A single serpentine flow field with an active area 72x72 mm^2 considered. Keeping the other dimensions mentioned in table 3.4.

Table 3.4 Dimensions for the model

	Dimension (mm)	Ref.		Dimension (mm)	Ref.
Membrane area	72x72	[27]	Channel width	1	
Electrolyte thickness	0.178		Channel height	1	
Gas Diffusion Layer (GDL) thickness	0.25	[58]	Current collector (CC) thickness	2	[58]
Catalyst Layer (CL) thickness	0.02		Rid width	1	

The variation of voltage with current density as observed in figure 3.2, a minimum deviation was observed, the reasons being the variation in water formation is higher at higher current densities, which is more precise in experiments due to multiphase in nature. With simulations other approximations like square cross section, sharp edges flow fields, and adiabatic conditions at the current collectors affected the output current density.[75]. The validation was common to all the flow field layouts.

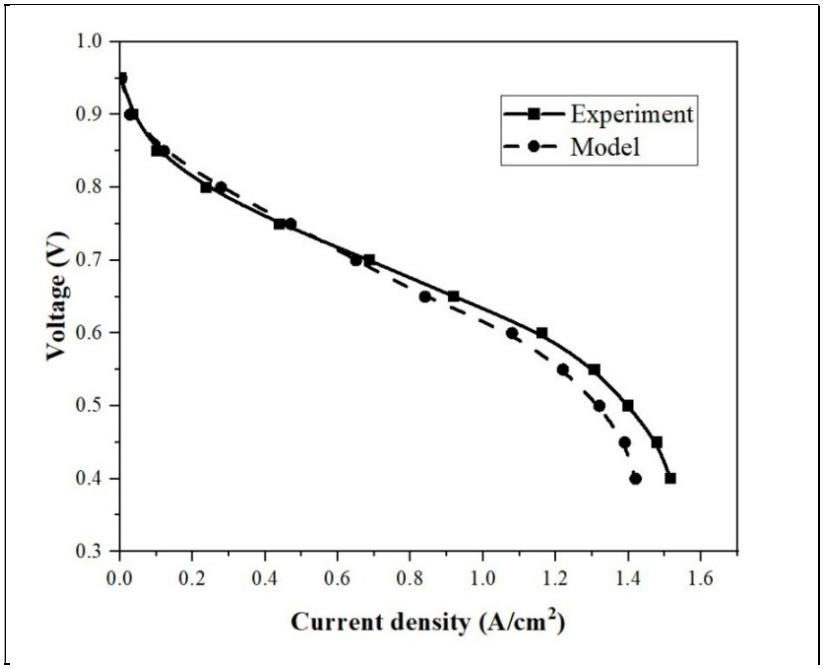

Figure 3.2 Validation of model with Ling Wang Experiments

The simulation's grid independence study and validation were consistent across all layouts. The results and discussion of the flow field study were divided into four chapters, each focusing on a specific design. Detailed information for each design was provided within its respective chapter 4,5,6 and 7.

RESULTS AND DISCUSSIONS

Chapter 4

OBJECTIVE 1

A Comparative Investigation of L-Serpentine and Single Serpentine Flow Fields Efficiency in Proton Exchange Membrane Fuel Cells Using Computational Fluid Dynamics

4.1.Model Development

For the current analysis, a small active area of 21mm x 21mm was chosen, as shown in figure 4.1 with layouts of Single Serpentine Flow Field (SSFF) on the left and L-Serpentine Flow Field (LSFF) on the right. The reasons for choosing small active are: i) large area minimizes the focus on the flow field; ii) a small active area/domain reduces the computational load. Furthermore, sharp edges at the turnings were considered to reduce computational load, though round or curved edges performs better. However, similarity for edges been considered in both designs [76]. All the inlet parameters were calculated as required for the active area. The main idea of the current work is to enhance the contact time of the reactants against the products, which doesn't require much time to evacuate. In view of the above, a LSFF was considered as it also avoids flooding in the channel.

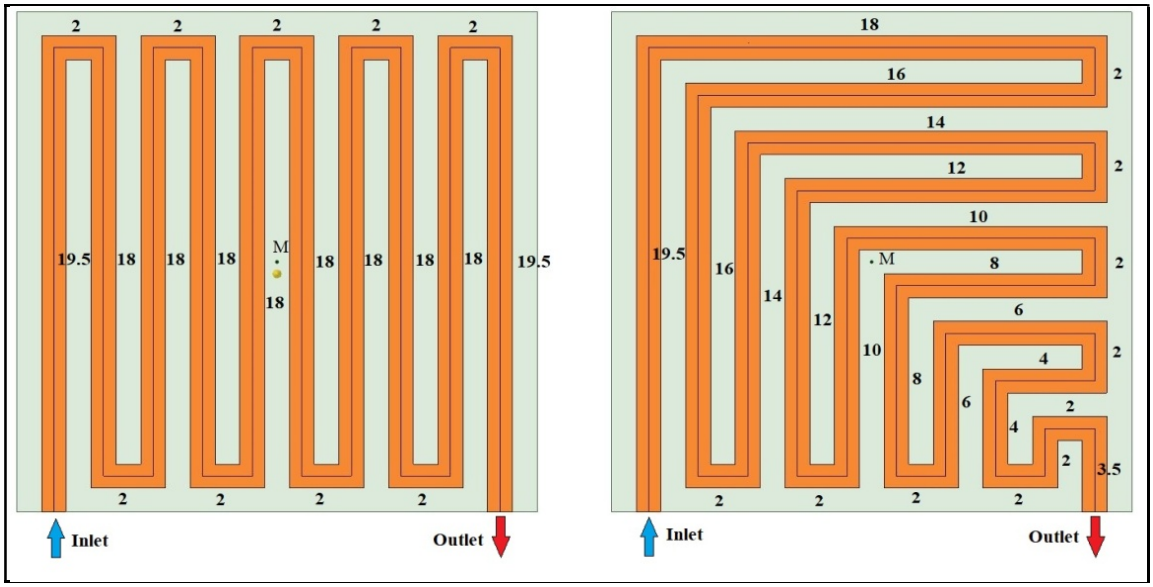

Figure 4.1 SSFF (Left) LSFF (Right)

Figure 4.1 depicted with average lengths in mm, the centre line drawn in the channels to measures total length. Both flow fields measured 201 mm and length is indicated at top,

bottom and sides respectively. Other dimensions were kept constant and they are given in table 4.1. In LSFF, from the midpoint to outlet, the length has been reduced by 40% approximately (where M indicates Midpoint) compared to SSFF.

Inlet and outlets are indicated with arrows as shown in figure 4.1, in all the subsequent sections same notation has been followed for both anode and cathode flow fields.

Table 4.1 Dimensions for the model

	Dimension (mm)	**Ref.**		**Dimension (mm)**	**Ref.**
Membrane area	21x21	[27][74]	Channel width	1	[58]
Electrolyte thickness	0.178		Channel height	1	
Gas Diffusion Layer (GDL) thickness	0.25	[58][74]	Current collector (CC) thickness	2	
Catalyst Layer (CL) thickness	0.02		Rid width	1	

4.2.**V-I & P-I Characteristics**:

In figures 4.2& 4.3, it is evident that as the temperature increases, the current density and power density also increase. Both the LSFF and SSFF flow fields show a similar trend, with the current density initially being minimum for lower voltages and gradually increasing as the voltage level drops. However, at higher temperatures, the LS80 exhibits a higher current density compared to the SS80. Similarly, the power density follows the same trend, with the LSFF model outperforming the SSFF model at higher temperatures within the same voltage range. At higher voltages, the variation in current density and power density becomes insignificant.

Numerical analysis was conducted on the considered models, spanning a temperature range of 60 - 80^0C, with 3 atm pressure as part of the study. The temperature range aimed to assess the effectiveness of the modified design. It is worth mentioning that the performance was less satisfactory at 60^0C due to sluggish reaction kinetics at lower temperatures. As the temperature increased beyond that point, the performance improved.

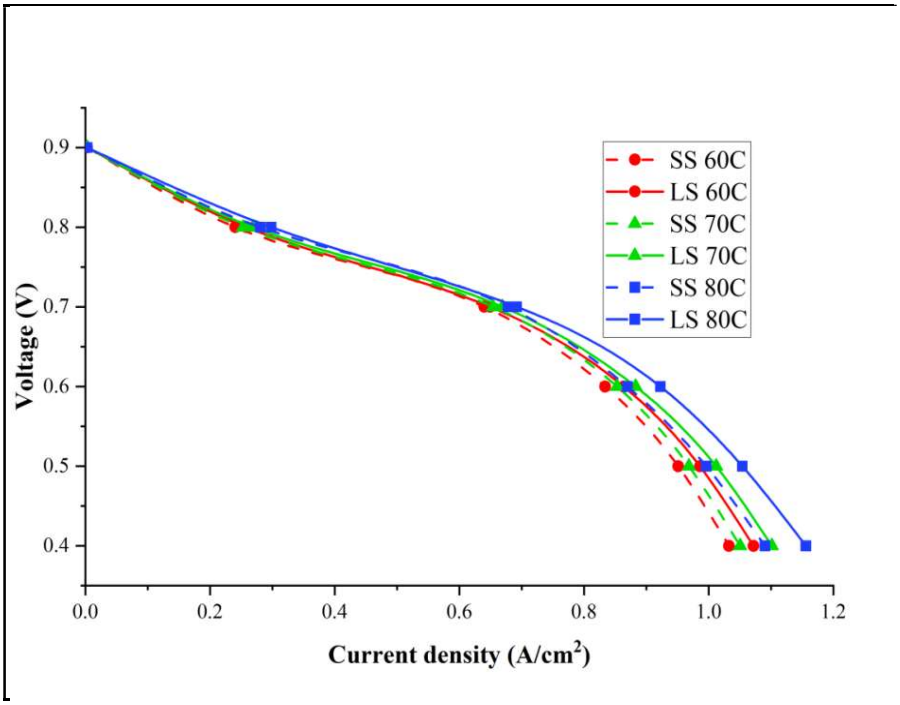

Figure 4.2 Voltage vs Current density of SSFC and LSFC

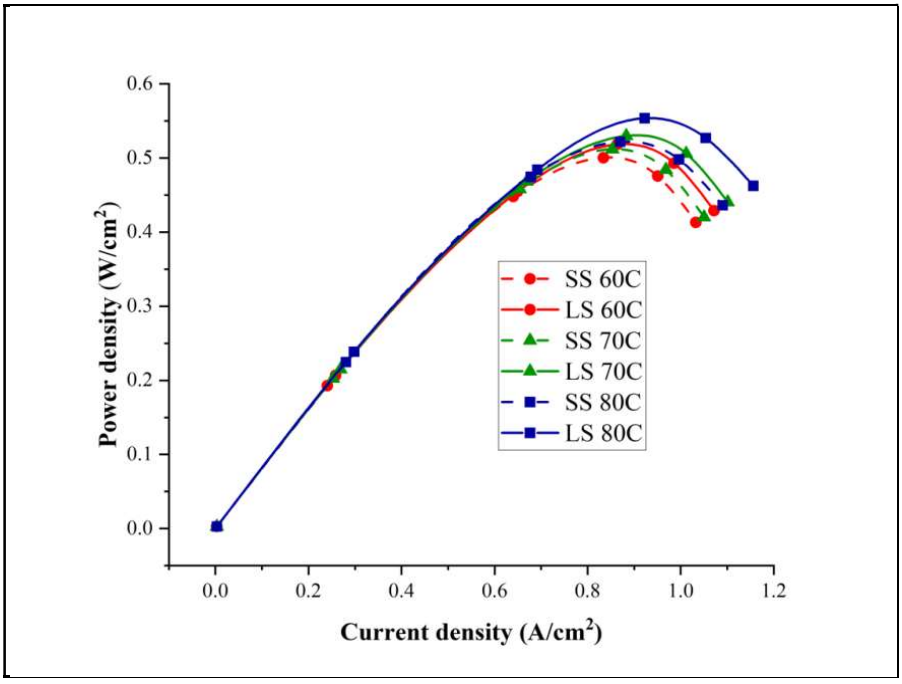

Figure 4.3 Power density vs Current density of SSFC and LSFC

These include potential membrane degradation, increased water loss through evaporation, enhanced electrode corrosion (which is directly proportional to temperature), and consequent increase in ohmic losses. Although performance generally improves with temperature, operating at high temperatures can negatively affect membrane conductivity [11][77]. To strike a balance, the optimum temperature for further analysis was determined to 70^0C. The

highest power and current densities were observed at 80^0C within this range. However, operating above 80^0C was not recommended due to several factors. The values of maximum power densities are observed at 0.6 V at different temperatures from the graphs shown in figure 4.3 The following characteristics were chosen for obvious reasons: i) Thermal (Temperature contours) ii) Flow (Pressure, Streamline contours) iii) species (H_2O, O_2 species contours) iv) Electric (V-I & P-I characteristics). All the contours in the subsequent sections are drawn at 70^0C and 0.6 V.

4.3.Thermal characteristics:

The temperature contours shown in figure 4.4 were plotted at the cathode GDL and CL interface. Temperature rise is more considerable on the cathode side than anode side [46]. The temperature rise in new design, i.e., LSFF, is only 2^0C, but in traditional SSFF rise was 14^0C and subsequently the rise in SSFF was mainly confined to the initial active area. In contrast, LSFF design displays a mostly uniform temperature rise.

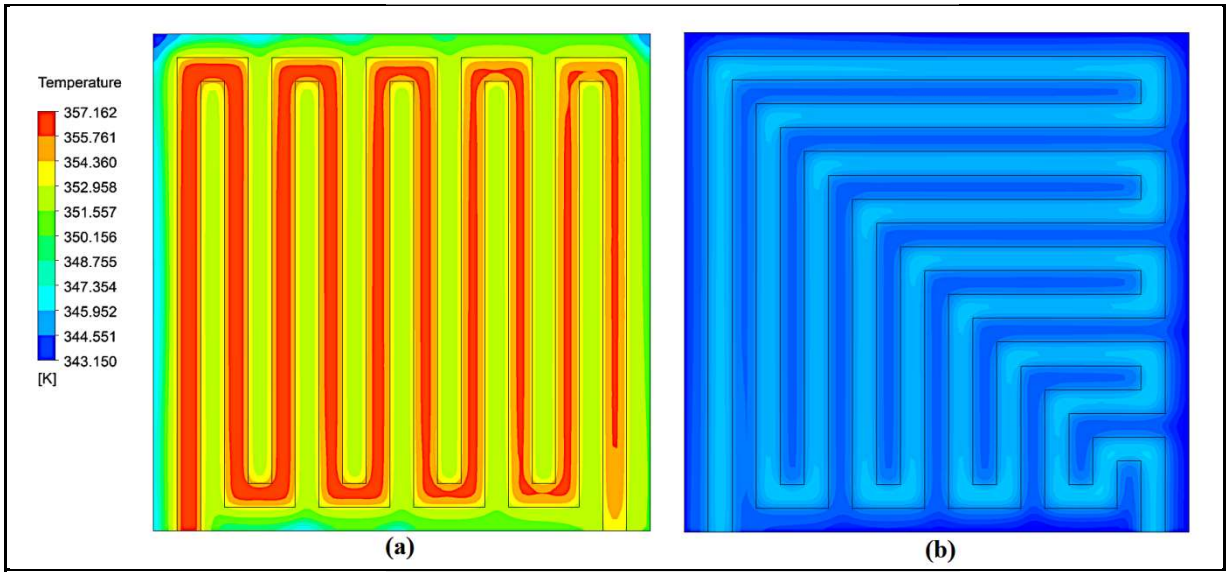

Figure 4.4 Temperature contours for SSFF and LSFF

From the same figure 4.4 it can be inferred that the sudden U-bend turn in SSFF gives rise to sudden drop in velocity of the reactants, thereby increased resident time at the U-bends. Hence temperature rise observed in the initial phase. Whereas in LSFC, due to the adoption on L-shape bends along with U-bends, it reduces the sudden velocity drop at L-bends compared to U-bends. Though the numbers of U-bends are same in both the designs, LSFC allows the species to spread throughout due to L-bends.

Furthermore, in SSFF, the temperature rise decreased in the later phase. This is due to the formation of water or accumulation of water at the end phase (which can be observed in H_2O mass fraction and MWC sections). The water formed absorbs the thermal energy thus reflected in the reduced temperature. However, in case of LSFF, the time available for products in flow channel was reduced. Furthermore, increasing in temperature decreases the condensation and decreases the moisture content [78], this has dried up the flow field area in SSFF which can be noticed from figure 4.8. Hence, LSFF design solves thermal management problem in the flow field. Moreover, constant temperature reduces thermal stresses in current collectors [79][80] [81].

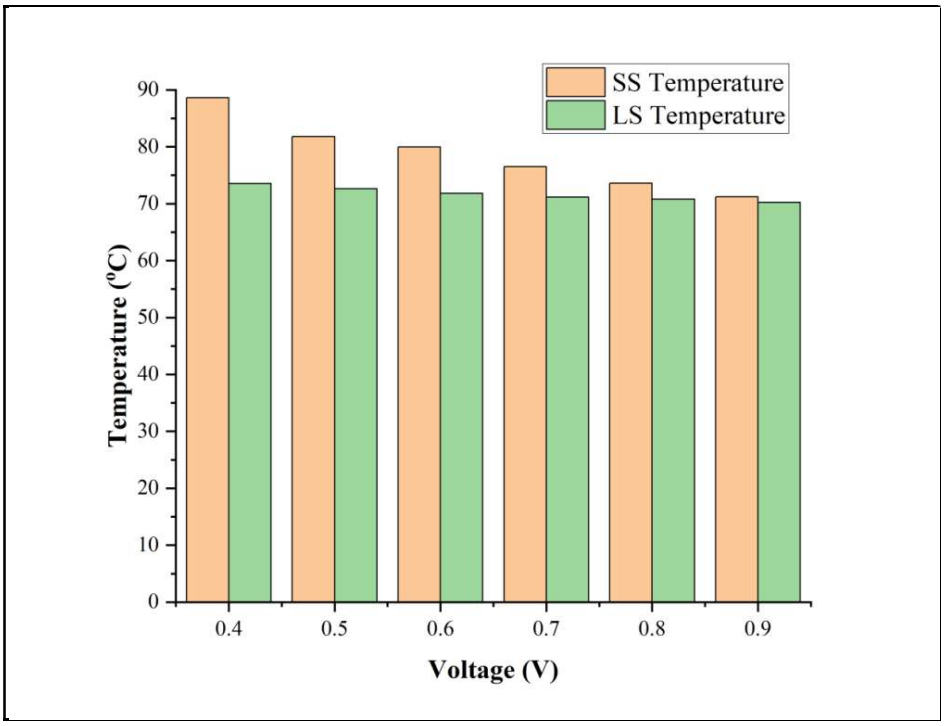

Figure 4.5 Maximum temperature attained at each voltage

Temperature rise at each voltage is been plotted in the figure 4.5 bar chart. At higher voltages the rise in temperature is almost similar in the both designs. At lower voltages, the rise in temperature is significant which corresponding to higher current density production, thus higher reactions happening in the cell produces higher temperature. Interestingly, the higher temperature of an LSFC is nearly identical for all voltage processes, making it an excellent design by eliminating exterior cooling without fluctuating heat burden. Notably, the temperature increase at each voltage in SSFF is greater than in LSFF. As previously stated, similar causes for higher temperatures can be extrapolated.

4.4.Pressure drop characteristics

The volume rendering method in Ansys post processing is used to calculate pressure drop in cathode channels.

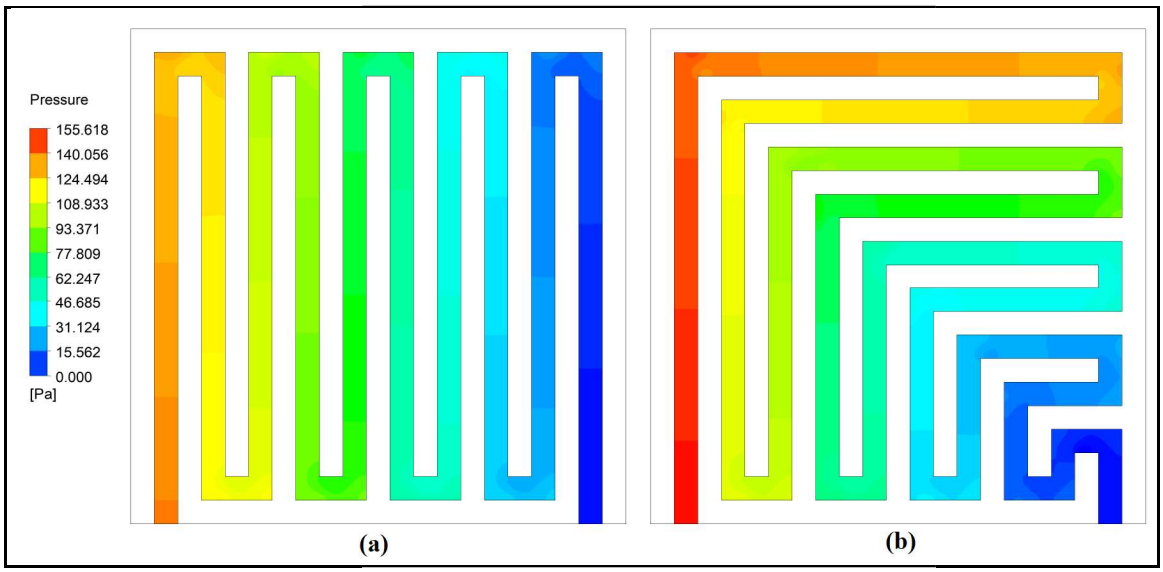

Figure 4.6 Pressure drop in Cathode channels of SSFF and LSFF

It is apparent from figure 4.6 that the pressure drop in the LSFF was higher as compared to SSFF. However, the percentage of pressure drops in the flow fields with respect to inlet pressure of 3 atm was 0.0464% and 0.051% respectively. This corresponds to 14 Pa higher inlet pressure requirements for LSFF.

The majority of new designs have a significant pressure drop, which is undesirable since it causes parasitic power losses. However, pressure drop is responsible for improved resident time of reactants in the flow field [55]. As a result, the temperature at the corners and U-bends rose sharply which can be observed in the preceding section (Temperature).

4.5.Streamline contours

The Streamline contours shown in figure 4.7 are plotted for cathode channels. The primary objective of these contours was to evaluate the occurrence of eddies at the sharp edges. After analyzing the contours, it becomes clear that the influence of secondary flows (indicated in Figure 4.7 as circles) on sharp edges is insignificant, resulting in a decreased turbulence effect. Initially, there were small secondary flows observed at the corners in the initial turns due to high velocity, but later these flows diminished. The decision to incorporate sharp edges was made in order to reduce the computational load. If curved edges had been

considered instead, small secondary flows would have been eliminated. The velocity distribution in the both channels seems uniform; the uniform velocity distribution of the reactants at the flow channel avoids parasitic current may be occurring due to potential difference [79].

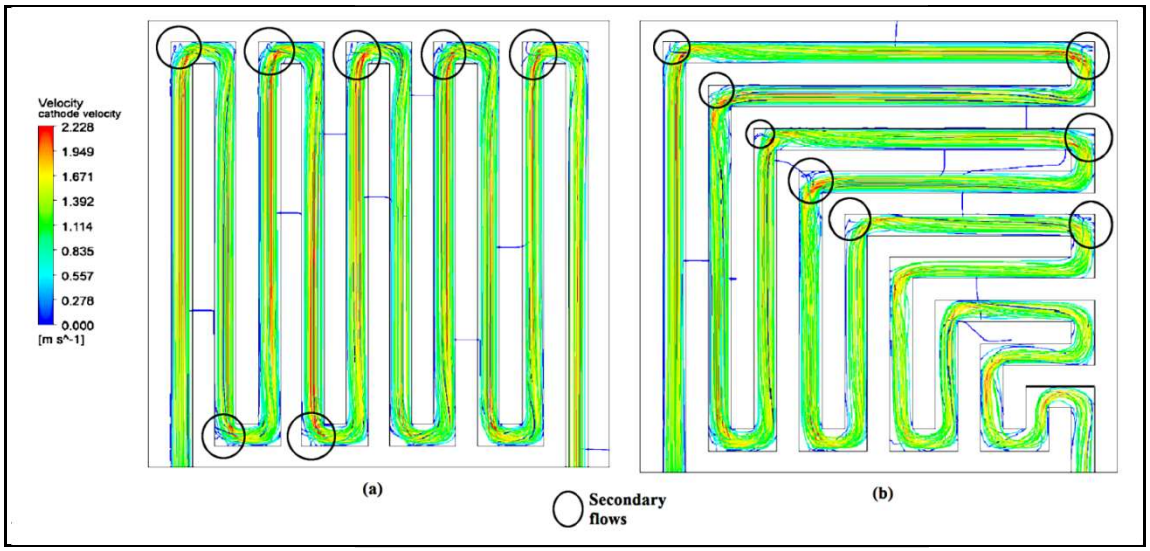

Figure 4.7 Cathode channel Streamline contours

4.6.Membrane water content characteristics:

The outlines shown in figure 4.8 were drawn at the membrane and CL on cathode side interfaces. Since, product water originates from the reactions at cathode end. The other reasons for water in the membrane are electro-osmotic drag and reverse diffusion [44]. The change in membrane water concentration (MWC) of SSFF is minimal, hovering around 14.Whereas, for LSFF it increased from 14 to 15.45 (with in the limits of range 14 to 22). Notably, if MWC > 14, then the membrane is fully saturated with water, which allows both water molecules and H_3O+ ions to move freely and easily through the membrane. This is the most desirable regime for PEMFCs, as it maximizes the proton conductivity and enhances the overall performance of the fuel cell [11]

Distribution of MWC in LSFF is more uniform than SSFF. In SSFF, due to higher temperatures in the initial phase has dried up the membrane. From figure 4.8 in SSFC, water is initially driven and accumulates towards the end due to the pressure difference, which is higher in the initial stages but reduces later on..

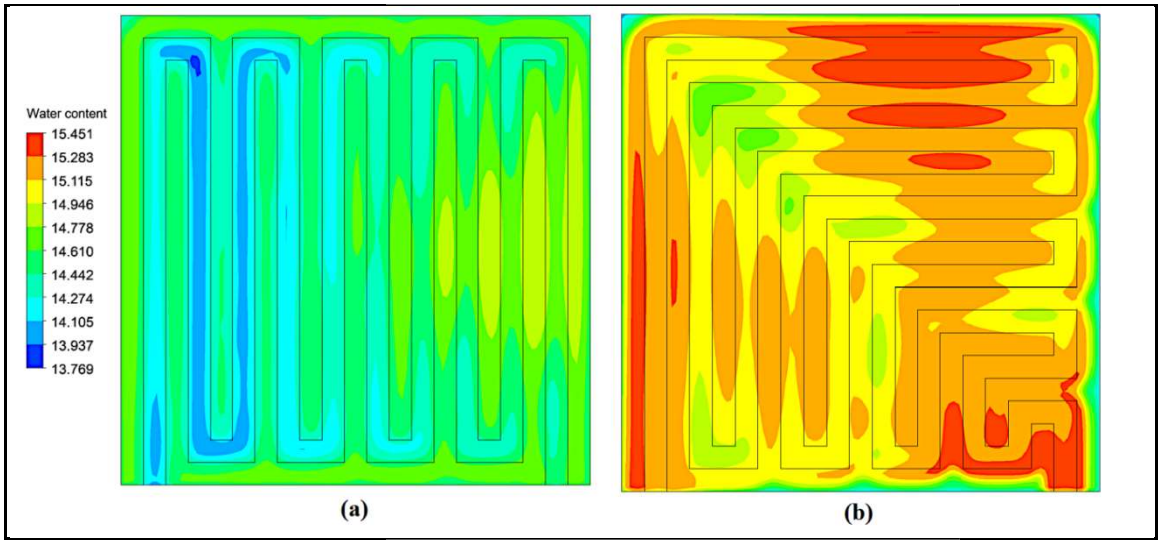

Figure 4.8 Membrane water content at Cathode side GDL and CL interface

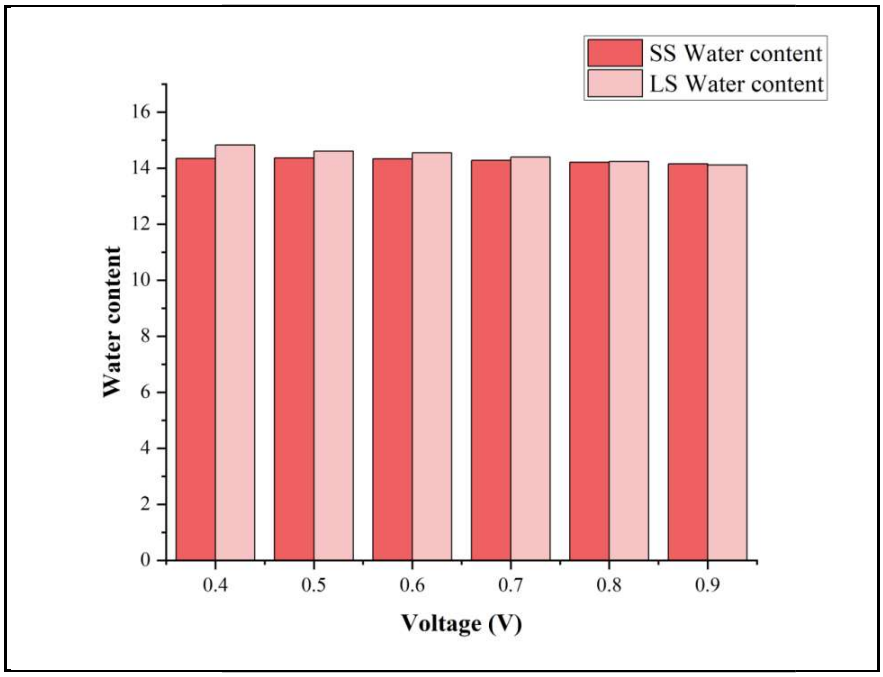

Figure 4.9 Average membrane water content vs Voltage

This pressure difference drives the water content. On the other hand, LSFC experiences a higher pressure drop in overall, but the sudden pressure drop at U-bend is reduced. Additionally, LSFC requires less pressure to remove product water near the outlet. Due to much available MWC, proton conductivity increased and led to increased power. In addition, this even distribution of MWC reduced hot spots, which extends the lifespan of the membrane [40]. The ability of water evacuation can be observed in the next section. Figure 4.9 depicts the average surface water content of the membrane with respect to voltage. It was

observed that the average water content is the same at higher voltages, but increases at lower voltage. Lower voltage (higher current) leads to the production of more amount of water.

4.7.H_2O mass fraction:

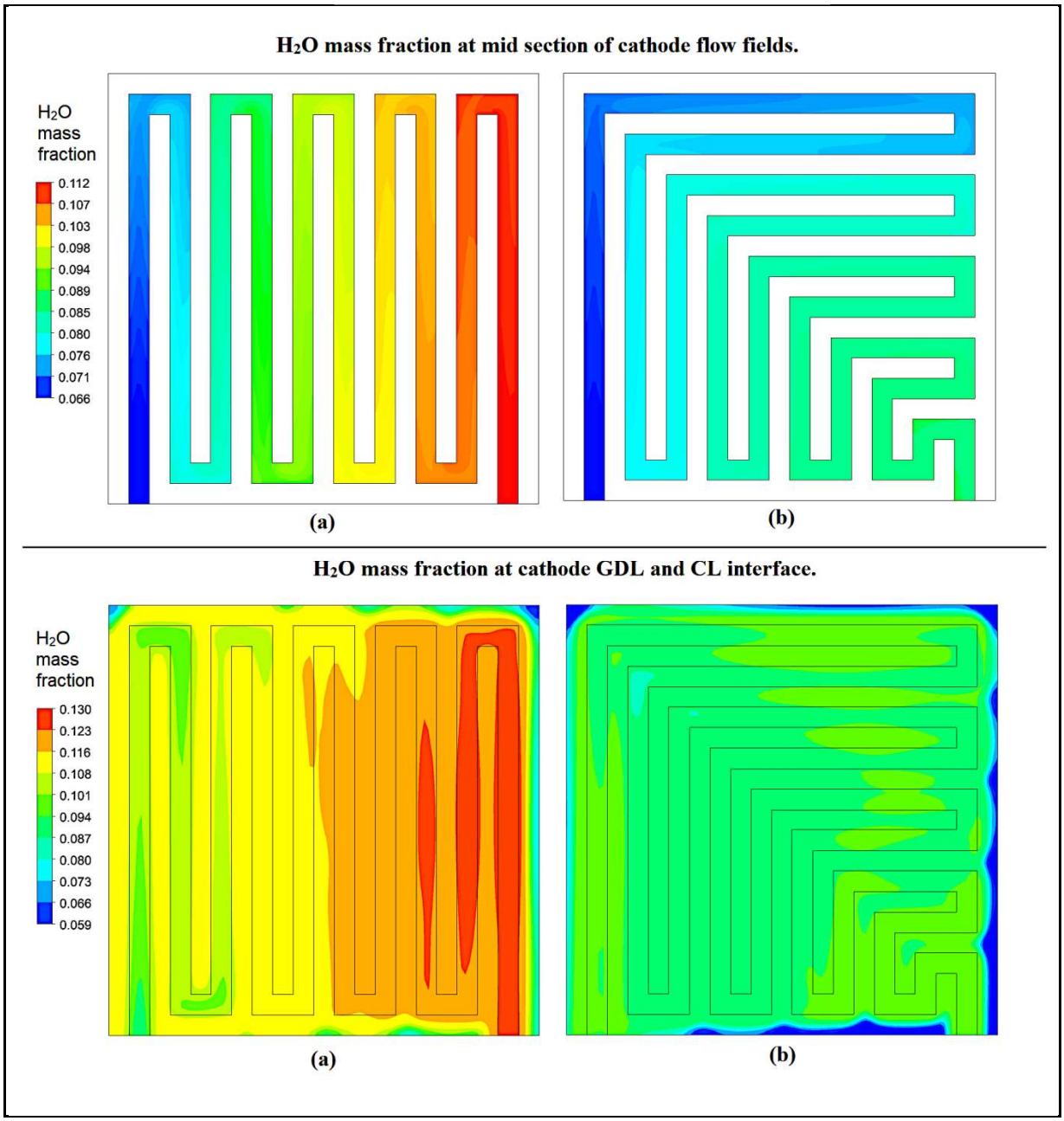

Figure 4.10 Cathode flow field H_2O mass fraction contours

To determine the H_2O mass fraction, a mid plane in the cathode channel was used. In figure 10 the contours show that in SSFF, H_2O mass fraction was increased from an input value of 0.066 to 0.112 whereas it is increased to 0.087 only in LSFF.

The increase in H_2O mass fraction demonstrates that H_2O has generated from the reactions and is increasing towards the channel's end. The buildup of H_2O in SSFF caused a drastic increase in mass fraction, but accumulation in LSFF was minimized due to shorter end phases. In contract, more H_2O indicates more reactions, but the less H_2O in LSFC can justified by observing MWC (Figure 4.10). These contours are co-related, MWC indicates how much water is produced during reactions and H_2O mass fraction tells the amount water at various locations. Hence, MWC of LSFC is higher ie. Membrane more humid compared SSFC design. Though equal amount of humidity provided at the inlet. Therefore, LSFC showed better membrane wetability and better water evacuation. Furthermore, LSFF assured improved removal of water content from the channels by 22.3% (22% approximately), which implicates a critical concern in the design of fuel cell flow channels.

4.8.O_2 mass fraction:

The contours in figure 4.11 were plotted on a mid plane created at the cathode channel. The range of O_2 mass fraction reduction in SSFF is less as compared to LSFF. The minimum mass fractions obtained at the outlet are 0.128 and 0.118 for SSFF and LSFF respectively.

O_2 mass fraction contours clearly justify H_2O mass fraction contours. LSFF has reduced oxygen mass fraction, indicating more consumption [75]. The modified designed allowed an increase in oxygen’s resident time in the initial phase. As a result, LSFF outperformed SSFF in terms of reactant use by 7.8% (approximately 8%). In both configurations, the decrease in H_2 mass fraction was small. Furthermore, the high dissociation energy of oxygen received the greatest attention in the literature too.

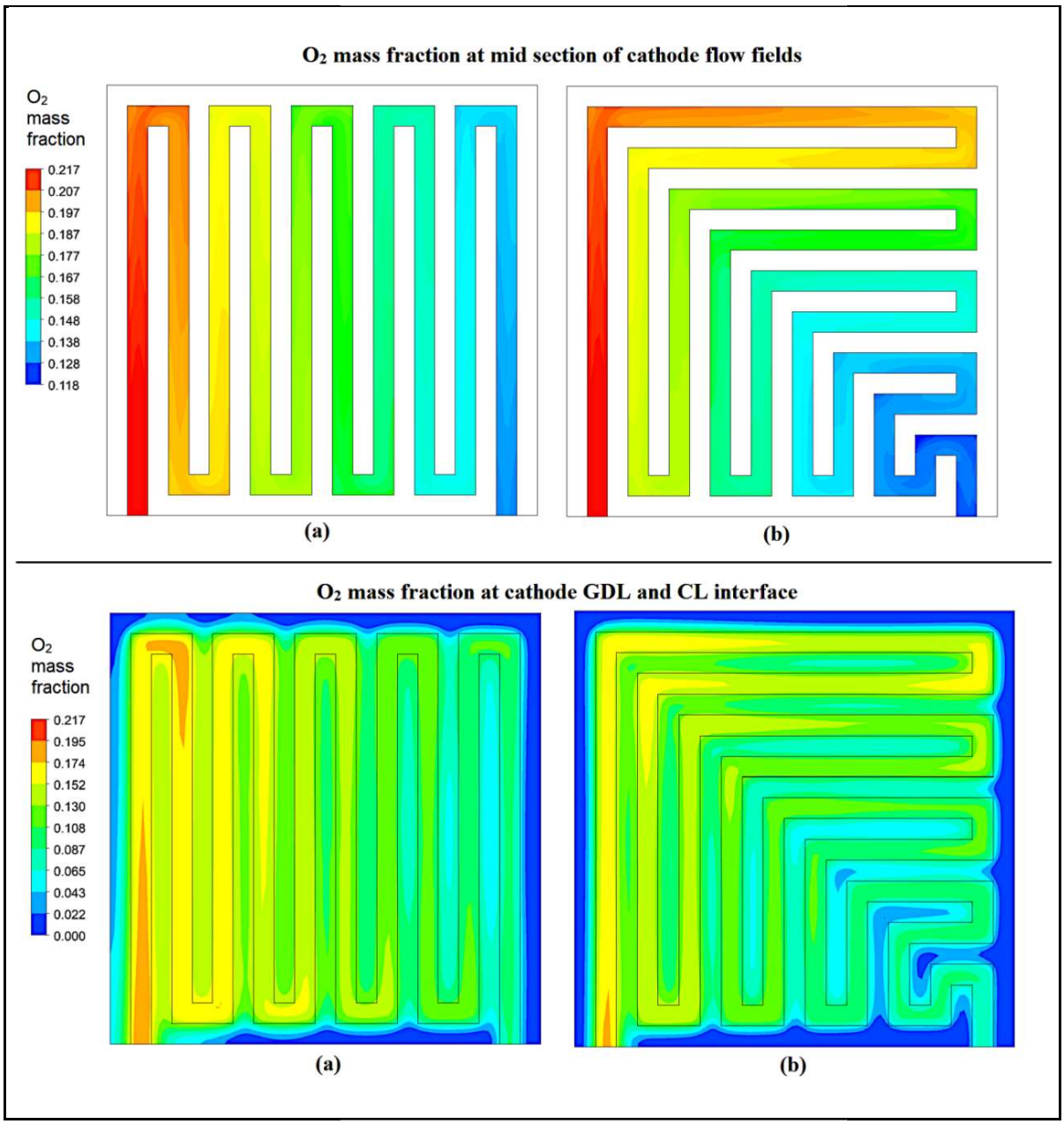

Figure 4.11 O_2 mass fraction in cathode flow fields

4.9.VI & PI characteristic curve for 70^0C:

The Overall performance of a fuel cell was evaluated using VI and PI curves. The graph in figure 4.12 was drawn for 70^0C and 3 atm pressure operating condition. It is very clear that LSFF current density or power density is higher compared to SSFF. At maximum power density, a 10% (approximately) rise was observed.

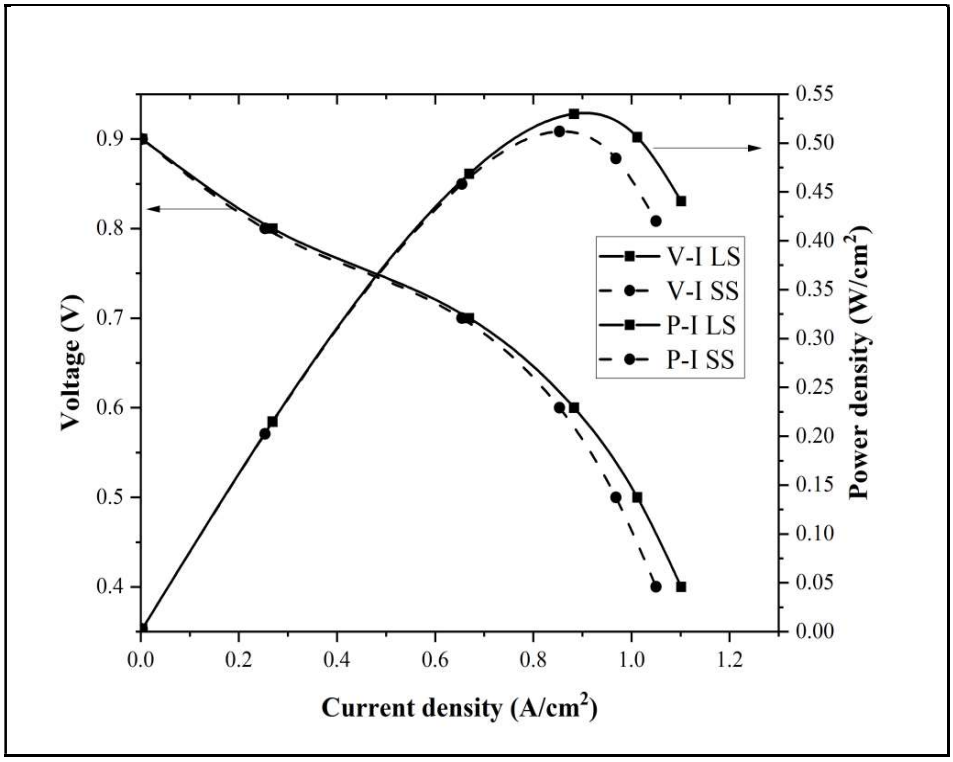

Figure 4.12 V-I and P-I characteristic curves

VI characteristic curves emphasizes the various losses. The losses are activation losses, ohmic losses and concentration losses. The modified design showed similar activation losses, since these losses are more dependent on catalyst. Ohmic losses found to be decreased because increased membrane content. Furthermore, concentration losses were reduced by increased current density, since the efficient product water evacuation helps the fresh reactant to reach the active site. Hence, polarization losses or the overvoltages were reduced with L-serpentine.

4.10. Objective 1 summary

The comprehensive numerical study of the innovative L-Serpentine flow field (LSFF) design compared to the standard single serpentine flow field (SSFF) design has yielded remarkable inferences. By adopting the LSFF, significant enhancements in performance have been achieved, addressing key challenges related to thermal management and water distribution within the fuel cell.

The findings highlight the following compelling conclusions from the LSFF-SSFF comparison:

- ❖ The incorporation of LSFF design effectively reduces the travel length for products by an impressive 40%, resulting in accelerated evacuation from the fuel cell.

- ❖ Remarkably, the LSFF design demonstrates minimal temperature rise and achieves near-uniform temperature distribution, alleviating thermal stresses on current collectors and bipolar plates.
- ❖ While LSFF shows a slightly higher pressure drop, requiring an additional 14 Pa of pressure, its impact on power density remains negligible, making it an attractive choice for fuel cell applications.
- ❖ The LSFF design showcases improved consumption of oxygen (O_2) and more efficient removal of water (H_2O) at the cathode end. This translates to an impressive 8% increase in O_2 consumption and a remarkable 22% enhancement in H_2O removal.
- ❖ Both the V-I (voltage-current) and P-I (power-current) characteristic curves demonstrate significant improvements in current density and power density outputs. The modified LSFF design exhibits an impressive 10% increase in both current density and power density.

Therefore, the LSFF design emerges as a promising solution for overcoming thermal and water management challenges in fuel cells. Further exploration should include investigations into the benefits of rounded edges to reduce pressure drop in flow fields, as well as the effects of larger active areas under various inlet conditions. These advancements hold tremendous potential for future studies in fuel cell technology.

Chapter 5

OBJECTIVE 2

Comparative Computational Fluid Dynamic analysis between Split and Dual Serpentine Flow Field for Proton Exchange Membrane Fuel Cells

5.1. Physical Model

The model was designed using ANSYS designing software "Spaceclaim". Two individual Single Serpentine Flow Fields were incorporated within the active area of 21 mm x 21 mm. To conduct a thorough investigation into various parameters, active area is restricted to 441 mm^2, with 10 flow fields as shown in Figure 2.1. Current collectors (CC), Gas diffusion layers (GDL) and Catalyst Layers (CL) were sandwiched to anode and cathodes of Proton exchange membrane (PEM) dimensions are table 5.1.

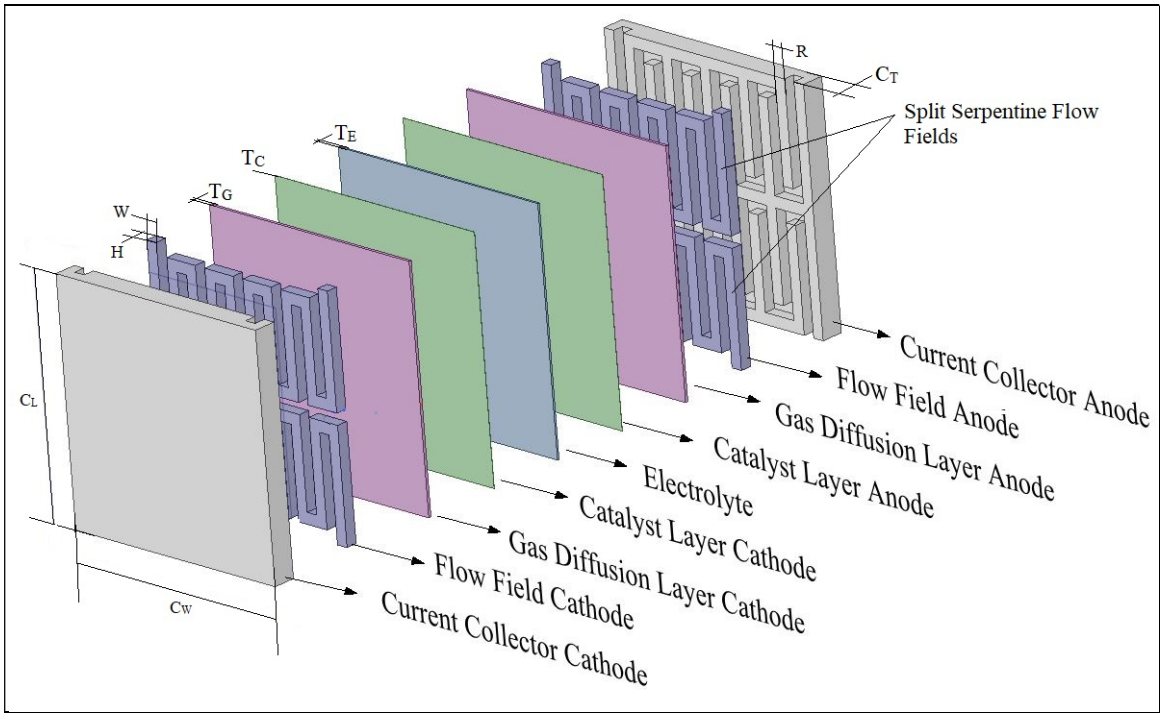

Figure 5.1 Exploded view of modified fuel cell

The dimensions indicated in figure 5.1. are given in table 5.1.

Table 5.1 Dimensions for the model

	label	Dimension (mm)	Ref.		label	Dimension (mm)	Ref.
Membrane area	C_L x C_W = A_{active}	21x21	[27]	Channel width	W	1	
Electrolyte thickness	T_E	0.178		Channel height	H	1	
Gas Diffusion Layer (GDL) thickness	T_G	0.25	[58]	Current collector (CC) thickness	C_T	2	[58]
Catalyst Layer (CL) thickness	T_C	0.02		Rid width	R	1	

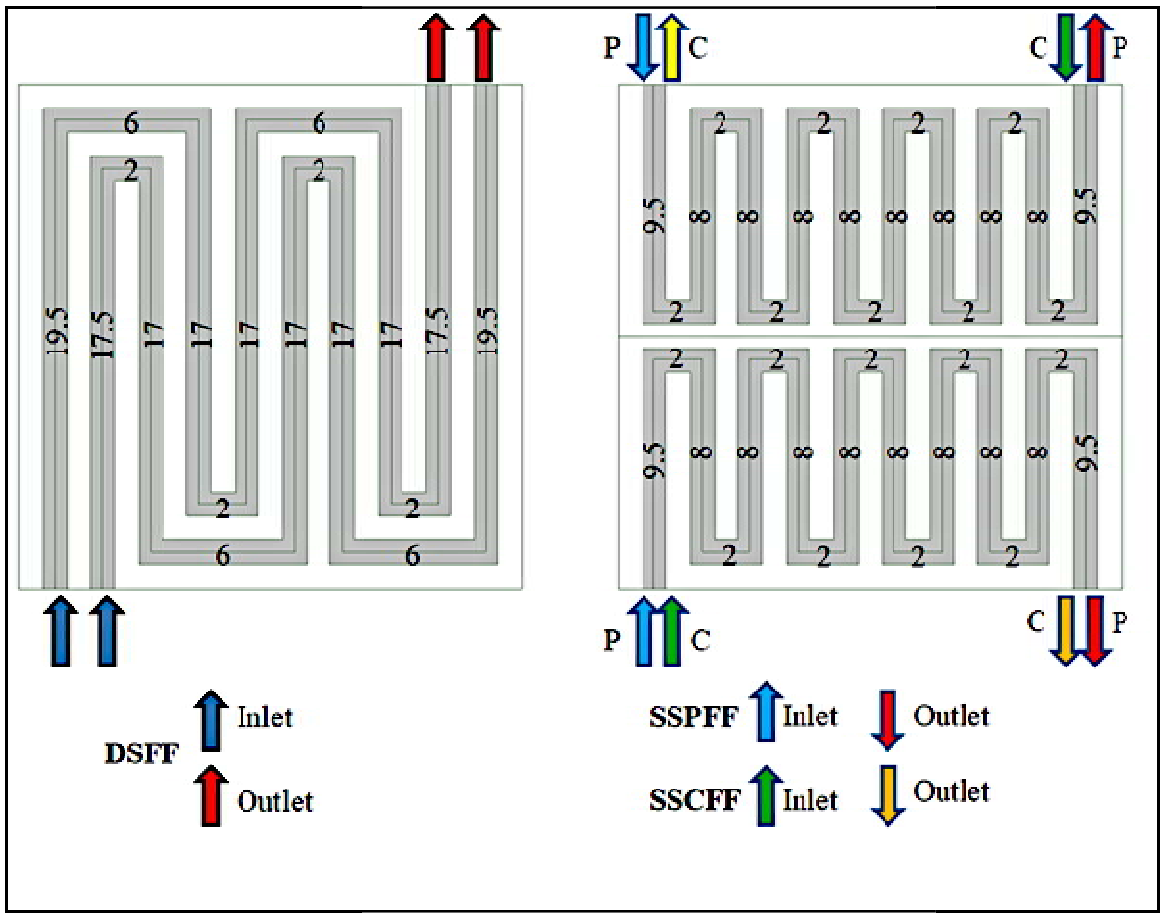

Figure 5.2 Flow field designs (a) DSFF (b) SSFF

In DSFF, flow direction is parallel to each other in both flow fields. For a Split Serpentine Flow Field (SSFF), it is further classified as parallel flow and counter flow. They are named as Split Serpentine Parallel Flow Field (SSPFF) for parallel flow directions and ii) counter flow as Split Serpentine Counter Flow Field (SSCFF), these can be observed in Figure 5.2, which shows the cross sectional top view of flow fields with flow directions. In the subsequent sections, flow directions were followed as indicated in Figure 5.2.

In the modified design, the distance traveled by the reactants remained the same, with both flow fields covering a distance of 202 mm. This measurement was taken by considering the path lines, and the lengths are marked at the center of each line in mm. Since the path length is the same in both layouts, it is feasible to make a comparison between them.

5.2.Results and Discussion

The performance of a fuel cell is evaluated through its voltage-current density (V-I), power density, and current density (P-I) curves. The amount of current produced is affected by the distribution of factors such as temperature, pressure, species, and current density. In this study, performance analyzed for a voltage range of 0.4-0.9V. However, results were discussed at 0.6 V, where the highest power density was obtained. As the effect of temperature, pressure, species, and current density was more prominent on the cathode side, the contours were only plotted for this side.

5.3.Temperature contours:

Temperature distribution within the fuel cell plays a vital role in understanding and managing thermal characteristics [82]. For thermal characteristics, temperature contours were plotted at i) (Gas Diffusion Layer cathode) GDLC and (Catalyst Layer Cathode) CLC interface ii) Cathode flow field mid section. A humidifying temperature of 343.15 K was applied at all inlets, approximately 3 K rise in temperature was observed in all the layouts at GDLC and CLC interface. However, maximum temperature obtained was higher in DSFF followed by SSPFF and SSCFF. Simultaneously, in the cathode flow field mid section in all the design very small increment in temperature was noticed.

In figure 5.3 (a1,b1, c1), dark blue color region indicates low temperature. On the other hand, red color region indicates the highest temperature attained. The difference in maximum temperatures between the three designs was found to be small, but its effect would be significant for large-sized active areas in practical applications. High temperature obtained

at any particular region implies more reactions occurring at that region. In the split serpentine flow fields for both parallel and counter flows, with an increase in number of bends with turns, the resident time of reactants increases, which in turn leads to upsurge in chemical reactions

On the other hand, cold spots were observed in central region of SSPFF and SSCFF due to drop in temperature because of restricted penetration of flow. This is more evident in case of SSPFF and less in case of SSCFF. However, in case of SSCFF, this temperature drop can be eliminated by reducing the gap between two counter flow fields; however keeping the flow penetration in consideration some gap is required hence a 1 mm gap is provided in this study.

Figure 5.3 (a2, b2, c2), shows the temperature rise in the flow fields. It is evident that increasing the number of turns has increased temperature distribution especially in both SSFFs. In case of SSPFF, a cold region is developed because of the parallel propagation of flow. Whereas in SSCFF, the cold spot were reduced due to the obvious counter flow effect.

The results showed that in the DSFF design, there were fewer hot spots distributed over a larger active area, resulting in a non-uniform distribution of active reaction sites. In contrast, the modified designs (SSPFF and SSCFF) had more hot spots distributed over a more active area, resulting in a uniform distribution of active reaction sites. SSCFF showed lesser temperature difference and uniform distribution among all other designs. Furthermore,, Uniform temperature distribution indicates reduced thermal strains within the current collectors [40]..

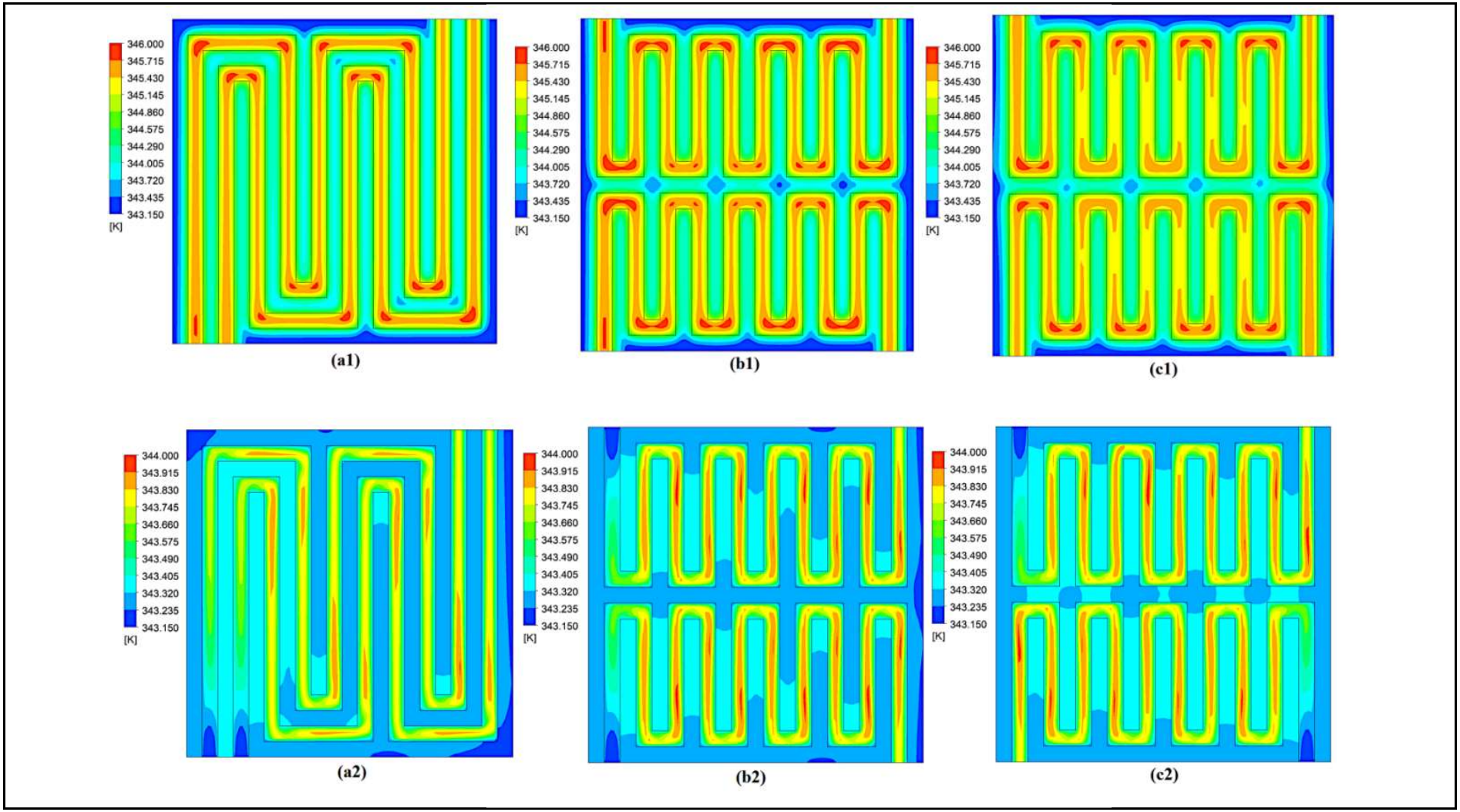

Figure 5.3 Temperature contours (a) DSFF (b) SSPFF (c) SSCFF

5.4.Pressure contours:

The pressure is highest at the flow field entrance and gradually decreases in the flow direction. The modified channels had higher pressure drops compared to DSFF due to the increased number of turns, which leads to an increase in the reactants' resident time. The pressure drops for each layout were calculated by considering the pressure difference between the inlets and outlets, and it is found to be 28.787 Pa for DSFF, 32.091 Pa for SSPFF and 31.905 Pa for SSCFF (figure 5.4). The pressure drop in SSPFF and SSCFF was almost same. The increase in pressure drop in SSFF helps to increase reactivity by prolonging resident time. It was found that the pressure drop in SSFF much less than a single serpentine channel, for the similar dimensions of single serpentine a 405 Pa pressure drop was noticed by Ozdemir and Taymaz [27].

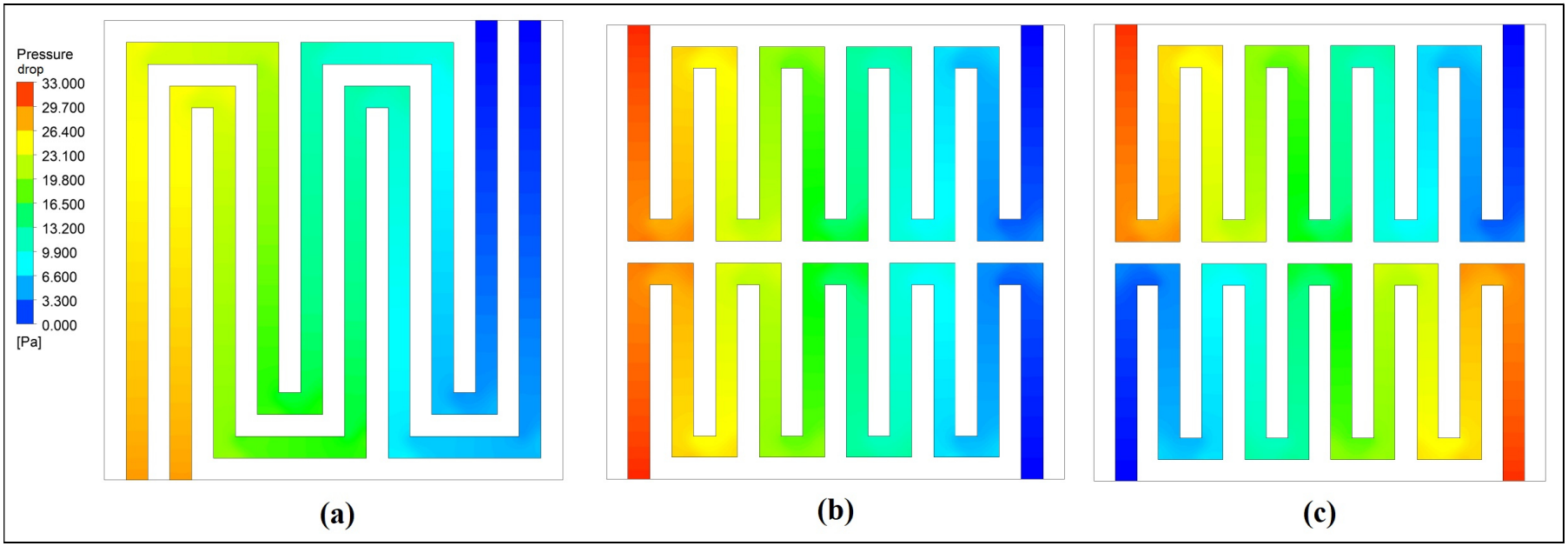

Figure 5.4 Pressure drop contours a) DSFF (b) SSPFF (c) SSCFF

5.5. Water content contours :

Membrane Water Content (MWC) was estimated using contours between membrane and catalyst layer interface on the cathode side. A uniform distribution of MWC increases proton conductivity in the membrane and decreases ohmic losses [83].

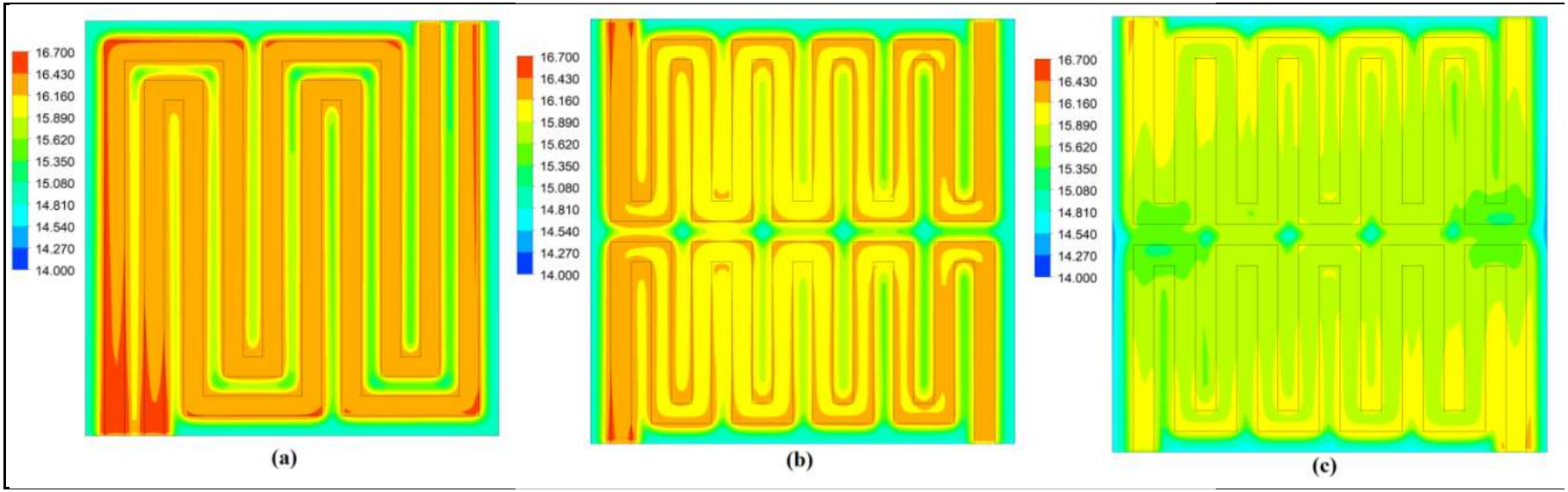

Figure 5.5 Membrane water content (a) DSFF (b) SSPFF (c) SSCFF

Maximum MWC of DSFF, SSPFF and SSCFF designs were found to be 16.676, 16.528 and 16.217 respectively. From figure 5.5, In DSFF, it is higher throughout the flow field and it is less under the rib. In case SSFF design it has better distribution in both flow configurations (counter and parallel flow). The recommended water content is 14 [40]. However, the high MWC is mainly due to the 100% RH provided to oxygen at the inlet, which can be lowered by reducing humidity through the cathode inlet flow. Nonetheless, 100% RH was considered in the

analysis to magnify the membrane water content effect. Another reason for the high MWC is the accumulation of product water, DSFF experienced increased humidity and more flooding due to water accumulation, while SSPFF showed better water content distribution. On the other hand, SSCFF demonstrated the most optimal and balanced MWC with only a minimal increase, resulting in a reduced risk of flooding.

5.6.Production of H_2O and distribution:

It is the amount of H_2O present in the flow channel as a product of chemical reactions at the cathode end. The water produced was removed from the flow field by pressure difference. The inlet mass fraction of H_2O was 0.066 (provided at the cathode inlet for humidification).

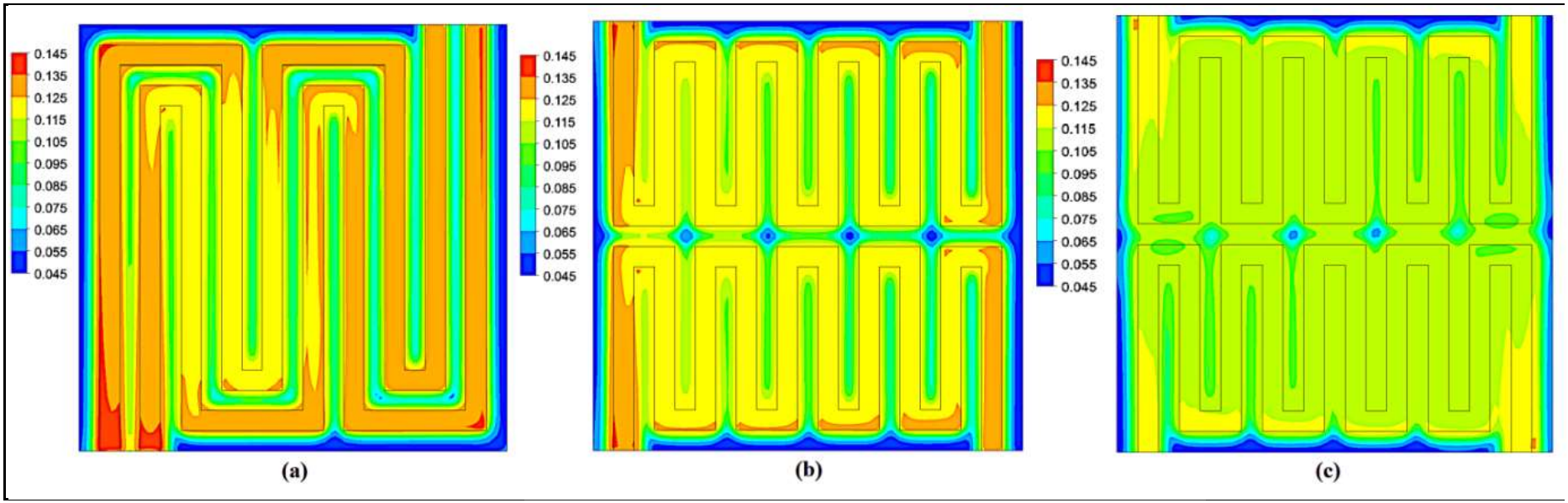

Figure 5.6 H_2O mass fraction contour a) DSFF (b) SSPFF (c) SSCFF

From figure 5.6 H_2O mass fractions contours obtained at GDL and CL interface on cathode side. It was observed that excessive water at start of the flow; this was due to the availability of moisture content with the reactants. It is decreasing towards the mid portion and then

increasing towards outlet. This signifies that the increase in mass fraction is the resultant of reactions happening in fuel cell, thus increases product water towards outlet. The driving capability of serpentine flow field increases product water toward the end. In the initial phases the reactants required time for products formation, so water forms little away from the inlet and the formed water can be easily driven out by the pressure difference. Furthermore, product water is high in the flow field area but it was comparatively less under the rib region in interval patterns. In case of SSFF and SSCFF layouts water content diffused evenly within the active area. In figure 5.6 (b) and (c), light blue spots were observed in the mid portion of SSPFF, whereas for SSCFF, these spots were reduced and water level increased in the mid section because of counter flow of species.

5.7.Reactant O_2 distribution:

O_2 mass fraction contour shown in figure 5.6 was drawn by considering a section plane in the cathode flow field. O_2 mass fraction of 0.217 was applied at the inlet and it was decreasing towards the outlet. The applied mass fraction has reduced towards the outlet because of consumption of O_2 during chemical reactions. In modified deigns consumption significantly increased due to increased number of turns has increased resident time. The difference in mass fractions can be observed in figure 5.7 (a1,b1& c1), these contours drawn at the mid section of cathode flow fields. The oxygen consumption of SSPFF has improved by 1.5% compared to DSFF, while that of SSCFF has improved by 5%. Among these designs, SSCFF showed better consumption due to added counter flow effect.

Contours were plotted at the GDL and CL interface on the cathode side in Figure 5.7 (a2, b2, and c2) to observe the flow effect in the corners of the modified design. The primary purpose of selecting these contours was to investigate the flow behavior in the corners of the system. Unlike SSFFs, DSFFs do not experience opposing flow, which made it essential to study the flow patterns. In parallel flow, there was some mixing of the flow in comparison to counter flow, but it did not have any significant impact on the current density. Additionally, the increased current density in SSCFFs indicated that counter flow helps to increase residence time, leading to increased consumption.

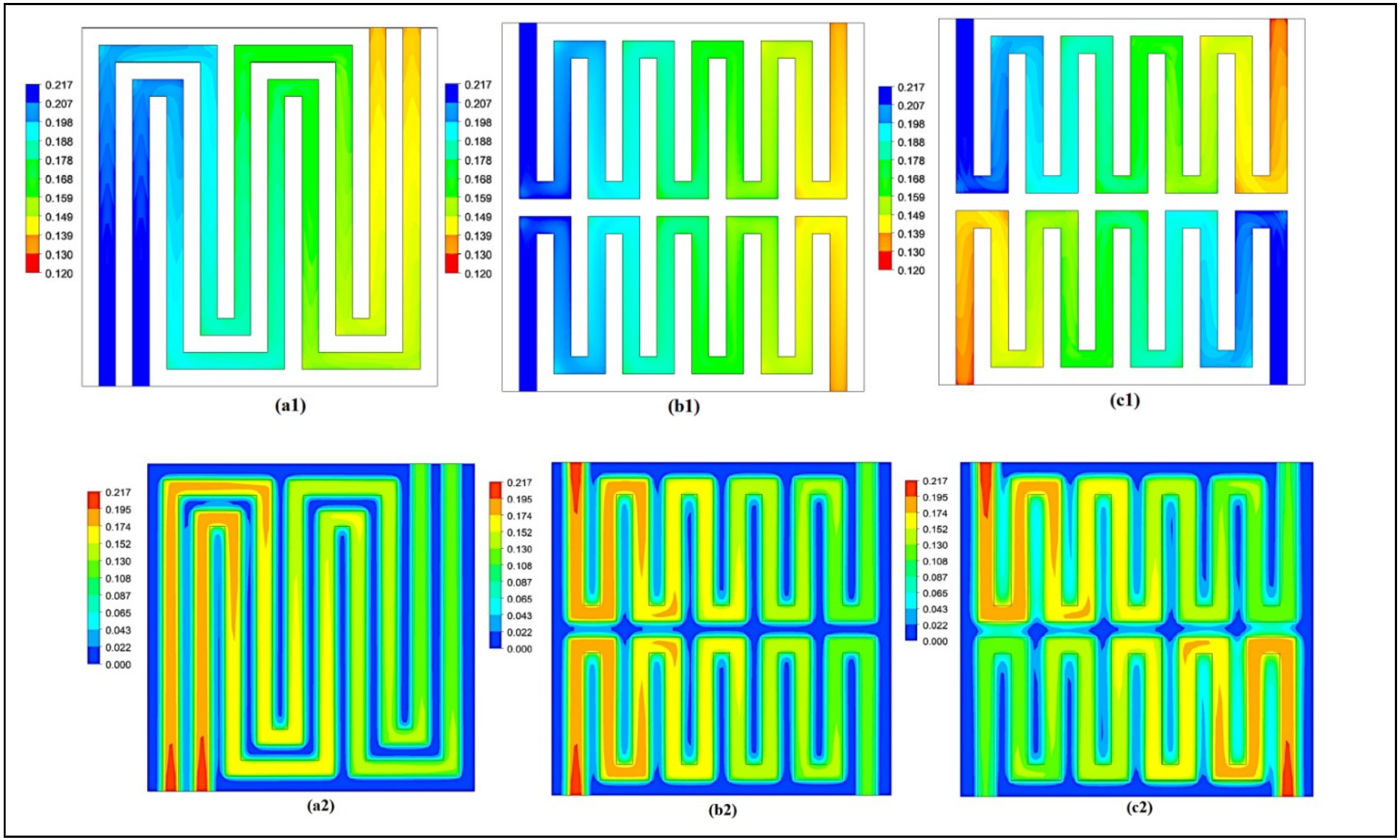

Figure 5.7 O_2 mass fraction in cathode flow fields (a) DSFF (b) SSPFF (c) SSCFF

5.8.Current density distribution contours:

Current density distribution was plotted at i) interface of GDLC and CLC and ii) Cathode flow field mid section. It was evident that maximum current density attained at maximum temperature spots available in active area. Therefore, temperature distribution (Figure 5.2- a1, b1, and c1) are in coherence with current density distribution for figure 5.8- a1, b1 and c1.

Contours in figure 5.8 (a1, b1 and c1) show that the current density distribution was concentrated as pockets at the corners and edges in all the configurations. However, in SSPFF and SSCFF the number of pockets either increased or it could be inferred as large area pockets broken into small pockets in the new design. Figure 5.8 (a2, b2 and c2) indicates the current collected by the ribs in all designs. In DSFF, higher current density is confined to particular region. In case SSFFs, extra rib portions helped to increase current distribution in the central region. For SSPFF, it has reduced towards the outlet. Whereas for SSCFF, current density distribution is extended further towards the outlet due to the availability of the counter flow. Furthermore, higher densities concentrated for particular regions has reduces average current density obtained [84]. Both SSFF configurations, enabled to increase of distribution to the central area due to the presence of bends, as bends are regions where the reactants gets enough resident time for reaction.

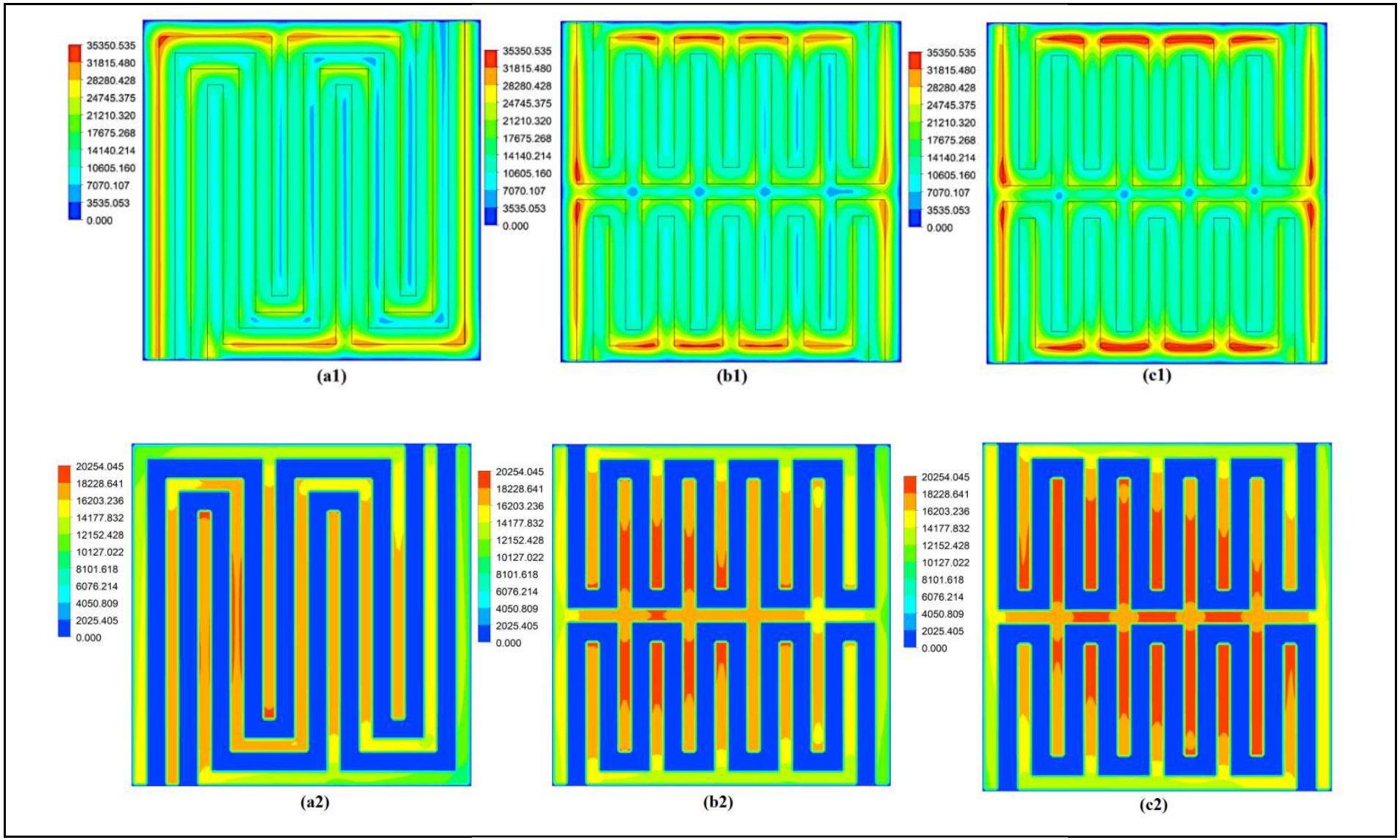

Figure 5.8 Current density distribution at cathode side (a) DSFF (b) SSPFF (c) SSCFF

5.9.Polarization characteristics:

The following subsections discuss the results obtained by drawing a comparison between the contours of DSFF, SSPFF and SSCFF. Thermal and water management were main focus of the discussion. VI characteristic curve is the ultimate measure of performance of the fuel cell, it is the reflection of all the characteristics discussed in the above sections [77]. From figure 5.9, it can be observed from VI and PI characteristics that SSCFF design was better in terms of current and power densities.

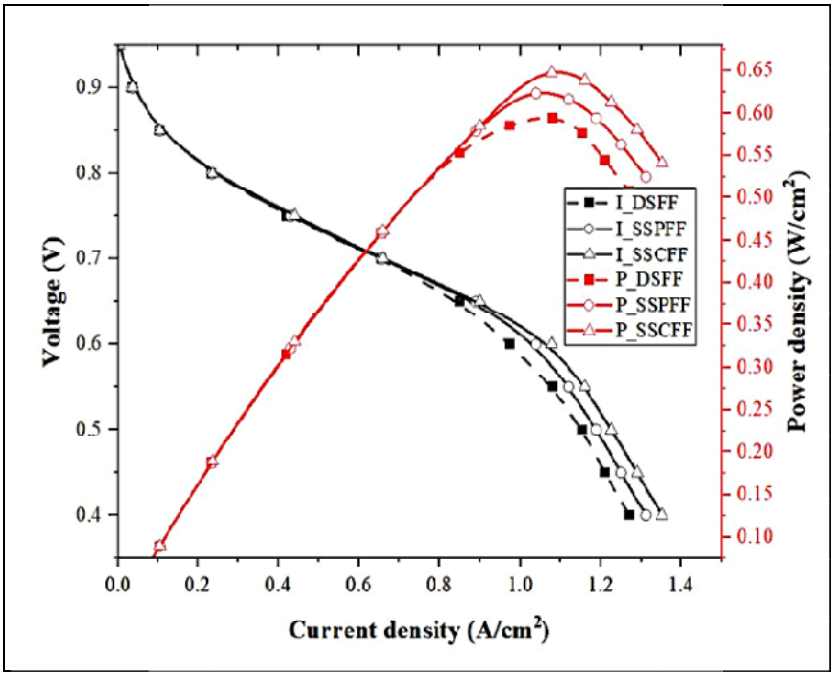

Figure 5.9 VI and PI comparison between DSFF, SSPFF and SSCFF

5.10.Objective 2 summary

The design presented in this chapter effectively balances the advantages of both single and parallel serpentine flow fields. With dual inlets and outlets, each featuring a single serpentine flow field, the proposed solution offers reduced pressure drop while maintaining high reactant driving capability. The increased number of u-bends results in a slight increase in pressure drop, but this increase helps to improve the resident time of the reactants. The split serpentine flow fields lead to improved distribution of membrane water content, current density, and temperature. Furthermore pressure drop is on the higher side compared to parallel flow fields. The use of counter flow was implemented to improve the distribution of heat and species in two directions. Although counter flow may create disturbances in the flow by consuming reactants near the inlets due to the opposite flow of products, these issues were not observed to have a significant impact. Therefore, the proposed design provides an overall

improvement in performance with reduced pressure drop and improved reactants distribution. A detailed comparative analysis as follows:

- The temperature profile showed more active spots in the single serpentine flow field (SSFF) compared to the dual serpentine flow field (DSFF). Although the maximum temperature reached was similar in all three designs, the number of hot spots increased in the SSFF, indicating a higher concentration of active regions. The SSCFF design had the smallest difference between the minimum and maximum temperature, making it more effective in reducing thermal stress.

- Pressure drop of SSFF layouts was higher than that of DSFF, but much lower than single serpentine flow field.

- Oxygen consumption increased significantly in modified designs. 1.5 % and 5% increase in oxygen consumption observed for SSPFF and SSCFF respectively. But no considerable change was observed in water production for all designs.

- Membrane water content distribution found to be uniformly distributed in modified designs but in case of DSFF distribution was non-uniform. Counter flow design showed even better distribution than parallel flow.

- Current density contours showed increased distribution for SSFFs, because of the increased rib region in the central region. Furthermore, SSFF counter flow current flux distributed even towards outlet.

- VI and PI curves showed better performance in case of modified designs as compared with DSFF. However, counter flow design showed better output in terms of current density and power density. In comparison to DSFF, SSPFF and SSCFF had a 6.5% and 10.6% improvement in current and power density, respectively.

To summarize, Split Serpentine Flow Field with counter flow proves to be a competitor for Dual serpentine flow field. Split serpentine provides curves and bends in the centre of the active area, which increases reaction sites. The increased active reaction sites reduce thermal strains in bipolar material. For the future scope, properties of a similar nature need to be checked for bigger active area of the membrane.

Chapter 6

OBJECTIVE 3

Assessment of Split Serpentine Flow Fields for Increased Active Area: Exploring Horizontal and Vertical Configurations

6.1.Physical Model

This chapter focuses on exploring the dimensional effects of split serpentine flow fields, as previously discussed in chapter 5. In chapter 5, the active area was 21x21 mm^2, forming a square shape. However, considering real-time applications, it is essential to have a larger active area. Therefore, active areas of 73x53 mm^2(Horizontal configuration) and 53x73 mm^2(Vertical configuration) were considered for comparison (depicted in figure 6.1 (a) and (b) respectively). To accommodate the larger flow field, an additional 3 mm was added to both sides of the design instead of using the previous dimensions of 50 mm or 70 mm. The flow directions, such as parallel flow and counter flow, were maintained the same as in chapter 5 for a consistent comparison. Apart from changing the dimensions effect of relative humidity has been studied in this chapter. Relative humidity (RH) changed from 20 to 100 in increment of 20%.

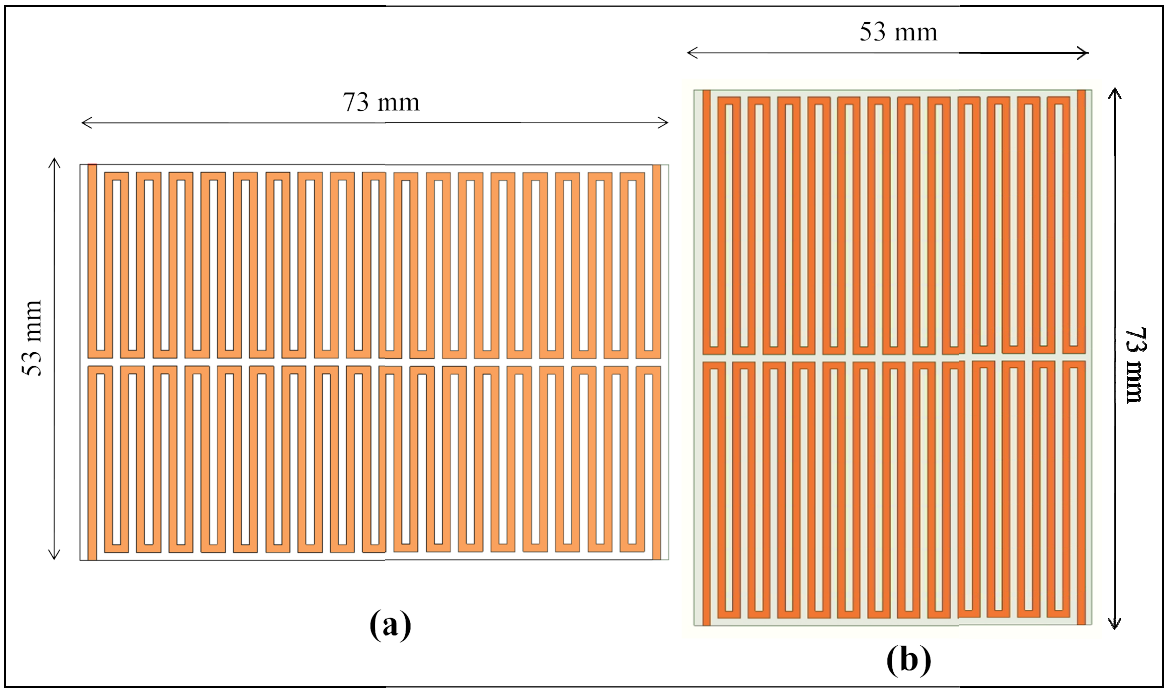

Figure 6.1 Split serpentine flow fields (a) 73x53 mm^2(Horizontal) and (b) 53x73 mm^2 (Vertical)

Dimensions of other components were maintained similar to chapter 5. Dimensions are given in table 6.1.

Table 6.1. Dimensions for the model

	Dimension (mm)	Ref.		Dimension (mm)	Ref.
Membrane area	73x53; 53x73	This study	Channel width	1	
Electrolyte thickness	0.178		Channel height	1	
Gas Diffusion Layer (GDL) thickness	0.25	[58][74]	Current collector (CC) thickness	2	[58]
Catalyst Layer (CL) thickness	0.02		Rid width	1	

6.2.Results and discussion:

In this study, four different layouts were investigated with parallel flow (PF) and counter flow (CF) configurations for two membrane sizes: 73x53 mm^2 and 53x73 mm^2.

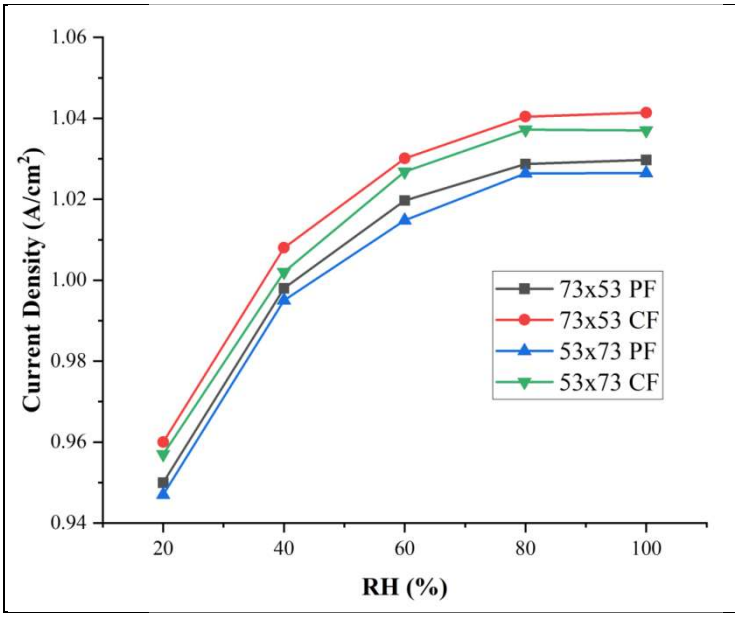

Figure 6.2. Current densities at various RH levels

These layouts were examined at various relative humidity (RH) levels ranging from 20% to 100%, and the voltage range was set between 0.4 V and 0.9 V. Upon comparing the Voltage-Current density (VI) curves for all four configurations, we observed that the highest power density was achieved at 0.6 V, which was consistent with previous research findings. To reduce data, a single graph showing current densities at 0.6 V for various RH levels is shown in figure 6.2.

The performance of the fuel cell varies at different relative humidity (RH) levels in figure 6.2 can be attributed to the following reasons:

a) At 20% RH, there is a significant drop in performance. The reduced water content in the PEM membrane leads to lower proton conductivity and higher membrane resistance (Ohmic losses). High current density also results in notable losses due to the transport of reactants and products.
b) At 40% RH, the fuel cell exhibits better performance compared to 20% RH. This improvement can be attributed to the higher water content in the PEM membrane, leading to improved proton conductivity and reduced membrane resistance.
c) At 60% RH, the fuel cell shows even better performance, with higher voltage and steeper slope. This is due to a better balance between proton conductivity and membrane resistance.
d) At 80% and 100% RH, the fuel cell reaches a peak in performance, with the highest voltage and steepest slope. This peak is achieved because of the optimal balance between proton conductivity and membrane resistance, resulting in the lowest losses and highest efficiency.

Considering that the current density is almost the same in both cases, a relative humidity level of 80% has been chosen for the further analysis. Remarkably, across all the layouts, the current densities at 80% RH, compared to the base case at 20% RH, demonstrated an increase of 8.3%. Furthermore, when comparing the two counter flow layouts, it was observed that the configuration with a 73x53 mm^2 membrane size resulted in a higher current density.The reason for improved current density in the counter flow configurations is discussed in the subsequent sections of the study.

6.3.Temperature and pressure characteristics:

Temperature rise was investigated at various locations across the 21x21 mm^2 active area, comparing the parallel and counter flow configurations. Surprisingly, no significant temperature differences were observed between the two setups. The maximum temperature obtained in the smaller size configuration is consistent with that of the larger active area (53x73 & 73x53).

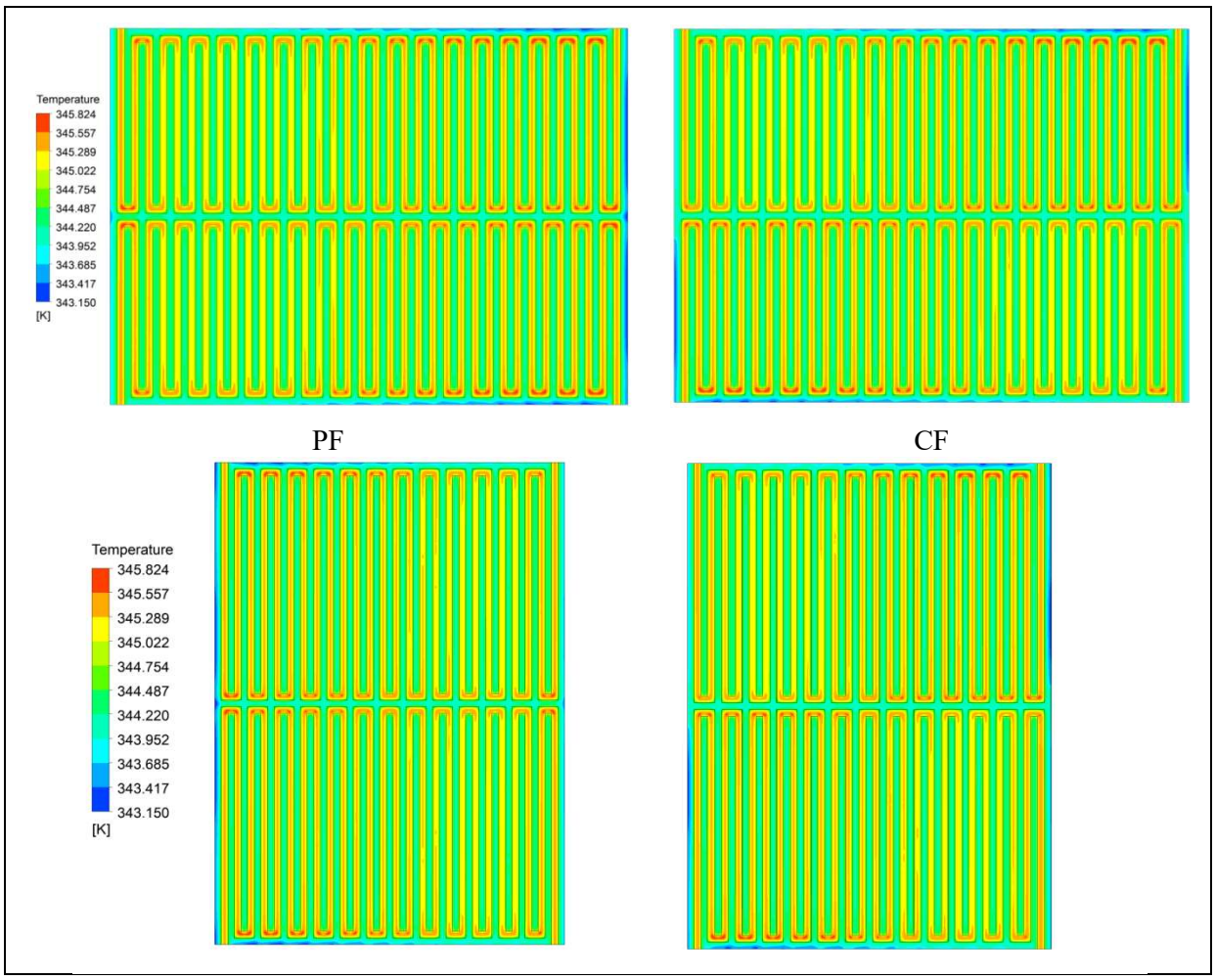

Figure 6.3 Temperature contours of 73x53 (above) and 53x73 (below)

In the 53x73 configuration, the distance between u-bends is larger, causing the high-temperature points to be located farther apart when compared to the 73x53 configuration. However, in the latter case, the maximum temperatures are closer together, resulting in a more even distribution of temperature.

Both parallel flow and counter flow configurations exhibit similar temperature distribution patterns. The main difference lies in the initial phase of the split serpentine, where the temperature is higher and gradually reduces towards the outlet in the mid-section

of each split serpentine (Figure 6.3). Overall, the temperature profiles in both flow directions show only minor variations.

In both configurations, the length of travel for the species remained constant regardless of the orientation or change in direction. However, the number of U bends in the flow path affected the pressure drop. The greater the number of U bends, the higher the pressure drop. Notably, the parallel flow configuration exhibited higher pressure drop compared to the counter flow configuration (figure 6.4 and 6.5).

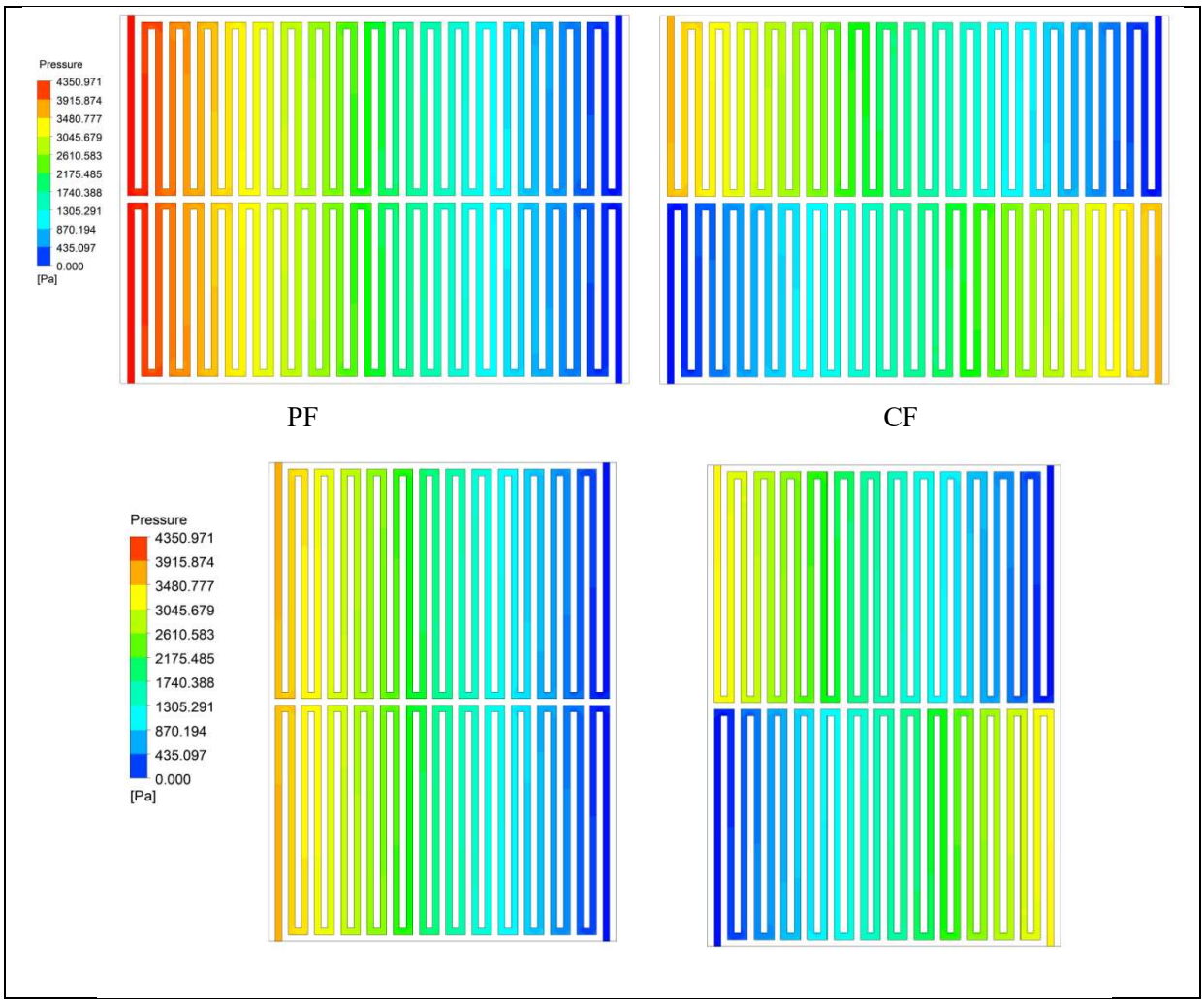

Figure 6.4 Pressure contours of 73x53 (above) and 53x73 (below)

In the case of counter flow, the proximity of the outlet of one split serpentine to the inlet of another split serpentine played a crucial role. This arrangement allowed high-pressure regions to balance out the low-pressure points, resulting in reduced pressure drop in the counter flow configuration. This phenomenon can be better understood by analyzing the oxygen distribution contours.

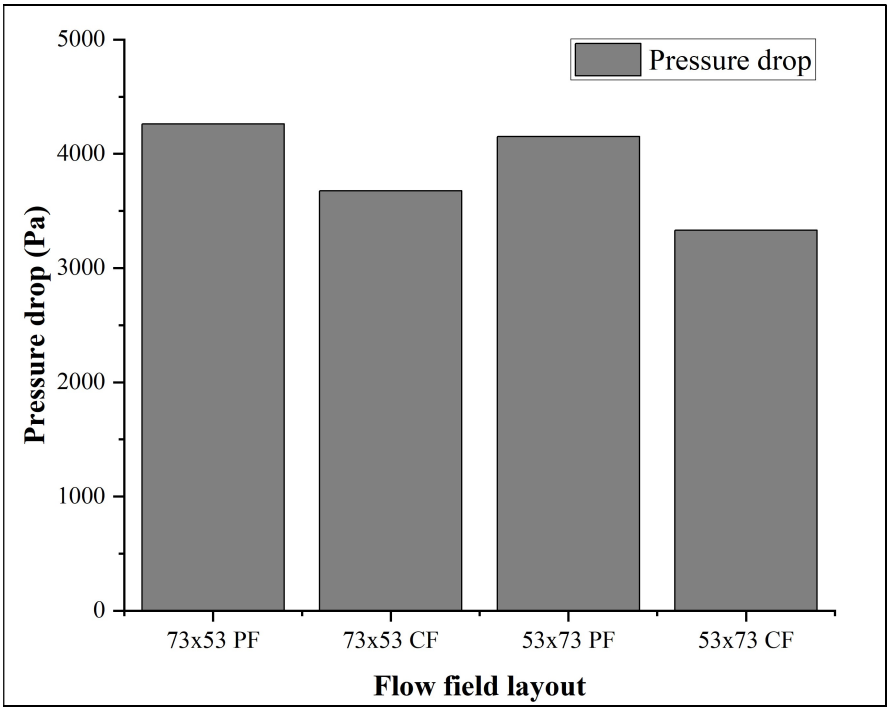

Figure 6.5 Pressure drops for 73x53 and 53x73 layouts with Parallel flow and counter flow

The percentage difference between parallel and counter flows for the 73x53 and 53x73 configurations is 16% and 24%, respectively. The higher pressure variation in the 53x73 setup can be attributed to the counter flow effect and the reduced number of u-bends.

6.4.Oxygen distribution

Figure 6.6 presents a visualization of the oxygen mass fraction distribution in the four types of cathode flow fields while operating at a cell potential of 0.6 V. When 0.22 mass fraction of O_2 is provided at the cathode inlets, it gradually decreases as it reaches the outlets. The contours were plotted at the interface between the Gas Diffusion Layer (GDL) and the Catalyst Layer (CL) on the cathode side.

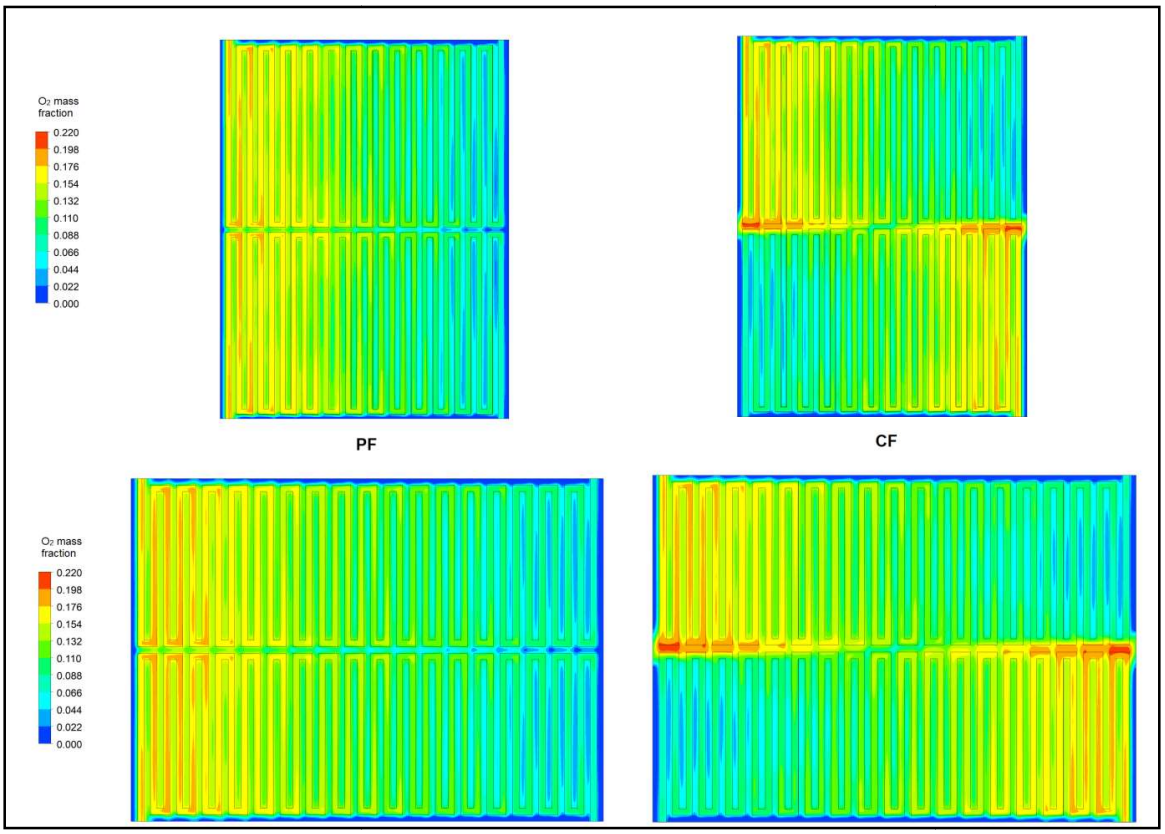

Figure 6.6 Oxygen distribution at GDL and CL interface on cathode end; vertical configuration (above), horizontal configuration (below)

In the parallel flow configurations, we observe that the oxygen mass fraction is initially higher on one side and depletes as it approaches the outlet. On the other hand, in the counter flow configurations, one of the inlets of the split serpentine is positioned near the outlet of the other. This setup facilitates the diffusion of some oxygen underneath the rib located at the center. This phenomenon not only helps to reduce pressure drop but also aids in the removal of product water accumulation towards the outlet.

However, one drawback of the counter flow configuration is that a higher depletion of oxygen occurs, as oxygen is predominantly scavenged towards the outlet. Despite this drawback, the benefits of reduced pressure drop and efficient product water removal are significant advantages offered by the counter flow design. Further studies required on rib width and operating pressures to understand the oxygen depletion.

6.5.Membrane water content and H_2O mass fraction:

Membrane water content and H_2O distribution are inter-related. So, inorder to make it more precise comparison, all horizontal and vertical configurations were compared individually in figure 6.7 and 6.8. Figure 6.7 illustrates the water accumulation towards the

outlet for both parallel and counter flow configurations, which also increases the membrane water content. A similar behavior can also be observed for the vertical configurations in figure 6.8.

The H_2O mass fraction distribution is measured at the interface of the cathode catalyst layer and the membrane. Interestingly, it closely aligns with the O_2 concentration distribution shown in figure 6.6. Regions with low O_2 concentration coincide with high H_2O concentration zones, which may lead to flooding or stagnant areas where no chemical reactions occur.

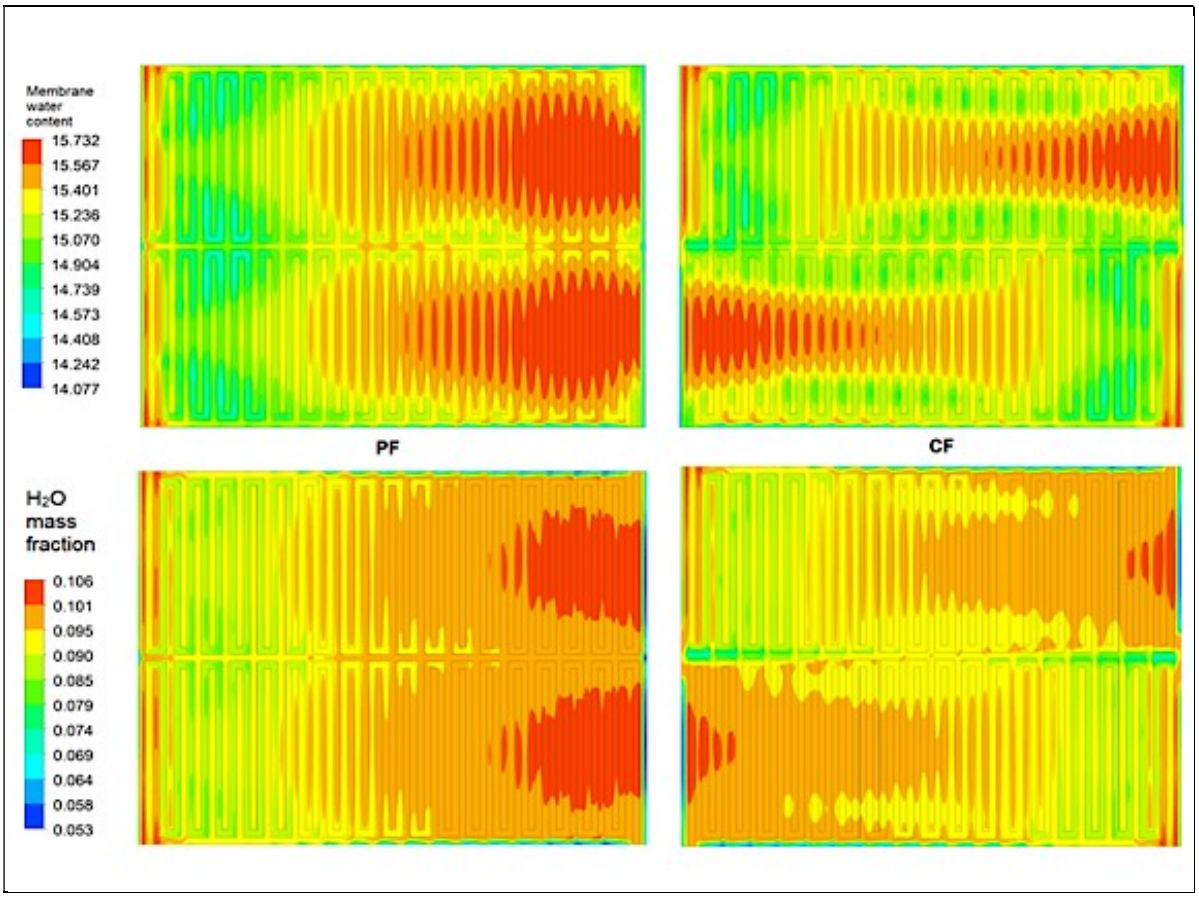

Figure 6.7. Horizontal configuration Membrane water content (above) and H_2O mass fraction (below) comparisons for parallel (left) and counter (right) flows

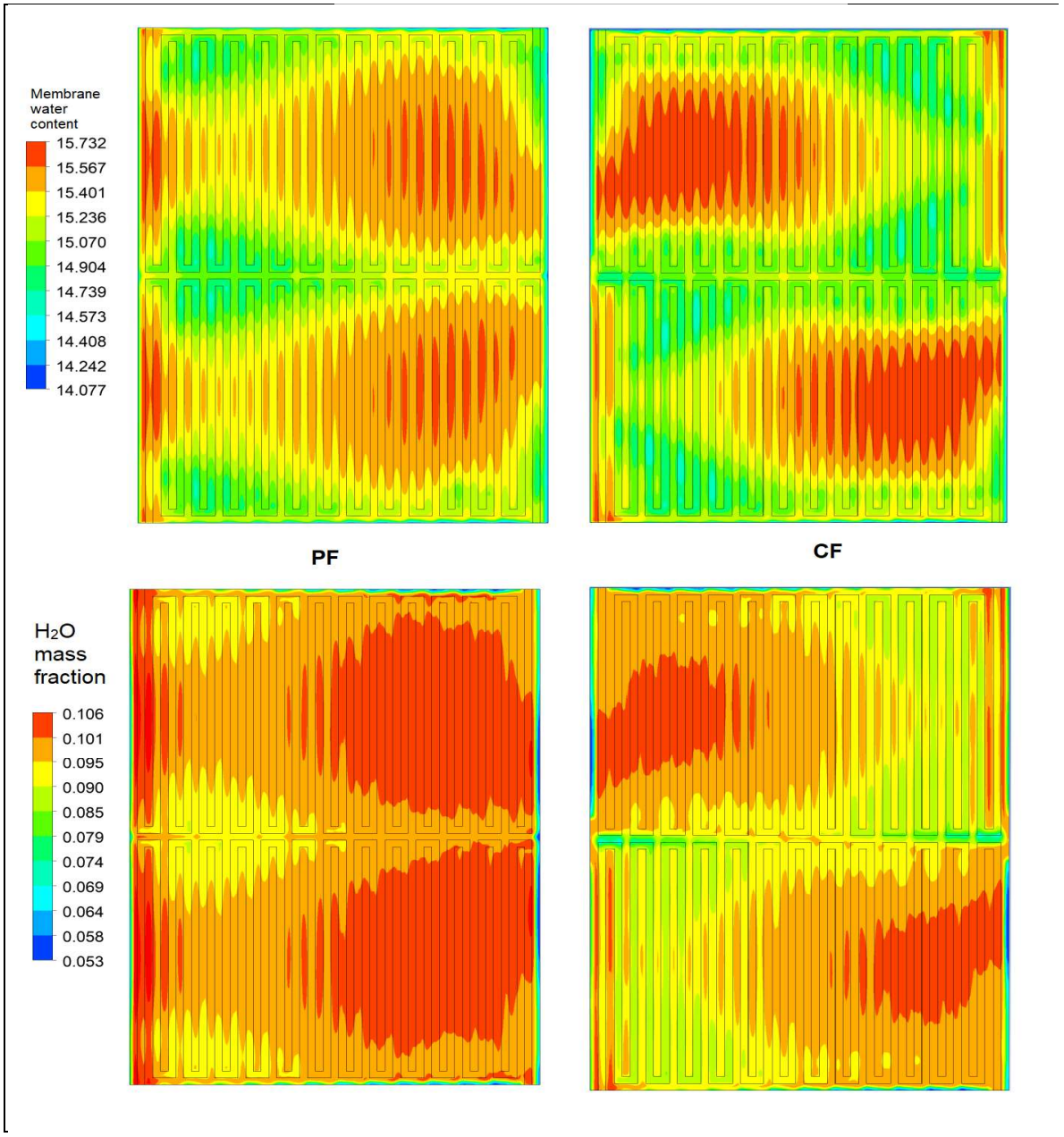

Figure 6.8 Vertical configuration Membrane water content (above) and H_2O mass fraction (below) comparisons for parallel (left) and counter (right) flows

In the larger active area, there is an observed increase in membrane water content and H_2O mass fraction as we move towards the outlet, particularly noticeable in the vertical configuration. This phenomenon is primarily due to the height of the flow field, which leads to a longer residence time for the species, allowing more water to accumulate.

In the case of the two parallel flow designs, water accumulation is more pronounced at the outlets, resulting in an uneven distribution. However, the counter flow designs show reduced water accumulation due to the induced oxygen flow towards the outlets from the

nearest inlet. This distribution of water improves further as the length is decreased. Among all the configurations, the 73x53 Counter Flow setup is identified as having the most favorable H_2O and membrane water content distribution.

6.6.Objective 3 summary

This study conduct a numerical analysis of the impact on performance in a fuel cell's flow field by altering factors such as the active area, orientation along with flow direction. The previously discussed results offer several crucial findings that need to be considered during the design of a fuel cell flow field. These findings are outlined below:

- With the increase in Relative Humidity Current Density also increases. Once we compare Parallel flow with counter flow at 80%, and 20% RH as base the change found to be 8.3% for both membrane sizes.

- For all the configurations the length of travel of the species remains the same irrespective of the orientation and change in direction. However, the number of u-bends decides the pressure drop. More the number of U bends more will be the pressure drop. Also Parallel flow has been found to have more pressure drop than counter flow. This can be attributed to the availability of high pressure near low pressure points that reduces the pressure drop. This phenomenon affected O_2, H_2O distribution thereby membrane water content.

- Oxygen concentration usually higher at the inlet and reduces towards the outlet, this phenomenon is same for parallel flow. Whereas, for counter flow the available oxygen from inlet of one of the split serpentine induces some oxygen to other split serpentine has increased the distribution of oxygen content in counter flow configurations.

- H_2O accumulation towards outlet was observed in all layouts. However, due to the available pressure in counter flows, it has reduced the H_2O accumulation to some extent. Similarly, membrane water content which in coherence with H_2Oproduction makes MWC levels better distributed.

Therefore, among all the configurations 73x53 mm^2 active area split serpentine flow field with counter flow found to be outperformed. Additionally, variable length method adoptionto split the serpentine flow fields will results in a reduction of water accumulation in the 73x53 counter flow configuration also. The effects of using variable lengths for this design were discussed in chapter 7.

Chapter 7

OBJECTIVE 4

Design and Performance Investigation of Variable Length Split Serpentine Flow Fields

7.1. Physical Model

In continuation with the chapter 6, where 73x53 mm^2 with counter flow found be good in terms of distribution of species. In this chapter, a new method called Variable Length Split Serpentine (VSS) is introduced for the same layout. VSS involves varying the length of each u-bend of the channel from the inlet to the outlet. Specifically, the distance between head-to-head u-bends was chosen as the variable length for that particular layout.

Figure 7.1 shows the geometry of two VSS configurations, (b) flow fields with 1mm variable length (c) flow fields with 2mm variable length and they are compared with Uniform Split Serpentine (USS) (figure 7.1 (a)). The geometry dimensions listed in table 7.1.

The reason for limiting the variable lengths to 1 mm and 2 mm is as follows: as the head-to-head distance between u-bends increases, the angle of inclination of variable lengths also increases. For 1 mm and 2 mm variable lengths, this inclination angle is found to be 14.04 and 26.57 degrees, respectively. However, for the 3 mm VSS, the angle becomes 36.87 degrees, which is higher than the diagonal angle of the 73x53 active area (35.37 degrees).

Due to the higher angle for the 3 mm VSS, some of the flow fields couldn't be accommodated within the active area. Otherwise, the layout would have to be changed to a uniform length up to a certain extent before converting to variable length, which couldn’t be considered as pure VSS. As a result, the study is limited to the 1 mm and 2 mm VSS configurations to ensure compatibility and practicality within the designated active area.

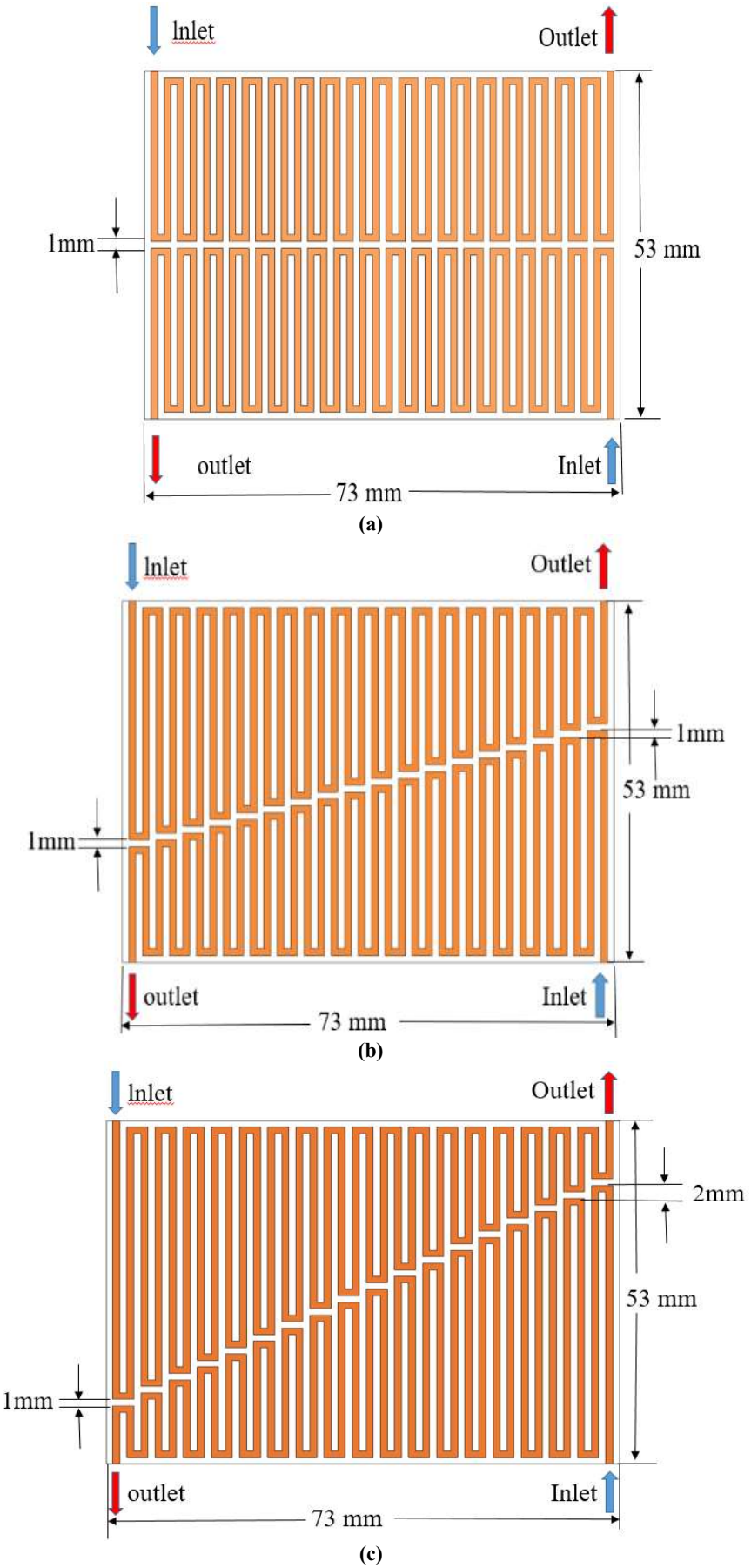

Figure 7.1 Flow field layouts (a) USS (b) 1 mm VSS (c) 2 mm VSS

Table 7.1 Dimensions for the model

	Dimension (mm)	Ref.		Dimension (mm)	Ref.
Membrane area	73x53	This study	Channel width	1	
Electrolyte thickness	0.178		Channel height	1	
Gas Diffusion Layer (GDL) thickness	0.25	[58][74]	Current collector (CC) thickness	2	[58]
Catalyst Layer (CL) thickness	0.02		Rid width	1	

7.2. Results and Discussion

The research examines the impact of variable length serpentine flow fields, similar to previous studies. The main objective is to analyze the performance of the fuel cell by observing crucial parameters like membrane water content, H_2O and O_2 mass fractions, temperature contours, and current density. Considering the previous study's findings on relative humidity (RH) levels, a value of 80% RH was chosen as it provided better results. Hence, all the contours discussed in this study are presented at the 80% RH level.

7.3. Temperature and Pressure characteristics

A humidifying temperature of 343.15 K provided at the inlets of anode and cathode. The temperature rise due to the reactions was observed to be 345 K in all USS and VSS. VSS layouts also showed similar temperature rise like USS (figure 7.2).

The pressure drop shows a decrease as the variable length is increased, Pressure drop values are 3676, 3572 and 3280 Pa for USS, 1 mm VSS and 2 mm VSS respectively (figure 7.3 &7.4). When compared to the 1 mm VSS and USS configurations, the pressure drop decreases by approximately 4.5%. Similarly, when compared to the 1 mm VSS and 2 mm VSS setups, the pressure drop decreases by approximately 8.85%. As discussed in chapter 6, this reduction in pressure drop is attributed to the inlet flow driving away the outlet products with extra pressure.

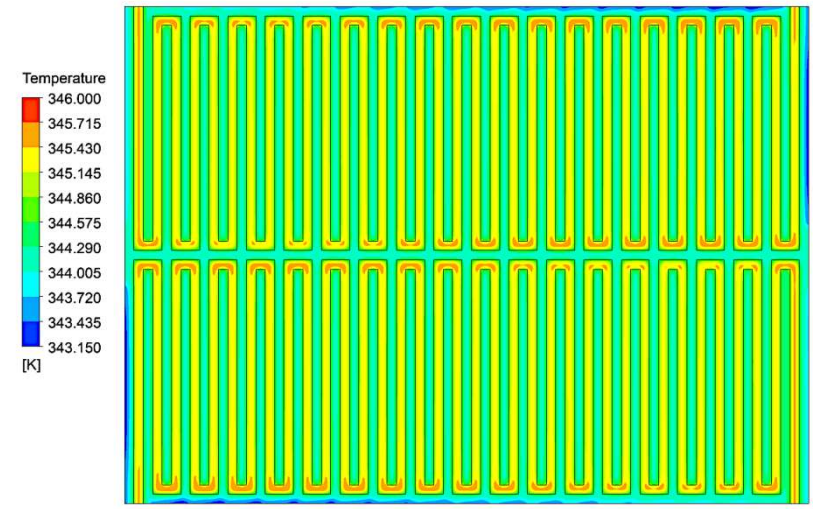

(a) USS

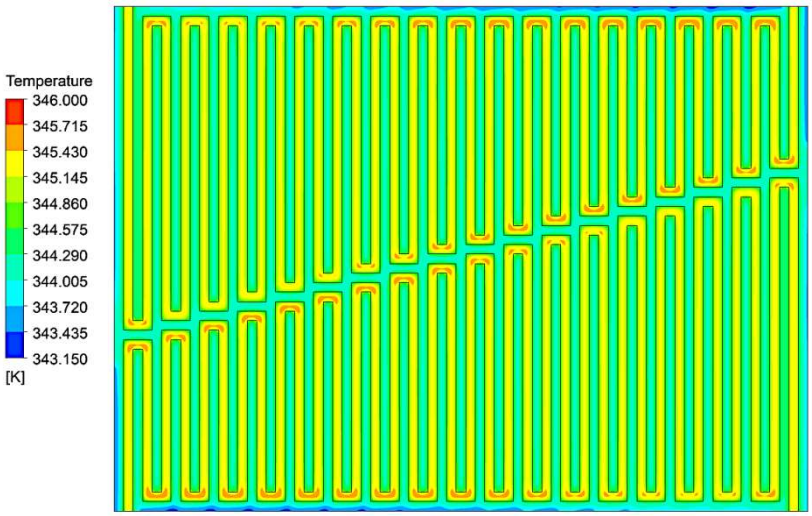

(b) 1 mm VSS

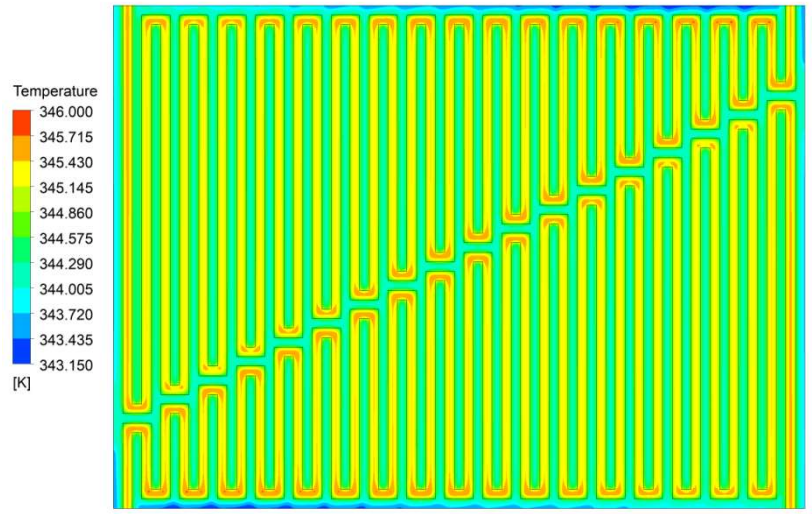

(c) 2 mm VSS

Figure 7.2 Temperature contours of (a) USS, (b) 1 mm VSS and (c) 2 mm VSS

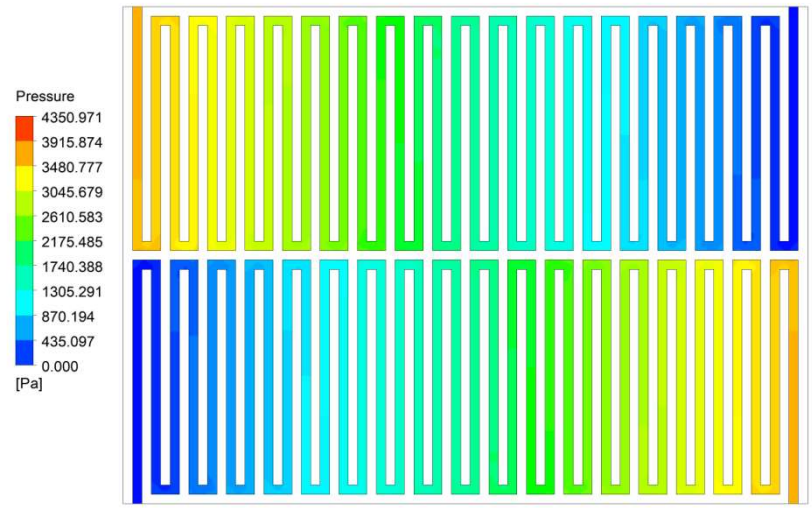

(a) USS

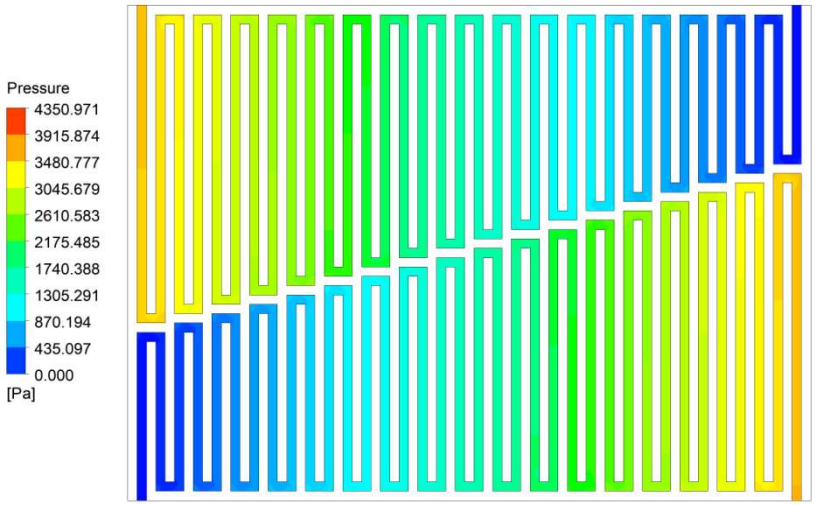

(b) 1 mm VSS

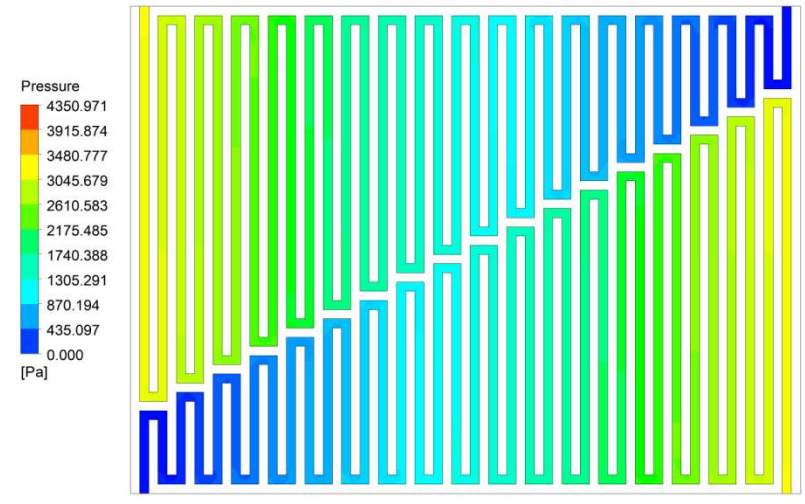

(c) 2 mm VSS

Figure 7.3 Pressure contours of (a) USS, (b) 1 mm VSS and (c) 2 mm VSS

However, with the increase in variable length, the length of the outlet u-bend decreases, bringing the inlet u-bend much closer to the outlet. At this point, it becomes challenging to determine which flow field is better, as other characteristics need to be further studied and considered for a comprehensive evaluation.

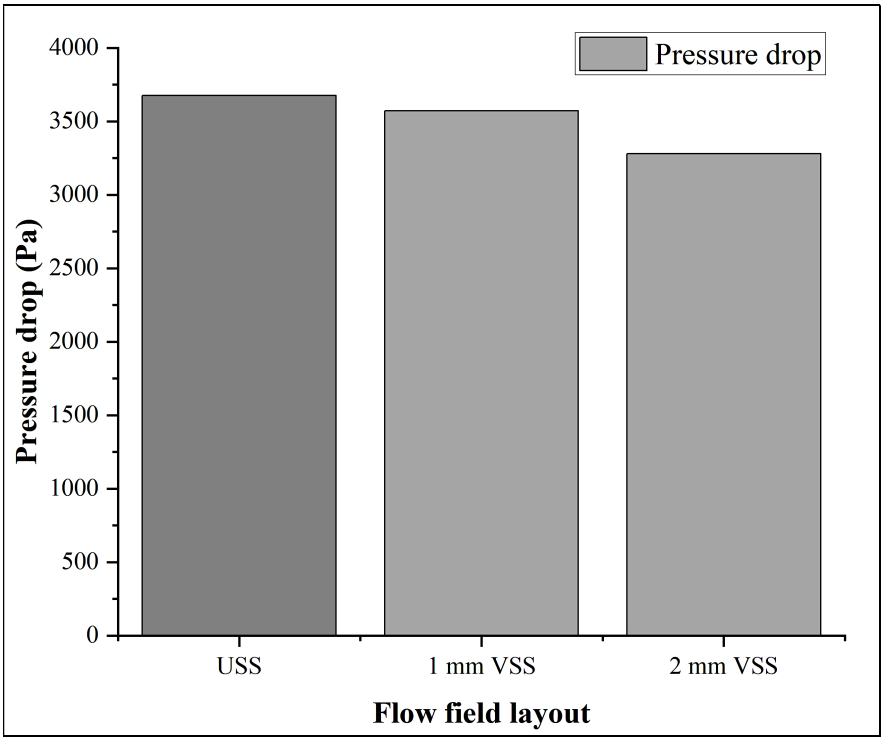

Figure 7.4 Bar chart indicating Pressure of USS, 1 mm VSS and 2 mm VSS

7.4. H_2O mass fraction distribution and Membrane water content profile

Variable length serpentine flow fields have demonstrated notable improvements in the distribution of Membrane Water Content (MWC) (figure 7.5 (a, b, c)). Specifically, when utilizing 1 mm variable length serpentine channels, MWC distribution was superior to that of uniform length serpentine channels. Furthermore, with 2 mm variable length serpentine channels, MWC distribution improved even further. This outcome can be attributed to the underlying assumption of the study, which revolves around increasing the residence time of reactants while concurrently reducing the residence time of products.

Figure 7.6 (a, b, c) presents the H_2O profile comparisons for uniform length, 1 mm, and 2 mm variable length serpentine channels. The contours clearly illustrate that the adoption of variable length serpentine flow fields in PEM fuel cells significantly enhances the H_2O profile. The consistent H_2O profile contributes to a reduction in concentration overpotential and overall improvement in fuel cell performance.

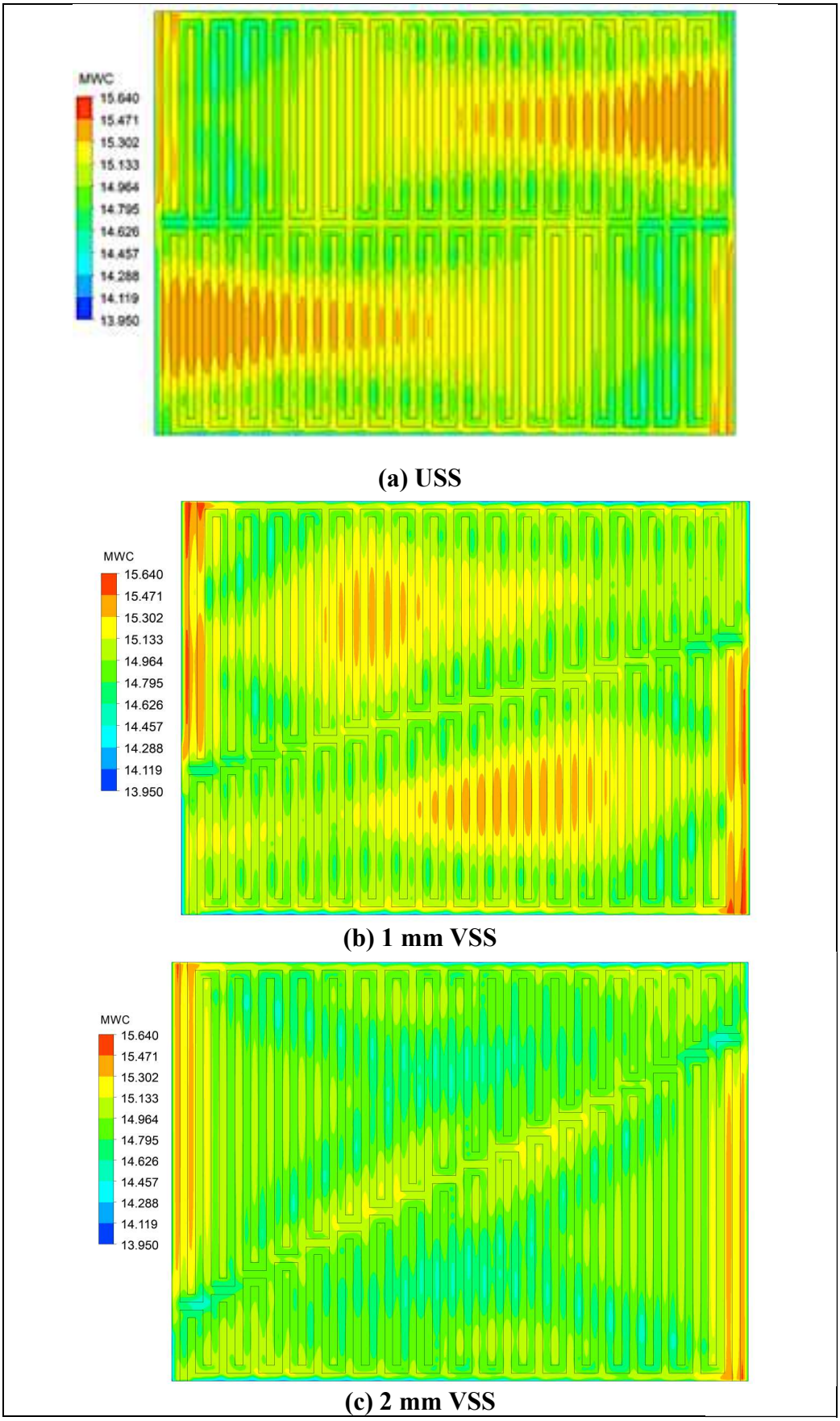

Figure 7.5 Variable length effect on Membrane water content and H_2O mass fraction (a) USS (b) 1 mm and (c) 2 mm

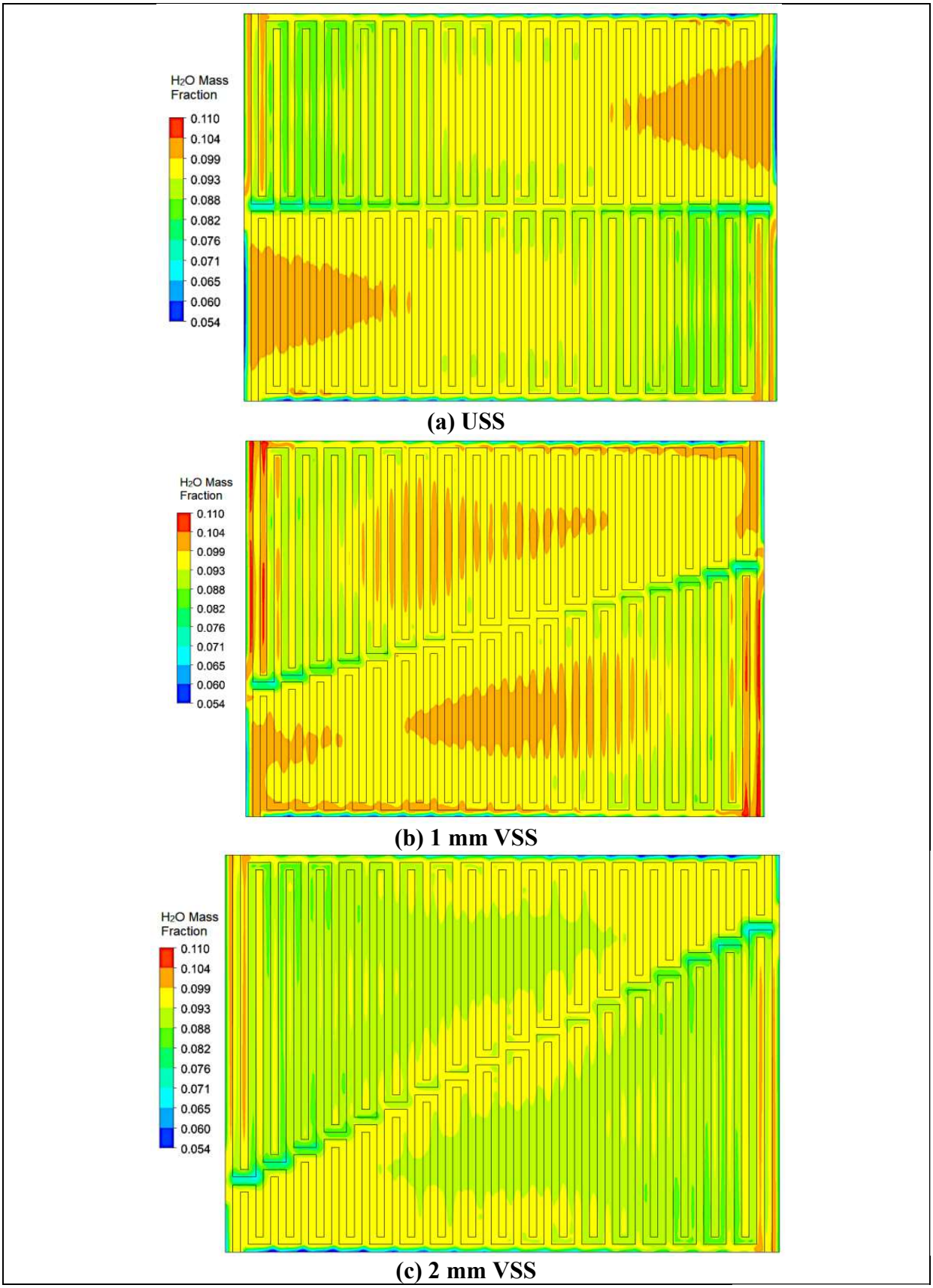

Figure 7.6 H_2O mass fraction distribution in (a) USS, (b) 1 mm VSS and (c) 2 mm VSS

The use of variable length serpentine channels ensures the uniform distribution of H_2O throughout the fuel cell, thereby minimizing the occurrence of flooding or drying. Additionally, consistent water distribution leads to increased membrane water content, thereby enhancing proton conductivity and ultimately improving the performance of the fuel cell.

7.5. Oxygen distribution

Figure 7.7 (a, b, and c) depicts the oxygen profiles for all three designs. The uniform oxygen profile plays a crucial role in reducing the concentration overpotentials, leading to improved fuel cell performance. The study reveals that employing variable length serpentine flow fields (Figure 7.7 b & c) results in a more uniform distribution of oxygen compared USS.

The study also examined the effect of inlet pressure, which was found to cause some oxygen diffusion towards the outlets. Though diffusion occurs even in USS still some region near outlet seems oxygen deficient in USS, due to its length of the channel. However, this diffusion could be considered as minimal. Since, the current counter was plotted at the catalyst layer (CL) and gas diffusion layer (GDL) interface, which means that the diffused oxygen still has a chance of being consumed at the catalyst. As the variable length increases, the probability of diffusion also increases. Therefore, a variable length of 1 mm appears to be the most effective in minimizing oxygen diffusion to the outlet.

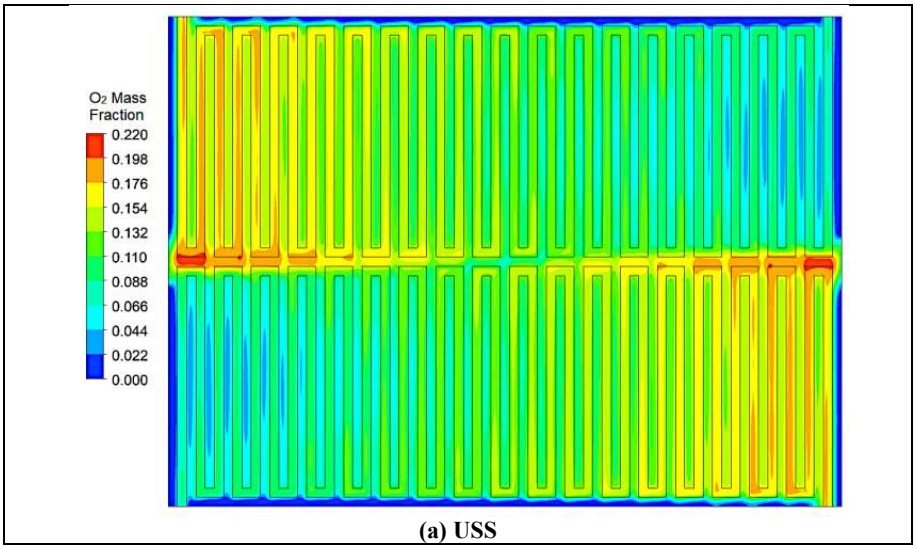

(a) USS

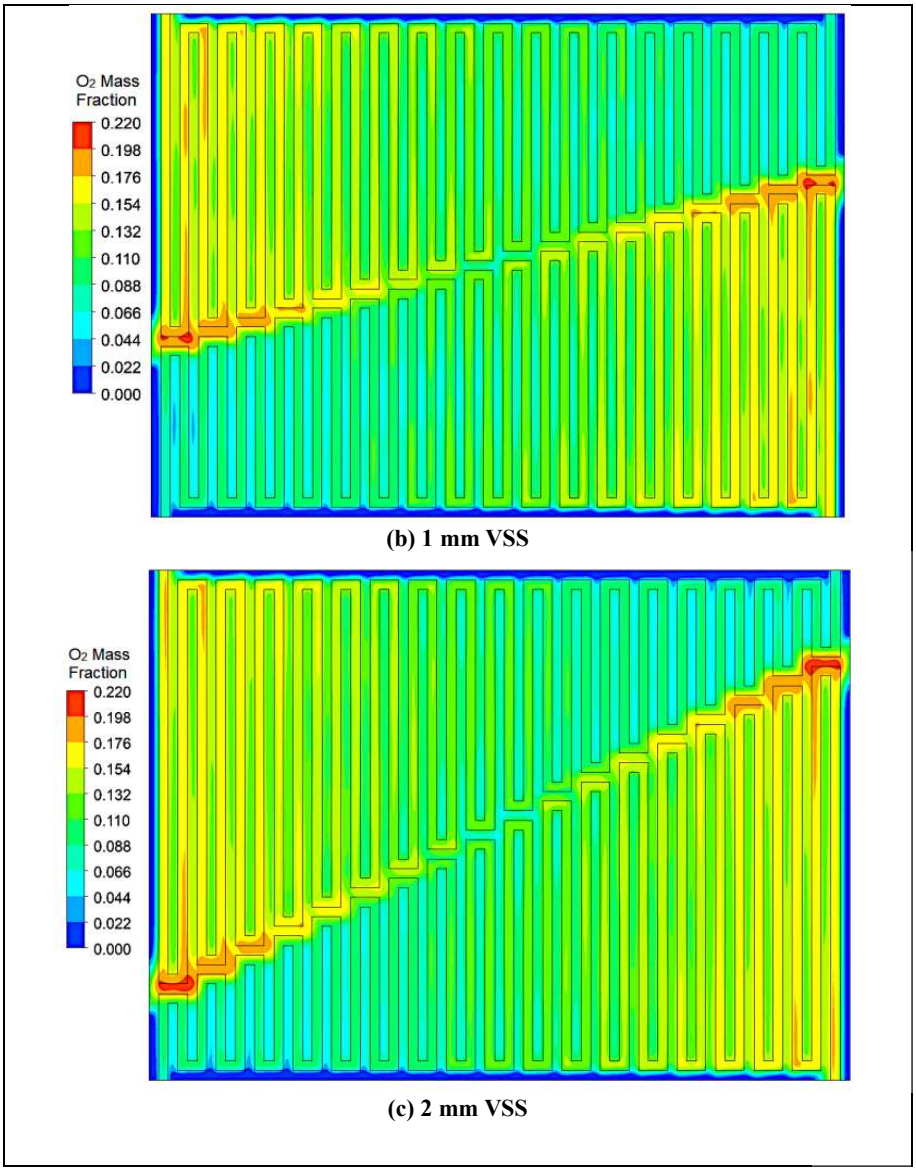

Figure 7.7 O_2 distribution contours (a) USS (b) 1 mm VSS (c) 2 mm VSS

7.6. VI characteristics with respect to relative humidity

Similar to Chapter 6, current densities were recorded at various relative humidity (RH) levels at 0.6 V, which corresponds to the point of maximum power density for all configurations. The reasons for the increase in current densities, as discussed in Chapter 6, are also applicable to this study (Figure 7.8).

As the variable length of the serpentine channels increased, the current density improved due to enhanced characteristics such as species distribution, MWC, and efficient evacuation of H_2O. A comparison between Uniform Serpentine Channels (USS) and 1 mm Variable Serpentine Channels (VSS) showed that the current density improvement was better by 2% at 80% RH. On the other hand, when comparing USS with 2 mm VSS, the current

density improvement was limited to 2.8%. The decrease in improvement in the latter case can be attributed to oxygen diffusion towards the outlets.

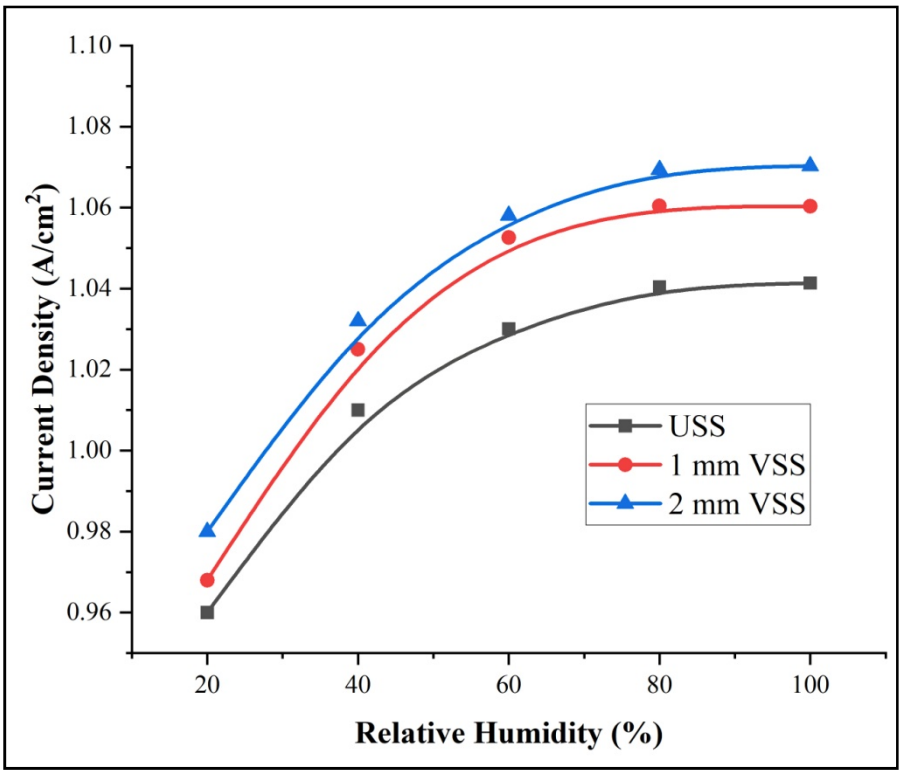

Figure 7.8 Current densities at various RH levels

7.7. Objective 4 summary

A thorough numerical analysis of the design investigation of variable-length split serpentine flow fields for PEMFCs is presented in this research. The study looks into how different channel lengths and relative humidity levels affect the fuel cell's performance. Comparison between VSS and USS design was carried out before optimizing the VSS design to 73x53mm^2.The outcomes are given below:

- ❖ The design of variable length flow fields upon the humidity level have a substantial impact on the PEMFC's performance like in chapter 6. It was discovered that a flow field with a length of 2 mm and an inlet relative humidity of 80% was the best combination of different lengths.
- ❖ In comparison to USS flow field design, it was discovered that the split serpentine flow field design with VSS channel lengths produced greater power output and distribution characteristics.
- ❖ The investigation process identified that 73x53 mm^2 design with 2 mm variable length is better and giving 2.3 % increase in power output compared to USS. Moreover, the

increase percentage of 1 mm VSS is of 2%. The amount increase in current densities are very small in between 1 mm VSS and 2 mm VSS.

- ❖ Pressure drop has decreased with VSS design adoption, due to the diffusion of inlet oxygen to nearby split serpentine. This has not only reduced the pressure drop but also reduced H2O accumulation towards the outlet and thereby good MWC.
- ❖ Among 1 mm VSS and 2 mm VSS, 2 mm VSS outperformed in all the characteristics like current density, membrane water content distribution, H2O and O2 distribution and pressure drop. However, 2 mm VSS outlet split serpentine is near to the outlet compared to 1 mm VSS, which arise a chance of evacuating some oxygen without reacting upon increasing the operating pressure. This arises ambiguity in choosing one among them as final one.

Therefore, it is difficult to finalize, which one better in this case. However, If the requirement is to maintained good distribution of species and current density, 2 mm VSS is better design with some penalties. If there is compromise on current density then 1 mm VSS would be better option.

Further studies are required on oxygen diffusion to outlet at various pressures and ever different active areas then it would simplify the choosing between them. Future work can focus on experimental validation of the optimized design and investigating other design parameters that can further enhance the performance of PEMFCs.

Chapter 8
CONCLUSIONS AND FUTURE SCOPE

8.1. Conclusions

This study conducts the performance evaluation of various novel flow fields design in comparison with the conventional flow fields available. The study of characteristics like VI, temperature, pressure drop, species distribution helps us to evaluate the performance of these designs. Using the CFD techniques the study shed light on study of these characteristics. Objective wise conclusions are discussed below:

Objective 1:

- In comparison between SS and LSFF, LSFF outperformed in these enhancements included a more uniform distribution of membrane water content, an impressive 8% increase in O_2 consumption, a remarkable 22% improvement in product evacuation demonstrated by the H_2O species profile, attributed to a 40% reduction in product travel distance. Additionally, a noteworthy 10% increase in power density was achieved.
- Temperature rise is higher in Single serpentine than the L- serpentine, since temperature reflects the reactions happening it requires further study on understanding this ambiguity.
- Pressure drop was higher in LSFF than SSFF. This increased pressure drop has evidently increased the resident time of the reactants and hence more consumption, this can be conformed to O_2 consumption profile.
- Membrane water content and H_2O distribution increased the water content to membrane and hence better proton conduction.

The study on LSFF and SSFF paved way for variable length flow fields, though some of the characteristics are ambiguous further studies would unveil the reason for peculiar behavior. With the better results obtained with this variable length designs, it helped us to try the same concept of variable length flow fields to split serpentine flow fields. Furthermore, though the pressure helps in reactivity it is always suggested to reduce it, so split serpentine with variable length, not only reduced the pressure drop but also increased the distribution characteristics.

Objective 2:

- An another attempt has been made to compare the flow behavior of parallel and counter split serpentine flow field with dual serpentine flow field. Polarization characteristics for all three cases were plotted and it was observed that split serpentine with counter flow field has better current density among other designs.
- In comparison to the dual serpentine flow field, split serpentine parallel flow and counter flow enhanced their power densities by 6.5% and 10.6%, respectively, and their oxygen consumption by 1.5% and 5%.
- This study seems to be completely different from the previous, however this study set the basic bench marks for the comparison of Split serpentine flow field characteristics with different sizes, orientation in objective 3.
  - Pressure drop has decreased almost by five fold in Split serpentine when compared to SS and LSFFs.
  - Interestingly, a counter flow configuration possible in split serpentine helped to adopted variable length flow concept to this design.

Objective 3:

- Orientation and size effects study conducted in this helps to understand the behaviour of split serpentine with the previous study (Objective 2).
- The current densities produced were low compared to 21x21 split serpentine, this can be attributed to increased area which induces more ohmic losses. The maximum current density was obtained in counter flow configuration in both sizes. Around 4% decrease in current density was observed with increase membrane area.
- Pressure drop has increased by 100 folds upon increasing the active area from 21x21 to 73x53 or 35x73. Due to the obvious reason of increased length of travel and increased flow resistance.
- With the adoption of bigger sizes the accumulation of water was observed towards the outlet. Moreover, the accumulation was higher in vertical configuration due to the length of the single flow field. Further the accumulation was reduced with counter flow configuration. However, this problem was further minimized with adoption of variable length to split serpentine (discussed in objective 4).

Objective 4:

- As anticipated various species distribution characteristics were enhanced with variable length flow fields. 73x53 with counter flow configuration performance was better in previous study, hence optimization of variable length study was conducted for the same.
- Since, current density and species distributions were enhanced with increasing the variable length, this study can't be considered as optimization study, however, it always required to choose among 1 mm and 2 mm VSS according to the importance current density or species distribution. Since, species distribution reduces the stresses induced to the current collector.
- Though the improved current density seems to be insignificant value of only around 2%. However, it is always to be noticed that this 2% is an additional current density obtained to increase 10% current density in split serpentine alone when compared to dual serpentine.

Overall comparison between SS & LS, Split Serpentine (Parallel and counter flow) SSP (Horizontal and vertical), SSC (Horizontal and vertical), Variable length SS 1mm, 2mm serpentine flow fields.

8.2. Future scope

- Comprehensive studies are required to test the dynamic nature of the developed designs.
- It is essential to consider various operating conditions during testing.
- The assumption of adopting variable length aims to increase the residence time of the reactants and reduce it for products. This assumption requires meticulous examination to how exactly this happening.
- The impact of variable lengths on High-temperature fuel cells needs to be evaluated to understand the advantages it offers.
- Further investigation is necessary to study the effect of rib width at the center, where reactant miscibility is possible.
- Oxygen scavenging in split serpentine counter flow fields need to be studied minutely to reduce the scavenging.
- Pressure drop in variable length split serpentines decreasing, since the pressure drop was calculated as the difference between inlet and outlet pressure. Due to escape of

some of the fuel to outlet pressure at various locations may vary. That need to be studied along with oxygen scavenging.

.

REFERENCES

[1]MOSPI GOI, "Energy Statistics India-2023," *Gov. India | Minist. Stat. Program. Implement.*, 2023, [Online]. Available: https://mospi.gov.in/web/mospi/home.

[2]Statista, "Global electricity consumption 1980-2021," *Stat. Res. Deparment*, 2023.

[3]F. Birol, "World Energy Investment," *Internatinal Energy Agency*, pp. 1–183, 2023.

[4]N. Armaroli and V. Balzani, "Towards an electricity-powered world," *Energy Environ. Sci.*, vol. 4, no. 9, pp. 3193–3222, 2011, doi: 10.1039/c1ee01249e.

[5]G. B. Katam, V. B. A., M. M. K., and G. S. Warkhade, "Review on algae for biodiesel fuel production, its characteristics comparison with other and their impact on performance, combustion and emissions of diesel engine," *World J. Eng.*, vol. 14, no. 2, pp. 127–138, 2017, doi: 10.1108/wje-06-2016-0012.

[6]A. Garai and D. K. Pandey, "EPRA International Journal of Research and Development (IJRD) Role of renewable energy for clean energy transition plan for india and determination of retariff under cerc terms and conditions of resources regulations , 2020 EPRA International Journal of," vol. 7838, no. July, pp. 51–56, 2022.

[7]P. T. Moseley, *Fuel Cell Systems Explained*, vol. 93, no. 1–2. 2001.

[8]S. E. Hosseini and M. A. Wahid, "Hydrogen production from renewable and sustainable energy resources: Promising green energy carrier for clean development," *Renew. Sustain. Energy Rev.*, vol. 57, pp. 850–866, 2016, doi: 10.1016/j.rser.2015.12.112.

[9]I. Dincer and C. Acar, "Review and evaluation of hydrogen production methods for better sustainability," *Int. J. Hydrogen Energy*, vol. 40, no. 34, pp. 11094–11111, 2014, doi: 10.1016/j.ijhydene.2014.12.035.

[10] S. Mohanty, A. N. Desai, S. Singh, V. Ramadesigan, and S. M, "Effects of the membrane thickness and ionomer volume fraction on the performance of PEMFC with U-shaped serpentine channel," *Int. J. Hydrogen Energy*, vol. 46, no. 39, pp. 20650–20663, 2021, doi: 10.1016/j.ijhydene.2021.03.252.

[11] F. Barbir, *PEM Fuel Cells*, Second Edi. 2013.

[12] A. Aiyejina and M. K. S. Sastry, "PEMFC flow channel geometry optimization: A review," *J. Fuel Cell Sci. Technol.*, vol. 9, no. 1, Feb. 2012, doi: 10.1115/1.4005393/439758.

[13] A. K. Shukla, R. K. Raman, and K. Scott, "Advances in mixed-reactant fuel cells," *Fuel Cells*, vol. 5, no. 4. pp. 436–447, 2005, doi: 10.1002/fuce.200400075.

[14] A. Ersoz, H. Olgun, and S. Ozdogan, "Reforming options for hydrogen production from fossil fuels for PEM fuel cells," *J. Power Sources*, vol. 154, no. 1, pp. 67–73, 2006, doi: 10.1016/j.jpowsour.2005.02.092.

[15] J. J. Baschuk and X. Li, "Carbon monoxide poisoning of proton exchange membrane fuel cells," *Int. J. Energy Res.*, vol. 25, no. 8, pp. 695–713, Jun. 2001, doi: 10.1002/er.713.

[16] S. Stolbov, M. A. Ortigoza, R. Adzic, and T. S. Rahman, "High CO tolerance of Pt/Ru nanocatalyst: Insight from first principles calculations," *J. Chem. Phys.*, vol. 130, no. 12, pp. 1–6, 2009, doi: 10.1063/1.3088843.

[17] T. V. Choudhary and D. W. Goodman, "CO-free fuel processing for fuel cell applications," 2002, doi: 10.1016/S0920-5861(02)00233-X.

[18] M. L. Perry, F. R. McLarnon, J. Newman, and E. Cairns, "Exploratory Fuel-Cell Research: I. Direct-Hydrocarbon Polymer-Electrolyte Fuel Cell II. Mathematical Modeling of Fuel-Cell Cathodes Energy and Environment Division," *Lawrence Berkeley Natl. Lab.*, 1996, Accessed: May 02, 2019. [Online]. Available: https://cloudfront.escholarship.org/dist/prd/content/qt4gk5f4bj/qt4gk5f4bj.pdf.

[19] B. Parackal, H. Khakdaman, Y. Bourgault, and M. Ternan, "An Investigation of Direct Hydrocarbon (Propane) Fuel Cell Performance Using Mathematical Modeling," *Int. J. Electrochem.*, vol. 2018, pp. 1–18, Dec. 2018, doi: 10.1155/2018/5919874.

[20] I. Korkischko, B. S. Carmo, and F. C. Fonseca, "Shape Optimization of PEMFC Flow-channel Cross-Sections," *Fuel Cells*, vol. 17, no. 6, pp. 809–815, Dec. 2017, doi: 10.1002/FUCE.201700168.

[21] R. Kumar, A. V. Babu, and S. H. Sonawane, "Performance evaluation of a trapezoidal

interconnector configuration of solid oxide fuel cell: A numerical study," *Int. J. Energy Res.*, Sep. 2022, doi: 10.1002/ER.8656.

[22] R. Kumar, A. V. Babu, and S. H. Sonawane, "Numerical investigation of a novel rhombohedral interconnector configuration for planar solid oxide fuel cells," *Int. J. Green Energy*, vol. 00, no. 00, pp. 1–12, 2022, doi: 10.1080/15435075.2022.2154609.

[23] T. Wilberforce *et al.*, "A comprehensive study of the effect of bipolar plate (BP) geometry design on the performance of proton exchange membrane (PEM) fuel cells," *Renew. Sustain. Energy Rev.*, vol. 111, no. May, pp. 236–260, 2019, doi: 10.1016/j.rser.2019.04.081.

[24] B. H. Lim, E. H. Majlan, W. R. W. Daud, T. Husaini, and M. I. Rosli, "Effects of flow field design on water management and reactant distribution in PEMFC: a review," *Ionics 2016 223*, vol. 22, no. 3, pp. 301–316, Feb. 2016, doi: 10.1007/S11581-016-1644-Y.

[25] M. Marappan *et al.*, "Performance Studies of Proton Exchange Membrane Fuel Cells with Different Flow Field Designs – Review," *Chem. Rec.*, vol. 21, no. 4, pp. 663–714, 2021, doi: 10.1002/tcr.202000138.

[26] Z. Liao, L. Wei, A. M. Dafalla, J. Guo, and F. Jiang, "Analysis of the impact of flow field arrangement on the performance of PEMFC with zigzag-shaped channels," *Int. J. Heat Mass Transf.*, vol. 181, p. 121900, 2021, doi: 10.1016/j.ijheatmasstransfer.2021.121900.

[27] S. N. Ozdemir and İ. Taymaz, "CFD Investigation of Different Flow Field Designs for Efficient PEMFC Performance," *Sak. Univ. J. Sci.*, no. June, 2021, doi: 10.16984/saufenbilder.901153.

[28] N. Limjeerajarus and P. Charoen-Amornkitt, "Effect of different flow field designs and number of channels on performance of a small PEFC," *Int. J. Hydrogen Energy*, vol. 40, no. 22, pp. 7144–7158, 2015, doi: 10.1016/j.ijhydene.2015.04.007.

[29] V. Velisala, G. Pullagura, N. Yarramsetty, S. Vadapalli, M. K. Boni, and K. K. Gorantla, "Three-Dimensional CFD Modeling of Serpentine Flow Field Configurations for PEM Fuel Cell Performance," *Arab. J. Sci. Eng.*, vol. 46, no. 12, pp. 11687–11700, 2021, doi: 10.1007/s13369-021-05544-4.

[30] R. R. Kumar, S. Suresh, T. Suthakar, and V. K. Singh, “Experimental investigation on PEM fuel cell using serpentine with tapered flow channels,” *Int. J. Hydrogen Energy*, vol. 45, no. 31, 2020, doi: 10.1016/j.ijhydene.2020.04.023.

[31] M. Liu, H. Huang, X. Li, X. Guo, T. Wang, and H. Lei, “Geometry optimization and performance analysis of a new tapered slope cathode flow field for PEMFC,” *Int. J. Hydrogen Energy*, vol. 46, no. 75, pp. 37379–37392, 2021, doi: 10.1016/j.ijhydene.2021.09.022.

[32] Z. Zhang, S. Wu, H. Miao, and T. Zhang, “Numerical Investigation of Flow Channel Design and Tapered Slope Effects on PEM Fuel Cell Performance,” *Sustain.*, vol. 14, no. 18, 2022, doi: 10.3390/su141811167.

[33] W. Li *et al.*, “Experimental and numerical analysis of a three-dimensional flow field for PEMFCs,” *Appl. Energy*, vol. 195, pp. 278–288, Jun. 2017, doi: 10.1016/J.APENERGY.2017.03.008.

[34] R. Gadhewal, S. K. Thamida, V. V. Ananthula, and V. S. Patnaikuni, “Hot spot identification in PEM fuel cell and its purging strategies,” *Chemical Papers*, vol. 76, no. 2. pp. 1199–1211, 2022, doi: 10.1007/s11696-021-01932-0.

[35] X. Li and I. Sabir, “Review of bipolar plates in PEM fuel cells: Flow-field designs,” *Int. J. Hydrogen Energy*, vol. 30, pp. 359–371, 2005, doi: 10.1016/j.ijhydene.2004.09.019.

[36] O. Ryan, C. Suk-Won, C. Whitney, and B. P. Fritz, “Fuel cell fundamentals,” *John Wiley sons, Inc., Hoboken,New Jersey*, pp. 1–603, 2009, doi: 10.1007/978-0-387-73532-0_1.

[37] L. Xing *et al.*, “A novel flow field with controllable pressure gradient to enhance mass transport and water removal of PEM fuel cells,” *Am. Inst. Chem. Eng.*, vol. 66, no. September 2019, pp. 1–13, 2020, doi: 10.1002/aic.16957.

[38] L. Rostami, M. Haghshenasfard, M. Sadeghi, and M. Zhiani, “A 3D CFD model of novel flow channel designs based on the serpentine and the parallel design for performance enhancement of PEMFC,” *Energy*, vol. 258, p. 124726, Nov. 2022, doi: 10.1016/J.ENERGY.2022.124726.

[39] A. L. R. Paulino, E. F. Cunha, E. Robalinho, M. Linardi, I. Korkischko, and E. I. Santiago, “CFD Analysis of PEMFC Flow Channel Cross Sections,” *Fuel Cells*, vol. 17, no. 1, pp. 27–36, Feb. 2017, doi: 10.1002/FUCE.201600141.

[40] S. Shimpalee, S. Greenway, and J. W. Van Zee, “The impact of channel path length on PEMFC flow-field design,” *J. Power Sources*, vol. 160, no. 1, pp. 398–406, 2006, doi: 10.1016/j.jpowsour.2006.01.099.

[41] D. S. Watkins, K. W. Dircks, and D. G. Epp, “Novel fuel cell fluid flow field plates,” *United States Pat.*, vol. 4,988,583, 1991.

[42] D. S. Watkins, K. W. Dircks, and D. G. Epp, “Fuel cell fluid flow plate,” *US State Pat.*, vol. 5,108,849, 1992.

[43] A. Kazim, H. T. Liu, and P. Forges, “Modelling of performance of PEM fuel cells with conventional and interdigitated flow fields,” *J. Appl. Electrochem.*, vol. 29, no. 12, pp. 1409–1416, 1999, doi: 10.1023/A:1003867012551/METRICS.

[44] S. Dutta, S. Shimpalee, and J. W. Van Zee, “Numerical prediction of mass-exchange between cathode and anode channels in a PEM fuel cell,” *Int. J. Heat Mass Transf.*, vol. 44, no. 11, pp. 2029–2042, 2001, doi: 10.1016/S0017-9310(00)00257-X.

[45] L. Wang, A. Husar, T. Zhou, and H. Liu, “A parametric study of PEM fuel cell performances,” *Int. J. Hydrogen Energy*, vol. 28, no. 11, pp. 1263–1272, 2003, doi: 10.1016/S0360-3199(02)00284-7.

[46] P. T. Nguyen, T. Berning, and N. Djilali, “Computational model of a PEM fuel cell with serpentine gas flow channels,” *J. Power Sources*, vol. 130, no. 1–2, pp. 149–157, 2004, doi: 10.1016/j.jpowsour.2003.12.027.

[47] Y. Ming and A. Su, “A three-dimensional full-cell CFD model used to investigate the effects of different flow channel designs on PEMFC performance,” *Int. J. Hydrogen Energy*, vol. 32, pp. 4466–4476, 2007, doi: 10.1016/j.ijhydene.2007.05.012.

[48] D. H. Jeon, S. Greenway, S. Shimpalee, and J. W. Van Zee, “The effect of serpentine flow-field designs on PEM fuel cell performance,” *Int. J. Hydrogen Energy*, vol. 33, no. 3, pp. 1052–1066, Feb. 2008, doi: 10.1016/J.IJHYDENE.2007.11.015.

[49] J. Zhang *et al.*, “Electrochimica Acta PEM fuel cell relative humidity (RH) and its

effect on performance at high temperatures," vol. 53, pp. 5315–5321, 2008, doi: 10.1016/j.electacta.2008.02.074.

[50] D. Chen, W. Li, and H. Peng, "An experimental study and model validation of a membrane humidifier for PEM fuel cell humidification control," vol. 180, pp. 461–467, 2008, doi: 10.1016/j.jpowsour.2008.02.055.

[51] X. Wang, X. Zhang, W. Yan, D. Lee, and A. Su, "Determination of the optimal active area for proton exchange membrane fuel cells with parallel , interdigitated or serpentine designs," *Int. J. Hydrogen Energy*, vol. 34, no. 9, pp. 3823–3832, 2009, doi: 10.1016/j.ijhydene.2008.12.049.

[52] L. I. N. Lin, Z. Xinxin, F. Huting, and W. Xiaodong, "Optimization of a serpentine flow field with variable channel heights and widths for PEM fuel cells," vol. 53, no. 2, pp. 453–460, 2010, doi: 10.1007/s11431-010-0009-4.

[53] X. D. Wang, W. M. Yan, Y. Y. Duan, F. B. Weng, G. Bin Jung, and C. Y. Lee, "Numerical study on channel size effect for proton exchange membrane fuel cell with serpentine flow field," *Energy Convers. Manag.*, vol. 51, no. 5, pp. 959–968, 2010, doi: 10.1016/j.enconman.2009.11.037.

[54] K. S. Choi, H. M. Kim, and S. M. Moon, "Numerical studies on the geometrical characterization of serpentine flow-field for efficient PEMFC," *Int. J. Hydrogen Energy*, vol. 36, no. 2, pp. 1613–1627, Jan. 2011, doi: 10.1016/J.IJHYDENE.2010.10.073.

[55] A. Iranzo, M. Muñoz, F. Rosa, and J. Pino, "Numerical model for the performance prediction of a PEM fuel cell. Model results and experimental validation," *Int. J. Hydrogen Energy*, vol. 35, no. 20, pp. 11533–11550, 2010, doi: 10.1016/j.ijhydene.2010.04.129.

[56] F. Hashemi, S. Rowshanzamir, and M. Rezakazemi, "CFD simulation of PEM fuel cell performance: Effect of straight and serpentine flow fields," *Math. Comput. Model.*, vol. 55, no. 3–4, pp. 1540–1557, 2012, doi: 10.1016/j.mcm.2011.10.047.

[57] J. Bachman, M. Charvet, A. Santamaria, H. Tang, J. Wan, and R. Walker, "Experimental investigation of the effect of channel length on performance and water accumulation in a PEMFC parallel flow field," *Int. J. Hydrogen Energy*, vol. 37, no.

22, pp. 17172–17179, 2012, doi: 10.1016/j.ijhydene.2012.08.023.

[58] J. M. Sierra, S. J. Figueroa-Ramírez, S. E. Díaz, J. Vargas, and P. J. Sebastian, "Numerical evaluation of a PEM fuel cell with conventional flow fields adapted to tubular plates," *Int. J. Hydrogen Energy*, vol. 39, no. 29, pp. 16694–16705, 2014, doi: 10.1016/j.ijhydene.2014.04.078.

[59] Y. Vazifeshenas, K. Sedighi, and M. Shakeri, "Numerical investigation of a novel compound flow-field for PEMFC performance improvement," *Int. J. Hydrogen Energy*, vol. 40, no. 43, pp. 15032–15039, 2015, doi: 10.1016/j.ijhydene.2015.08.077.

[60] Y. Wang, L. Yue, and S. Wang, "New design of a cathode flow-field with a sub-channel to improve the polymer electrolyte membrane fuel cell performance," *J. Power Sources*, vol. 344, pp. 32–38, 2017, doi: 10.1016/j.jpowsour.2017.01.075.

[61] D. Singdeo, T. Dey, S. Gaikwad, S. J. Andreasen, and P. C. Ghosh, "A new modified-serpentine flow field for application in high temperature polymer electrolyte fuel cell," *Appl. Energy*, vol. 195, pp. 13–22, 2017, doi: 10.1016/j.apenergy.2017.03.022.

[62] E. Alizadeh, M. Rahimi-Esbo, S. M. Rahgoshay, S. H. M. Saadat, and M. Khorshidian, "Numerical and experimental investigation of cascade type serpentine flow field of reactant gases for improving performance of PEM fuel cell," *Int. J. Hydrogen Energy*, vol. 42, no. 21, pp. 14708–14724, 2017, doi: 10.1016/j.ijhydene.2017.04.212.

[63] A. N. A. Mubin, M. H. Bahrom, M. Azri, Z. Ibrahim, N. A. Rahim, and S. R. S. Raihan, "Analysis performance of proton exchange membrane fuel cell (PEMFC)," *IOP Conf. Ser. Mater. Sci. Eng.*, vol. 210, no. 1, 2017, doi: 10.1088/1757-899X/210/1/012052.

[64] V. Velisala and G. N. Srinivasulu, "Numerical Simulation and Experimental Comparison of Single, Double and Triple Serpentine Flow Channel Configuration on Performance of a PEM Fuel Cell," *Arab. J. Sci. Eng.*, vol. 43, no. 3, 2018, doi: 10.1007/s13369-017-2813-7.

[65] S. Abdulla and V. S. Patnaikuni, "Detailed analysis of polymer electrolyte membrane fuel cell with enhanced cross-flow split serpentine flow field design," *Int. J. Energy Res.*, vol. 43, no. 7, pp. 2806–2820, 2019, doi: 10.1002/er.4368.

[66] M. K. Vijayakrishnan *et al.*, “Numerical and experimental investigation on 25 cm2 and 100 cm2 PEMFC with novel sinuous flow field for effective water removal and enhanced performance,” *Int. J. Hydrogen Energy*, vol. 45, no. 13, pp. 7848–7862, 2020, doi: 10.1016/j.ijhydene.2019.05.205.

[67] R. Gundlapalli and S. Jayanti, “Effective splitting of serpentine flow field for applications in large-scale flow batteries,” *J. Power Sources*, vol. 487, no. December 2020, p. 229409, 2021, doi: 10.1016/j.jpowsour.2020.229409.

[68] D. Ponnaiyan, M. Chandran, T. Kumaresan, J. Ramasamy, K. Palaniswamy, and S. Sundaram, “Experimental study of temperature distribution effect on proton exchange membrane fuel cell using multi-pass serpentine channels,” *Mater. Lett.*, vol. 320, p. 132361, Aug. 2022, doi: 10.1016/J.MATLET.2022.132361.

[69] A. Hamrang, M. Abdollahzadeh, M. J. Kermani, and S. M. Rahgoshay, “Numerical simulation of the PEM fuel cell performance enhancement by various blockage arrangement of the cathode serpentine gas flow channel outlets/inlets,” *Int. J. Heat Mass Transf.*, vol. 186, p. 122475, 2022, doi: 10.1016/j.ijheatmasstransfer.2021.122475.

[70] A. Iranzo, C. H. Arredondo, A. M. Kannan, and F. Rosa, “Biomimetic flow fields for proton exchange membrane fuel cells: A review of design trends,” *Energy*, vol. 190. Elsevier Ltd, p. 116435, Jan. 01, 2020, doi: 10.1016/j.energy.2019.116435.

[71] S. R. Badduri, G. N. Srinivasulu, and S. S. Rao, “Influence of bio-inspired flow channel designs on the performance of a PEM fuel cell,” *Chinese J. Chem. Eng.*, vol. 28, no. 3, pp. 824–831, 2020, doi: 10.1016/j.cjche.2019.07.010.

[72] S. R. Badduri, G. N. Srinivasulu, and S. S. Rao, “Experimental analysis of PEM fuel cell performance using lung channel design bipolar plate,” *Int. J. Green Energy*, vol. 16, no. 15, pp. 1591–1601, 2019, doi: 10.1080/15435075.2019.1677238.

[73] S. Abdulla and V. S. Patnaikuni, “Performance evaluation of Enhanced Cross flow Split Serpentine Flow Field design for higher active area PEM fuel cells,” *Int. J. Hydrogen Energy*, vol. 45, no. 48, 2020, doi: 10.1016/j.ijhydene.2020.01.199.

[74] G. Amarnath and A. V. Babu, “Comparative computational fluid dynamic analysis between split and dual serpentine flow field for proton exchange membrane fuel

cells.," *Chem. Pap.*, 2023, [Online]. Available: https://doi.org/10.1007/s11696-023-02841-0.

[75] L. Yuan, Z. Jin, P. Yang, Y. Yang, D. Wang, and X. Chen, "Numerical analysis of the influence of different flow patterns on power and reactant transmission in tubular-shaped pemfc," *Energies*, vol. 14, no. 8, 2021, doi: 10.3390/en14082127.

[76] A. M. Prasad, P. Lavanya, P. Hara Gopal, T. Praveen Sagar, and S. Pavani, "Experimental investigation of proton exchange membrane (Pem) fuel cell using different serpentine flow channels," *Mater. Sci. Forum*, vol. 969 MSF, pp. 461–465, 2019, doi: 10.4028/WWW.SCIENTIFIC.NET/MSF.969.461.

[77] E. E. Kahveci and I. Taymaz, "Assessment of single-serpentine PEM fuel cell model developed by computational fluid dynamics," *Fuel*, vol. 217, no. August 2017, pp. 51–58, 2018, doi: 10.1016/j.fuel.2017.12.073.

[78] X. Liu, H. Guo, F. Ye, and C. F. Ma, "Flow dynamic characteristics in flow field of proton exchange membrane fuel cells," *Int. J. Hydrogen Energy*, vol. 33, no. 3, pp. 1040–1051, Feb. 2008, doi: 10.1016/j.ijhydene.2007.11.018.

[79] V. Lakshminarayanan and P. Karthikeyan, "Optimization of Flow Channel Design and Operating Parameters on Proton Exchange Membrane Fuel Cell Using," *Period. Polytech. Chem. Eng.*, vol. 60, no. 3, pp. 173–180, 2016, doi: 10.3311/PPch.8461.

[80] Y. Amadane, H. Mounir, A. El Marjani, E. M. Karim, and A. Awan, "Numerical investigation of hydrogen consumption in Proton Exchange Membrane Fuel Cell by using computational fluid dynamics (CFD) simulation," *Mediterr. J. Chem.*, vol. 7, no. 6, pp. 396–415, 2019, doi: 10.13171/mjc7618121415ya.

[81] D. Rohendi, E. H. Majlan, A. B. Mohamad, W. R. W. Daud, A. A. H. Kadhum, and L. K. Shyuan, "Effects of temperature and backpressure on the performance degradation of MEA in PEMFC," *Int. J. Hydrogen Energy*, vol. 40, no. 34, pp. 10960–10968, 2015, doi: 10.1016/j.ijhydene.2015.06.161.

[82] H. Liu *et al.*, "Three-dimensional multi-phase simulation of cooling patterns for proton exchange membrane fuel cell based on a modified Bruggeman equation," *Appl. Therm. Eng.*, vol. 174, Jun. 2020, doi: 10.1016/J.APPLTHERMALENG.2020.115313.

[83] K. Jiao and X. Li, “Water transport in polymer electrolyte membrane fuel cells,” *Prog. Energy Combust. Sci.*, vol. 37, no. 3, pp. 221–291, Jun. 2011, doi: 10.1016/J.PECS.2010.06.002.

[84] T. V. Reshetenko, G. Bender, K. Bethune, and R. Rocheleau, “A segmented cell approach for studying the effects of serpentine flow field parameters on PEMFC current distribution,” *Electrochimica Acta*, vol. 88. pp. 571–579, 2013, doi: 10.1016/j.electacta.2012.10.103.

Publications:

1. Numerical comparative analysis of Single Serpentine Flow Field with L - Serpentine Flow Field for Proton Exchange Membrane Fuel Cells, Renewable Energy Research and Applications (RERA), DOI: 10.22044/RERA.2023.12943.1213 (ESCI).

2. Comparative Computational Fluid Dynamic analysis between Split and Dual Serpentine Flow Field for Proton Exchange Membrane Fuel Cells, Chemical Papers, Springer, DOI:10.1007/s11696-023-02841-0 CHPA-D-23-00385R1 (SCIE).

3. Optimization of the tapering angle of the flow channels of the PEM Fuel cell: a numerical study, Renewable Energy Research and Applications (RERA), DOI: 10.22044/RERA.2023.12517.1193 (ESCI).

4. Effect of anode material composition on intermediate products generated in low-temperature direct methane fuel cells, Advances in Energy Research, Techno Press (ESCI) (Under review).

5. Evaluation of orientation effect of split serpentine flow fields in parallel and counter flow configuration by using 73x53 mm^2 and 53x73 mm^2 active areas. Sage Part A: Energy source. Taylor and Francis (SCIE) (Under review).

6. Optimization of Variable length in Split serpentine flow fields using the active areas 73x53 mm^2 and 53x73 mm^2, Energy and Environment, Inderscience publications (SCIE) (Under review).

APPENDIX-I

A simple python calculator was used to obtain the mass flow rates, mass fractions of hydrogen and oxygen at anode and cathode respectively, for change in active area, Relative humidity and Temperature.

```
## Step 1: Calculate the mole fraction of hydrogen and oxygen at
# anode and cathode respectively##
P= 303975 # Operating pressure
T = 343.15 # Humidifying temperature
Psat = 31201 # Saturation pressure at humidifying temperature
R = 8.314 #ideal gas constant J/mol.K
I_ref = 10000 #Reference current A/cm2
X_H2O = (Psat/P)
X_H2 = 1- X_H2O
A_mem = float(input("Enter the Active area of the membrane:"))
A_ff = 1e-6 ## area of cross section of flow channel
print("Mole fraction of Hydrogen at anode=", X_H2)
print("Mole fraction of Water at anode=", X_H2O)
X_O2 = (1-X_H2O)*21/(100)
print("Mole fraction of Oxygen= ", X_O2)

## Step 2: velocities
ua = (2*10000*R*T*A_mem)/(2*96485*X_H2*P*A_ff)## inlet velocity at anode
uc = (2*10000*R*T*A_mem)/(4*96485*X_O2*P*A_ff)## inlet velocity at cathode
print("u_a", ua)
print("u_c",uc)

## Step 3: Calculated the specific humidity at anode
R_H2 = 4124 ##j/kg.K
R_H2O = 461.52 ## J/kg.K
RH_a = float(input("Relative Humidity in percentage at anode (0 to 1): "))
Pa_H2O = RH_a*Psat ## saturation temperature
P_H2 = P - Pa_H2O ## partial pressure of hydrogen
```

```
v_H2 = (R_H2*T)/(P_H2)
va_H2O = (R_H2O*T)/(Pa_H2O)
v_a = (v_H2 * va_H2O)/(v_H2+va_H2O)
print("specific volume at anode: ", v_a)

## step 4: calculate the specific humidity at cathode
RH_c = float(input("Relative humidity of air at cathode (0 to 1): "))
R_a = 286.9 ##j/kg.K
Pc_H2O = Psat*RH_c
P_a = P - Pc_H2O
Omega_c = 0.622 * (Pc_H2O/P_a)
print("kg of water content per kg of air= ", Omega_c)
v_o = (R_a*T)/P_a
vc_H2O = (R_H2O*T)/Pc_H2O
v_c = (v_o*vc_H2O)/(v_o+vc_H2O)
print("specific volume at cathode: ",v_c)

## Step 5: Mass flow rates
Uc= uc*A_ff
print(Uc)
m_dota = ua*A_ff/v_a
m_dotc = uc*A_ff/v_c
print("Mass flow rate at anode= ", m_dota)
print("Mass flow rate of cathode= ", m_dotc)

## Step 6: Mass fractions at anode
## Mass fraction kg of H2O per kg of H2
Omega_a = (Pa_H2O/P_H2)*(R_H2/R_H2O) print("kg of water content per kg of Hy
drogen=",  Omega_a)
m_H2 = m_dota/(1+Omega_a)
y_H2 = m_H2/m_dota
y_H2O = 1-y_H2
print("Mass fraction of Hydrogen at anode= ", y_H2)
```

```
print("Mass fraction of Water content at anode= ", y_H2O)

## Step 7: Mass fractions of water content at cathode
mc_air = m_dotc/(1+Omega_c)
yc_H2O = (m_dotc-mc_air)/m_dotc

## Step 8: Mass fraction of Oxygen at cathode
N_air = mc_air/28.946
N_O2 = N_air/4.76
m_O2 = N_O2*32
y_O2 = m_O2/m_dotc
print("Mass fraction of Oxygen at cathode= ", y_O2)
print("Mass fraction of Water content at cathode= ",yc_H2O)
```

Sample output:

```
Enter the Active area of the membrane:441e-6
Mole fraction of Hydrogen at anode= 0.8973566905173123
Mole fraction of Water at anode= 0.10264330948268773
Mole fraction of Oxygen=  0.18844490500863556
u_a 0.4780461659285889
u_c 1.1382051569728306
Relative Humidity in percentage at anode (0 to 1): 1
specific volume at anode:  2.5656470720614837
Relative humidity of air at cathode (0 to 1): 1
kg of water content per kg of air=  0.071146890832704
specific volume at cathode:  0.336960638576501
1.1382051569728305e-06
Mass flow rate at anode=  1.863257698746856e-07
Mass flow rate of cathode=  3.3778579058408953e-06
kg of water content per kg of Hydrogen= 1.0221006673393749
Mass fraction of Hydrogen at anode=  0.49453522079876117
Mass fraction of Water content at anode=  0.5054647792012388
Mass fraction of Oxygen at cathode=  0.21682304353611648
Mass fraction of Water content at cathode=  0.0664212270432813
8
```